DOCTORAL THESIS

Calorimetric and Dilatometric Studies on Glass Transitions under High Pressure

by
Shuichi Takahara

Department of Chemistry
Faculty of Science
Osaka University

1995

Abstract

The heat capacities of the glassy, liquid and crystalline 3-bromopentane were measured with an adiabatic calorimeter in the temperature range 7-300 K. From these data, the configurational entropy S_C of the liquid and undercooled liquid states was evaluated in the temperature range of 107 - 298 K. The relation between the configurational entropy and dielectric relaxation time reported by Berberian and Cole was reproduced well by the Adam-Gibbs theory over the entire temperature range covering the relaxation time from 10 ps to 1 ks. The configurational entropy of a cooperative domain, the number of molecules in a cooperative domain, and the molar activation free energy were determined in the framework of the Adam-Gibbs theory.

The heat capacities of 1-propanol and 3-methylpentane were measured in the temperature range 50 - 180 K (50 - 130 K for the latter) and at three different pressures (0, 108, 198 MPa) by using an adiabatic high-pressure calorimeter. For both substances, the glassy states were readily realized by cooling their liquids and the respective glass transitions were observed calorimetrically at every pressure. Thermodynamic quantities associated with the fusion of the crystalline phase were measured at the three pressures for 1-propanol and at 108 MPa for 3-methylpentane. The pressure dependences of the glass transition and fusion were accurately determined. Experimental data for the entropy of fusion and the heat capacity difference between the glass and the liquid were combined to calculate the temperature dependence of the configurational entropy S_C at each pressure. The pressure dependence of the Kauzmann temperature

T_0, at which S_c tends to vanish, was also determined. It was found that the quantity TS_c was constant at T_g for different pressures, indicating the validity of the entropy theory proposed by Adam and Gibbs.

A novel adiabatic calorimeter was constructed for the simultaneous measurement of enthalpy and volume under high pressure. This calorimeter works under constant pressure up to 100 MPa and in the temperature range between 80 and 380 K. The sample is pressurized hydrostatically using liquid pressure transmitting medium (e.g., 3-methylpentane, Fluorinert and 1-butanol). The sample volume is measured with a new type of volume measurement system using a bellows installed in the cell. As the calibration and test experiments, the heat capacities and volumes (in the low resolution mode) of toluene, water and Fluorinert were measured at atmospheric pressure in the temperature range between 275 and 380 K. The accuracies of heat capacity and thermal expansivity (in the low resolution mode) were ±0.2 % of total sample heat capacity and $\pm 2\times10^{-5}$ K^{-1}, respectively. The test of the volume measurement in the high resolution mode showed that the resolution was $\pm10^{-5}$ % of total sample volume, which is more than 10 times improvement over that of the best previous dilatometer.

The enthalpy and volume of atactic polystyrene were measured simultaneously around the glass transition (T_g = 350 K) at 0.1 MPa and 21 MPa with the above apparatus. The heat capacity gap ΔC_p, thermal expansivity gap $\Delta\alpha$, the isothermal compressibility gap $\Delta\varkappa$ at T_g and the pressure dependence of the glass transition temperature dT_g/dP were determined to be 0.33 J K^{-1} g^{-1}, 0.34 kK^{-1}, 0.17 GPa^{-1}, and 0.34 K MPa^{-1}, respectively. It was found

that $TV\Delta\alpha/\Delta C_p$ agreed with dT_g/dP within the experimental error, indicating that the entropy theory is much better than the free volume theory to describe the pressure dependence of T_g. Prigogine-Defay ratio ($\Pi \equiv \Delta C_p \Delta\kappa / TV(\Delta\alpha)^2$) was calculated to be 1.6, indicating that more than one internal parameters are required to describe the glassy state thermodynamically. The relaxation rates of configurational enthalpy and volume near the glass transition were measured simultaneously as functions of temperature. The temperature dependences of the two relaxation rates were different from each other. This result indicates that the relaxation functions of the enthalpy and volume differ from each other at states far from the equilibrium.

The structural relaxation of atactic polystyrene was investigated around the glass transition temperature by the simultaneous measurement of enthalpy and volume for long time (ca. 80 h). The initial state of the relaxation was prepared by cooling the liquid rapidly to the glass transition region. These data provided the relaxation path in the ΔH_C-ΔV_C plane (ΔH_C: the departure from the equilibrium configurational enthalpy, ΔV_C: the departure from the equilibrium configurational volume). The relaxation path was reproduced by a straight line which is significantly different from the equilibrium line. This result indicates that the relaxation functions of ΔH_C and ΔV_C are similar to each other in a vicinity of equilibrium but the fictive temperature concept is invalid in the structural relaxation of polystyrene. The relaxation path was discussed also on the ΔG_C contour map as functions of ΔE_C and ΔV_C (ΔG_C: the departure from the equilibrium Gibbs free energy, ΔE_C: the departure from the equilibrium internal

energy). It was found that the coupling coefficient between ΔE_c and ΔV_c relaxations is quite significant in the structural relaxation of polystyrene.

Contents

Chapter 1

General Introduction

1-1 Thermodynamic Aspect of Glass Transition

It is well known that the glassy state is a non-equilibrium state of a liquid and that the glass transition occurs as a result of freezing of its microscopic structure. The relation between the equilibrium liquid, glass and crystal is described schematically in the entropy diagram shown in Fig. 1-1. As the temperature decreases, the structural relaxation time τ of the liquid increases and the short range order develops in its structure. The entropy of the liquid decreases because of the development of the structural order. If the crystallization does not occur and the liquid supercools far below T_{fus}, then below a certain temperature T_g the relaxation time τ may become longer than a typical experimental time (ca. 10^3 s) of a thermodynamic measurement. The liquid structure is then frozen in an immobile state. The temperature T_g is known as a glass transition temperature. On further cooling the liquid deviates further from the equilibrium line. The abrupt change of the slope of the entropy corresponds to a step-like change of the heat capacity.

The entropy of a liquid consists of the vibrational entropy S_{vib} and the configurational entropy S_c. The latter does not change below T_g. Since the entropy of the crystal S_{cr} usually consists only of S_{vib}, S_c is given by

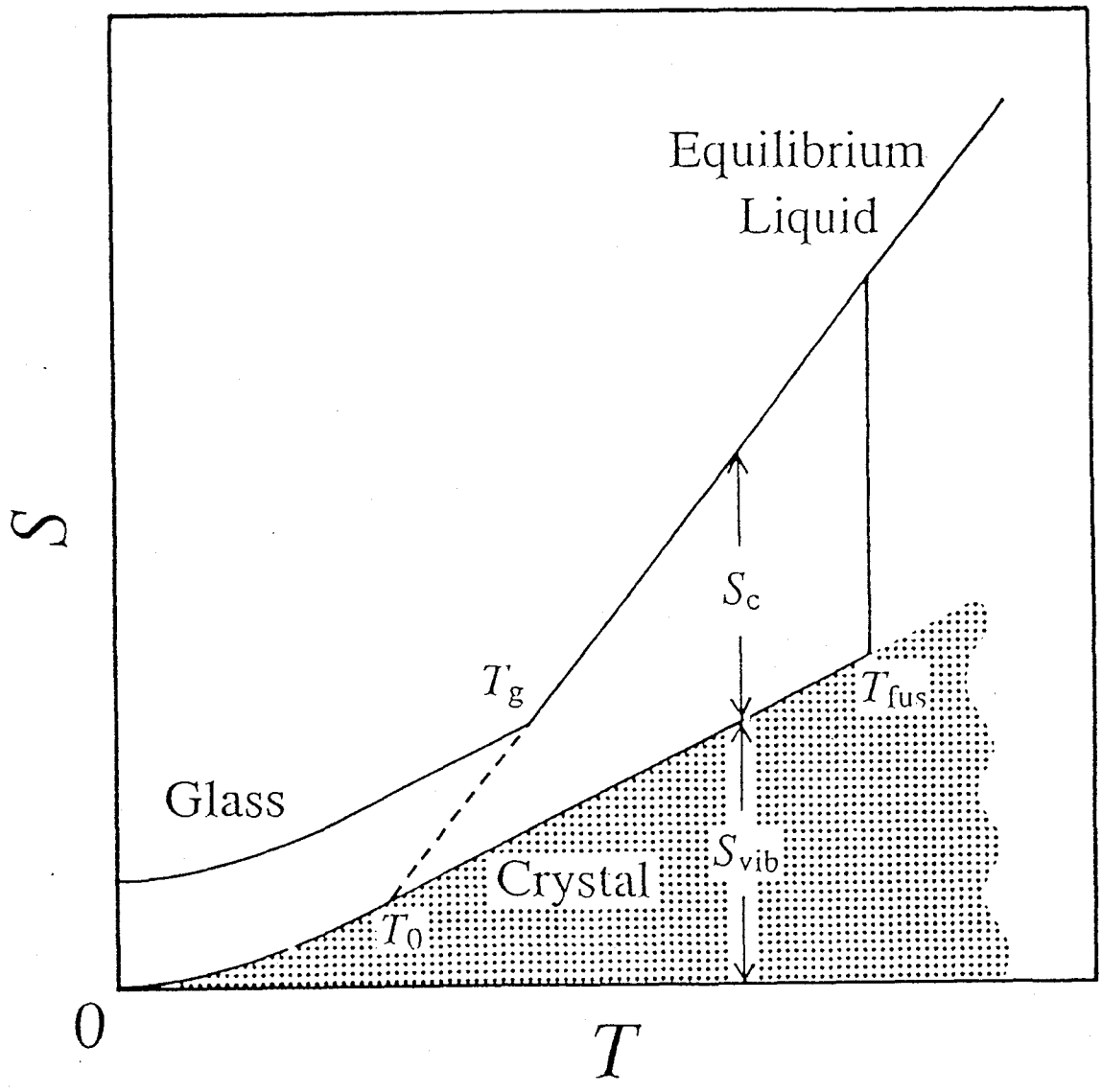

Fig. 1-1. A schematic entropy diagram of a glass-forming system.

$$S_C = S_{liq} - S_{cr}. \qquad (1\text{-}1)$$

Configurational parts of the enthalpy, volume and other thermodynamic quantities are given by relations similar to eq. 1-1. The temperature at which S_C vanishes is known as Kauzmann temperature T_0 [1].

1-2 Structural Relaxation

The structural relaxation in the undercooled liquid and the glass is one of the current topics on condensed-matter physics [2]. The important properties of the structural relaxation are the non-Arrhenius temperature dependence of the structural relaxation time and the non-exponential (non-Debye) nature of the relaxation function. The origin and mechanism of these properties have not been explained coherently, although a number of experimental and theoretical studies have been performed. The entropy theory [3-7] and free volume theory [8-10], which will be discussed in this thesis, were proposed to explain the non-Arrhenius temperature dependence of the structural relaxation time. These theories have been applied also to the pressure dependence of the structural relaxation time and glass transition temperature [5,11-17].

By definition the structural relaxation time near the glass transition temperature is comparable with the experimental time

scale of thermodynamic measurements. The structural relaxation is observed as the relaxations of the various physical quantities (e.g., enthalpy and volume) in the time domain experiments. This is because the glass is in the non-equilibrium state far from the equilibrium and its structure changes significantly with the progress of the relaxation. Since such a changing structure itself dominates the following relaxation, the relaxation function depends on the sign and magnitude of the initial departure from the equilibrium state.

In equilibrium thermodynamics, a homogeneous isotropic liquid is described by a surface representing its equation of state in the p-T-V space. A point on this surface corresponds to a point on a surface representing the Gibbs free energy as a function of p and T. The enthalpy and entropy may be represented similarly as surfaces in the p-T-H and p-T-S space, respectively. Non-equilibrium states cannot be represented in this way, because they are situated off the surface of the equation of state. However, one can imagine, for a given T and p, a space spanned by three axes representing the deviations, ΔV and ΔH, of the volume and enthalpy from their equilibrium values and the Gibbs energy. In this apace a non-equilibrium state is represented by any point in the ΔV-ΔH plane other than the origin. The origin represents the equilibrium Gibbs energy of the liquid at p and T. The Gibbs energy surface is at a minimum at the origin. It is important to distinguish the surfaces representing the Gibbs energy (or any other equilibrium thermodynamic quantities) as a function of p and T and the surface representing the Gibbs energy as a function of

ΔV and ΔH. Any point on the former surface corresponds to an equilibrium state, whereas on the latter only the origin represents one. Relaxation of a liquid to an equilibrium state may be represented as a trajectory approaching the origin in the ΔV-ΔH plane. It is first necessary to determined the entropy (enthalpy) and volume as functions of temperature and pressure to construct the Gibbs free energy surface both in the glassy and liquid states. It is then required to determine the enthalpy and volume during the relaxation as a function of time to obtain the relaxation path on the Gibbs energy surface. This type of experiment has not been performed before because of the difficulty of the experimental techniques.

1-3 The Purpose of the Present Study

The present study has two purposes roughly divided. The first one is to examine the validity of the entropy theory (especially the Adam-Gibbs theory [7]) and free volume theory. The second is to investigate the structural relaxation in glassy state through the comparison between the enthalpy and volume relaxations.

The following three experiments were performed to attain the first purpose. In Chapter 2, the heat capacity of 3-bromopentane was measured at atmospheric pressure. The Adam-Gibbs theory was examined over a wide temperature range using the configurational entropy and the dielectric relaxation time reported before. In Chapter 3, the heat capacities of 3-methylpentane and 1-propanol

were measured under high pressure. Two entropy theories were examined through the pressure dependence of T_g and the configurational entropy under high pressure. In Chapter 5, the gaps of heat capacity, thermal expansivity, and isothermal compressibility at T_g were determined in polystyrene under pressure. Using these data and the pressure dependence of T_g, the entropy theory and the free volume theory were examined. The Prigogine-Defay ratio was also discussed.

For the second purpose, the simultaneous measurement of enthalpy and volume is essential since the same non-equilibrium state can not be realized in separate experiments. In Chapter 4, construction of a new type of adiabatic calorimeter is desired which enabled simultaneous measurement of enthalpy and volume under high pressure. Chapters 5 and 6 describe an investigation of the structural relaxation of glassy polystyrene by the use of this apparatus.

References to Chapter 1

[1] W. Kauzmann, Chem. Rev. 43 (1948) 219.

[2] K.L. Ngai, E. Riande and G.B. Wright, eds., "Relaxations in Complex Systems", J. Non-Cryst. Solids 172-174 (1994); K.L. Ngai, and G.B. Wright, eds., "Relaxations in Complex Systems", J. Non-Cryst. Solids 131-133 (1991).

[3] J.H. Gibbs and E.A. DiMarzio, J. Chem. Phys. 28 (1958) 373.

[4] E.A. DiMarzio and J.H. Gibbs, J. Chem. Phys. 28 (1958) 807.

[5] M. Goldstein, J. Chem. Phys. 39 (1963) 3369.

[6] A.B. Bestul and S.S. Chang, J. Chem. Phys. 40 (1964) 3731.

[7] G. Adam and J.H. Gibbs, J. Chem. Phys. 43 (1965) 139.

[8] A.K. Doolittle, J. Appl. Phys. 22 (1951) 1471.

[9] M.H. Cohen and D.Turnbull, J. Chem. Phys. 31 (1959) 1164.

[10] D. Turnbull and M.H. Cohen, J. Chem. Phys. 34 (1961) 120.

[11] T. Nose, Polymer J. 2 (1971) 445.

[12] C.A. Angell, E. Williams, K.J. Rao and J.C. Tucker, J. Phys. Chem. 81 (1977) 238.

[13] R.O. Davies and G.O. Jones, Adv. Phys. 2 (1953) 370.

[14] J.M. O'Reilly, J. Polym. Sci. 57 (1962) 429.

[15] M. Goldstein, J. Phys. Chem. 77 (1973) 667.

[16] M. Naoki and T. Nose, J. Polym. Sci. Polym. Phys. Ed. 13 (1975) 1747.

[17] T. Atake and C.A. Angell, J. Phys. Chem. 83 (1979) 3218.

Chapter 2

Heat Capacity of 3-Bromopentane: Correlation between the Structural Relaxation Time and Configurational Entropy

2-1 Introduction

One of the important properties of the structural relaxation of the undercooled liquid is the non-Arrhenius temperature dependence of the structural relaxation time τ. This is prominent especially in the slow relaxation regime as discussed in Chapter 1 [1,2]. A number of theoretical models [1-6], including the Adam-Gibbs (AG) theory [7], have been proposed to explain this feature.

The AG theory is based on the existence of cooperatively rearranging assemblies of molecules, which is called "domains" in this thesis. The most important prediction of this theory is that τ is related to the molar configurational entropy S_C and temperature T, by the equation

$$\tau = \tau_0 \exp(\Delta\mu s_C^*/kTS_C). \qquad (2\text{-}1)$$

Here, τ_0 is the frequency factor, $\Delta\mu$ the molar activation free energy, k the Boltzmann constant and s_C^* the configurational entropy of a domain. Eq. 2-1 implies that τ diverges at the Kauzmann temperature T_0 where S_C vanishes [8]. The number of the molecules in a domain, z, is related to S_C by the equation

$$z = s_C^* N_a / S_C, \qquad (2\text{-}2)$$

where N_a is the Avogadro constant. According to eq. 2-2, S_c tends to $s_c^* N_a$ in the high-temperature limit where z tends to 1.

A number of studies [9-17] have been performed to test the validity of the AG theory. It is now believed that the AG theory gives a qualitatively adequate description of the fragility of undercooled liquids [9]. Among the predictions by the AG theory, one relevant to the present study is that the fragile liquids exhibit large heat capacity jump at T_g, corresponding to strong temperature dependence of S_c [9,11]. The quantitative approaches were also successful for polymers [18]. For molecular liquids, however, the situation is less conclusive, even though both experimental and theoretical studies have been abundantly devoted to the dynamics of molecular systems.

Complexity of the structural relaxation in molecular liquids arises from, among other things, the existence of the overall and intramolecular rotations. For polymers, only the latter need be considered. A single glass transition is observed in most of the molecular liquids in spite of the difference in the activation energy between the intramolecular and overall rotations. This indicates that two types of the rotation are coupled in the dynamics of the configurational rearrangement. Therefore, s_c^* should be related to the combined number of the intramolecular and intermolecular configurations and be larger than k ln 3 multiplied by the number of C-C bonds. This value is usually assumed in the AG analysis of polymers. Actually, the molar entropy of fusion, which is equal to S_c at the fusion point, is usually much larger than R ln 3 multiplied by the number of C-C bonds. Therefor the

experimental values of s_C^* (= S_C/N_a at $T = \infty$) pertain both to the intra- and intermolecular configurational degrees of freedom. In most of the previous studies on molecular liquids [12-15], however, s_C^* was assumed to be equal to k ln 2. This assumption is invalid since the entropy of fusion alone exceeds this value for practically all the molecular crystals. The s_C^* values must be evaluated experimentally. $\Delta\mu$ should be also associated with the coupled motion of the intramolecular and intermolecular degrees of freedom. For 3-bromopentane, the barrier to the overall molecular rotation is 11.5 kJ mol^{-1} from the dielectric data [19], whereas the barrier to internal rotation is not known. However, for some hydrocarbons, the internal barrier height has been calculated (13-15 kJ mol^{-1} for butane [20]). These inter- and intramolecular barrier heights may be compared with the outcome of the analysis based on the AG theory.

The purpose of the present study is to make a quantitative test for the validity of the AG theory in molecular liquids. The heat capacity of 3-bromopentane was measured with an adiabatic calorimeter to determine the temperature dependence of S_C. This substance was chosen for the experiment because the relaxation time has been determined in a wide frequency interval [19]. The parameter s_C^* was estimated from S_C data at high temperatures. Using the calorimetric data and the temperature dependence of τ reported by Berberian and Cole [19], the validity of the AG theory was demonstrated over the wide temperature and time ranges. The values of $\Delta\mu$ and z obtained by comparison between the theory and experiment were also examined.

2-2 Experimental

Commercial reagent of 3-bromopentane, whose purity was stated to be 97 %, were purchased from Aldrich Chemical Company, Inc. The sample was dehydrated with Molecular Sieves 3A 1/16 (Wako Pure Chemical Industries, Ltd.) and fractionally distilled twice under reduced pressure (ca. 16 kPa) with a concentric type of rectifier HC-5500-F (Shibata Kagakukikai Kogyo Co., Ltd.). The main distillate was degassed and distilled again in vacuo with a home-made vacuum-line. The final purity of the sample was checked by gas chromatography (Perkin-Elmer F21) and no trace of organic impurity was detected. A Karl-Fischer test was also carried out and the amount of water in the sample was found to be sufficiently small (0.03 mol%).

The quantity of the sample loaded in the calorimeter cell was 19.3725 g (0.128255 mol). Helium gas (2.06×10^{-4} mol) was charged into the dead space (4.96 cm^3) of the sample cell to enhance the thermal equilibration between the sample and the cell.

The heat capacity measurement was carried out by an intermittent heating mode with the adiabatic calorimeter described elsewhere [21]. The imprecision of the heat capacity was within 1 % in the temperature region T < 15 K, 0.3 % in 15 K < T < 30 K, and 0.1 % in T > 30 K. The temperature was measured with a Rh-Fe resistance thermometer calibrated on the temperature scale EPT76 (T < 30 K) and IPTS68 (T > 30 K). The heat capacity difference caused by the conversion to the new temperature scale ITS90 [22]

was estimated to be smaller than 0.05 % over the temperature range 7-300 K.

The heat capacities of the sample in the liquid, glassy and crystalline states were determined. A sample in which 99 % of the material was crystalline was formed by annealing the undercooled liquid for 5 days. The contribution from the remaining liquid (1 %) was small enough to be neglected in the following discussion. The heat capacities of the glassy and undercooled liquid states were obtained from the heat capacity of a rapidly cooled liquid sample (cooled at 3-4 K min^{-1}). The sample was 68.8 % crystalline as determined from the heat capacity of the crystalline state, the enthalpy of crystallization, and the enthalpy of fusion. The heat capacities of a fully glassy sample were calculated from those of the mixture by assuming an additivity.

2-3 Results and Discussion

2-3-1 Heat Capacity

Molar heat capacities of the glassy-liquid (open triangles and circles) and crystalline (closed circles) states of 3-bromopentane are summarized in Table 2-1 and plotted in Fig. 2-1. In the glassy-liquid states, a large heat capacity jump ($\Delta C_{p,g}$ = 76.4 J K^{-1} mol^{-1}) due to the glass transition was observed at 107.4 K. Crystallization occurred above the glass transition so that the heat capacity data of the undercooled liquid are missing between 119 and 160 K. In the crystalline state (closed circles), a large

Table 2-1. Molar heat capacity of 3-bromopentane.

T	C_p	T	C_p	T	C_p	T	C_p	T	C_p
K	J K^{-1}mol^{-1}	K	J K^{-1}mol^{-1}	K	J K^{-1}mol^{-1}	K	J K^{-1}mol^{-1}	K	J K^{-1}mol^{-1}
		62.28	59.93			265.60	182.0	40.32	42.13
crystal		63.72	61.04	liquid		267.91	182.5	41.62	43.19
		65.17	62.06			270.25	183.0	42.93	44.13
7.05	1.877	66.62	63.06	160.39	168.8	272.60	183.6	44.25	45.25
7.42	2.180	68.08	64.08	161.99	168.9	274.97	184.2	45.56	46.39
7.83	2.536	69.54	65.11	163.61	168.9	277.35	184.7	46.88	47.45
8.25	2.946	71.01	66.13	165.24	168.9	279.75	185.1	48.21	48.54
8.69	3.391	72.49	67.10	166.90	169.0	282.17	185.8	49.53	49.62
9.18	3.913	73.97	68.12	168.57	169.1	284.61	186.5	50.86	50.67
9.72	4.532	75.46	69.06	170.25	169.1	287.05	186.9	52.19	51.78
10.30	5.219	76.95	70.00	171.96	169.2	289.52	187.6	53.52	52.86
10.89	5.960	78.45	70.99	173.68	169.2	291.99	188.2	54.86	53.84
11.50	6.752	79.96	71.96	175.42	169.3	294.49	188.6	55.65	54.31
12.13	7.584	81.47	72.94	177.18	169.4	297.00	189.4	56.81	55.19
12.76	8.441	82.99	73.88	178.95	169.6	299.53	189.8	58.17	56.13
13.42	9.338	84.52	74.80	180.74	169.7			59.54	57.14
14.11	10.30	86.07	75.75	182.55	169.8			60.91	58.43
14.82	11.30	87.65	76.69	184.37	169.9	glass and liquid		62.29	59.32
15.54	12.33	89.25	77.59	186.21	170.1			63.66	60.37
16.29	13.39	90.85	78.56	188.07	170.2	7.15	3.870	65.09	61.33
17.06	14.49	92.48	79.47	189.95	170.3	7.50	4.355	66.55	62.38
17.85	15.61	94.11	80.38	191.84	170.5	7.88	4.909	68.03	63.44
18.65	16.76	95.76	81.28	193.75	170.7	8.29	5.494	69.52	64.50
19.48	17.92	97.42	82.22	195.67	170.9	8.74	6.119	71.03	65.53
20.33	19.11	99.10	83.13	197.61	171.1	9.24	6.844	72.55	66.61
21.23	20.33	100.79	84.05	199.57	171.2	9.79	7.581	74.09	67.71
22.24	21.70	102.49	84.95	201.65	171.4	10.36	8.379	75.63	68.87
23.31	23.11	104.21	85.89	203.59	171.6	10.95	9.164	77.19	70.04
24.38	24.47	105.94	86.83	205.54	171.9	11.56	10.05	78.77	71.20
25.46	25.80	107.68	87.86	207.51	172.1	12.18	11.00	80.35	72.48
26.60	27.16	109.43	89.07	209.49	172.3	12.83	11.85	81.95	73.67
27.84	28.65	111.19	90.01	211.49	172.6	13.51	12.77	83.56	75.04
29.13	30.21	112.96	90.88	213.50	172.9	14.21	13.72	85.18	76.34
30.39	31.63	114.71	91.73	215.53	173.2	14.93	14.69	86.82	77.66
31.66	32.98	116.51	92.63	217.57	173.5	15.68	15.75	88.46	79.12
33.01	34.48	118.33	93.50	219.63	173.7	16.45	16.80	90.12	80.60
34.37	35.96	120.66	94.60	221.71	174.0	17.23	17.84	91.80	82.13
35.70	37.32	122.78	95.63	223.79	174.3	18.04	18.99	93.48	83.62
37.04	38.66	124.92	96.68	225.90	174.6	18.88	20.09	95.18	85.18
38.40	39.94	127.07	97.76	228.02	175.0	19.73	21.25	96.89	86.96
39.77	41.29	129.23	99.02	230.15	175.3	20.64	22.46	98.62	88.84
41.15	42.53	131.40	100.4	232.30	175.7	21.66	23.73	100.37	91.01
42.53	43.79	133.58	101.6	234.46	176.1	22.74	24.95	102.13	93.77
43.91	45.04	135.78	102.8	236.64	176.5	23.82	26.14	103.90	97.45
45.30	46.28	137.99	104.2	238.83	176.9	24.91	27.37	105.67	104.2
46.70	47.52	140.21	105.6	241.03	177.2	26.06	28.48	107.39	124.7
48.10	48.69	142.44	107.0	243.25	177.6	27.32	29.65	108.97	163.3
49.50	49.85	144.67	108.9	245.48	178.0	28.63	31.14	110.55	164.7
50.90	51.07	146.89	111.5	247.69	178.4	29.93	32.67	112.14	165.0
52.31	52.26	149.11	114.3	249.86	178.8	31.24	33.68	113.74	164.9
53.72	53.38	151.33	117.3	252.06	179.3	32.54	35.34	115.37	164.9
55.14	54.53	153.53	121.9	254.27	179.7	33.84	36.26	117.01	164.8
56.56	55.66	155.70	127.9	256.50	180.2	35.14	37.55	118.67	164.8
57.98	56.76	157.80	138.0	258.75	180.4	36.43	38.74		
59.41	57.84	159.79	156.0	261.01	181.1	37.73	39.97		
60.85	58.87	161.60	189.4	263.29	181.5	39.02	41.09		

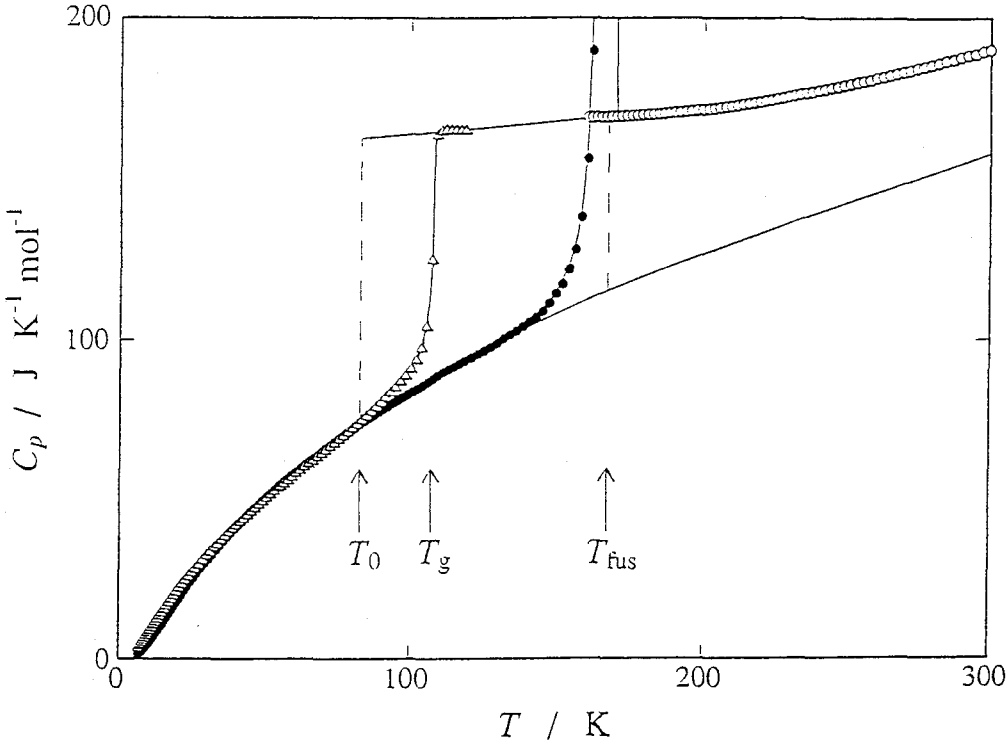

Fig. 2-1. Heat capacities of liquid (open circles), glassy-undercooled liquid (open triangles) and crystalline (closed circles) states of 3-bromopentane. The solid curves represent the extrapolations of the heat capacities used for the determination of the configurational entropy as a function of temperature (see text for the details).

heat capacity peak due to the fusion occurred at 167.3 K. The enthalpy $\Delta_{fus}H$ = 8.398 kJ mol^{-1} and the entropy of fusion $\Delta_{fus}S$ = 50.19 J K^{-1} mol^{-1} were determined by the standard method of adiabatic calorimetry.

To evaluate the configurational entropy as a function of temperature, the heat capacities of both liquid and crystalline states are needed over the whole temperature range above the Kauzmann temperature T_0. The heat capacities of the liquid state in the temperature range 112-119 K and 160-175 K were expressed by a straight line and used for the extrapolation down to T_0 (see the solid line in Fig. 2-1). A model function was fitted to the heat capacities of the crystalline state as described below and used for extrapolation to above T_{fus};

$$C_p = C_{lat} + C_{rot} + C_{vib} + \Delta C_{corr} \qquad (2\text{-}3)$$

where C_{lat}, C_{rot} and C_{vib} are the heat capacities due to the lattice vibration, rotational vibration (libration) and intramolecular vibration, respectively. The last term in eq. 2-3 gives the correction for the difference between C_p and C_V. C_{lat} was approximated by a Debye function and C_{rot} by an Einstein function, each having 3 degrees of freedom. From the Raman and infrared spectroscopic data for 3-bromopentane [23] and the related compounds [24,25], it was found that 3-bromopentane has 10 intramolecular vibrational modes which contribute to C_{vib} in the present temperature range (T < 300 K). C_{vib} was therefore approximated by two Einstein functions having 4 and 6 degrees of freedom. Other combinations of the weights were also possible but

the final result did not change significantly within a reasonable range of the change in the functional form. The C_p-C_V correction term was represented as usual by

$$\Delta C_{corr} = AC_p^2T \qquad (2\text{-}4)$$

where A is a constant and T the temperature. The Debye temperature $\theta_D(3)$ and the Einstein temperatures $\theta_E(3)$, $\theta_E(4)$, $\theta_E(6)$ and the correction coefficient A, where the numbers in the parentheses represent the degrees of freedom, were determined by the least-squares fitting to the experimental heat capacities in the temperature range 7-136 K. The optimum values were $\theta_D(3)$ = 69.6 K, $\theta_E(3)$ = 102.9 K, $\theta_E(4)$ = 209.3 K, $\theta_E(6)$ = 475.9 K and A = 4.79×10^{-6} mol J^{-1}. The fitting was satisfactory as shown by the solid curve in Fig. 2-1. The extrapolations of the liquid and crystalline heat capacities thus calculated were sufficiently accurate for the following discussion.

2-3-2 Configurational Entropy

The temperature dependence of the configurational entropy was calculated by the equation

$$S_c(T) = \Delta_{fus}S - \int_{T}^{T_{fus}} [C_p(l) - C_p(cr)] / T \; dT. \qquad (2\text{-}5)$$

Here, T_{fus} and $\Delta_{fus}S$ are the temperature and entropy of fusion, respectively, and $C_p(l)$ and $C_p(cr)$ are the heat capacities of the liquid and crystalline states, respectively. Fig. 2-2 shows the temperature dependence of the configurational entropy calculated

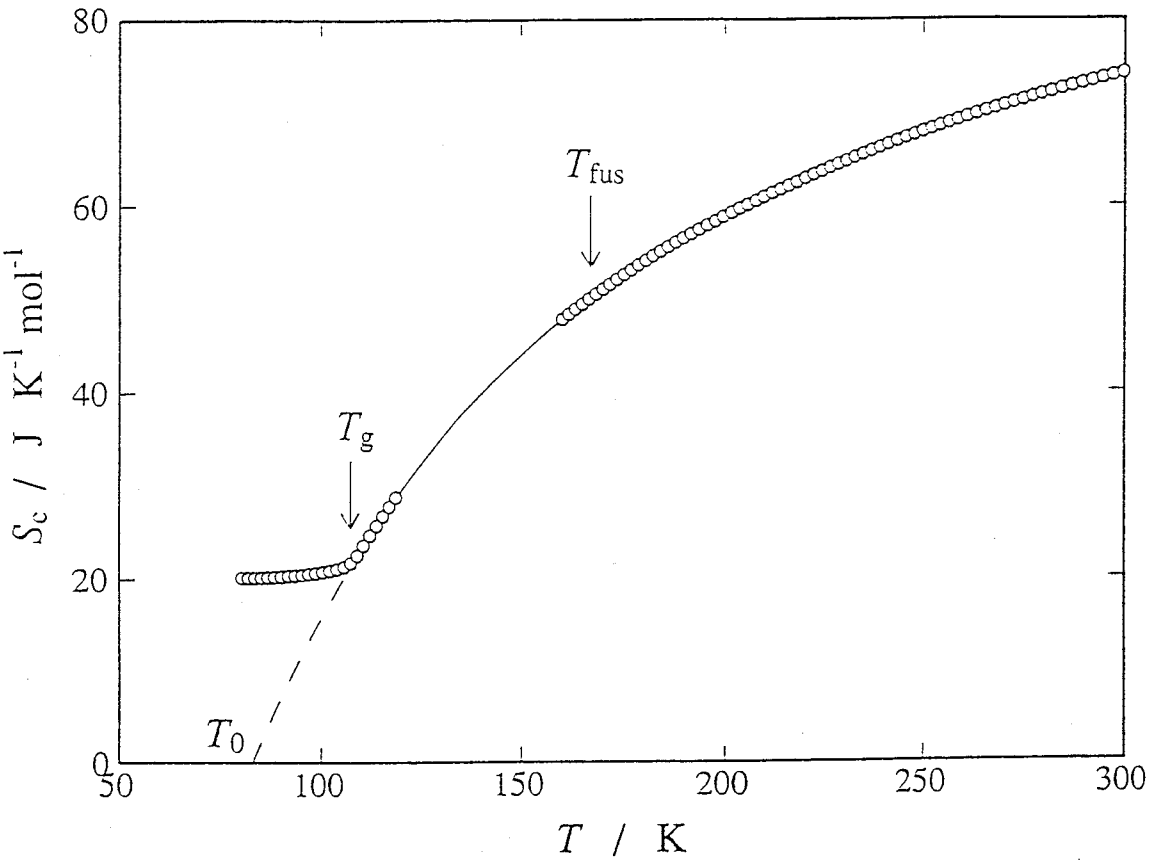

Fig. 2-2. Temperature dependence of the configurational entropy of 3-bromopentane.

by eq. 2-5 and the heat capacity functions described above. T_0 (Kauzmann temperature) was determined to be 82.5 K by extrapolating S_C vs. T curve to $S_C = 0$.

Fig. 2-2 shows that S_C became constant below T_g, corresponding to the freezing of the structure and the resulting residual entropy in the glassy state. At high enough temperature, S_C should approach a constant value $s_C^* N_a$ according to the AG theory. This value was estimated to be 80-100 $JK^{-1}mol^{-1}$ from the S_C vs. T curve. It is noteworthy that $s_C^* N_a$ is much larger than R ln 2 (= 5.76 JK^{-1} mol^{-1}), in agreement with the argument in Section 2-1; i.e., $s_C^* \gg k$ ln 2. It is known from IR spectroscopic study [23] that 3-bromopentane molecule has four conformers. If the energy difference among these conformers is neglected, the entropy due to the intramolecular rotation is R ln 4 (= 11.6 J K^{-1} mol^{-1}). The entropy due to the overall rotation is therefore 70-90 J K^{-1} mol^{-1} (= $s_C^* N_a$ - R ln 4), corresponding to R ln (4000-40000). For the simplest model of an Ising type, the number of the available orientations is 2. The large number (4000-40000) obtained here indicates that the molecules have a large variety of orientations in the disordered environment formed by adjacent molecules.

2-3-3 Examination of the Adam-Gibbs Theory

Fig. 2-3 shows log τ plotted against $(S_C T)^{-1}$ for the equilibrium liquid of 3-bromopentane. The structural relaxation times τ were obtained from the dielectric permittivity data reported by Berberian and Cole [19]. The data points are reproduced very well by a straight line, indicating the validity

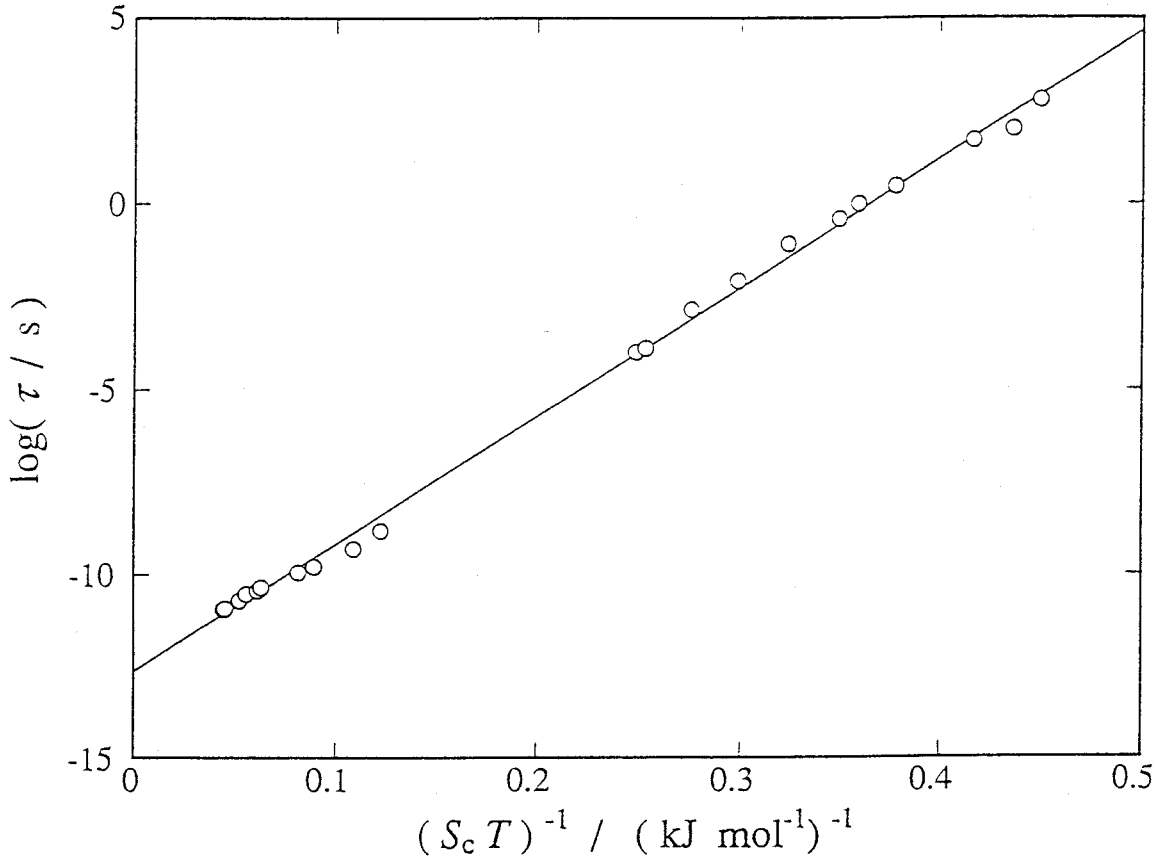

Fig. 2-3. Log τ versus $(S_C T)^{-1}$ plot for the equilibrium liquid of 3-bromopentane. The τ data were taken from the dielectric study [19].

of the AG theory. The AG theory is thus confirmed over wide temperature (107-298 K) and time (10 ps - 1 ks) ranges.

The intercept and slope of the straight line are $\log(\tau_0/s)$ = -12.6 and $\Delta\mu s_c^*/k$ = 79.6 kJ mol^{-1}, respectively. The slope combined with the value of $s_c^* N_a$ estimated above gives $\Delta\mu$ (molar activation free energy) = 6.6-8.2 kJ mol^{-1}, while the intercept gives τ_0 (frequency factor) = 0.25 ps. The frequency factor corresponds to 6.4×10^{11} Hz (= 21 cm^{-1}), a likely value for rotational vibration of a molecule in a condensed phase. The $\Delta\mu$ value obtained from the fit is comparable with but smaller than the intramolecular activation barrier of a hydrocarbon chain (13-15 kJ mol^{-1} for butane [20]). This result is reasonable considering that both the intra- and intermolecular processes are involved in the actual relaxation mechanism and that the latter process will be less hindered for a molecule of this size. It is worth pointing out that the activation energy reported previously, 11.5 kJ mol^{-1}, is comparable with the $\Delta\mu$ value, but it is based on a traditional Arrhenius analysis while the present value was arrived at in an entirely different method involving experimental evaluation of the configurational entropy as a function of the temperature. Thus the frequency and energetic parameters obtained from the present data and the dielectric relaxation times using eq. 2-1 are both of physically reasonable magnitude as a description of the elementary process in a liquid. This, in turn, supports the AG theory as a theory of the relaxation time in the liquid state.

Fig. 2-4 shows the temperature dependence of z (the number of molecules in a cooperative domain). These values were calculated from S_C and $s_C^* N_a$ (= 80 J K^{-1} mol^{-1}) by using eq. 2-2. The solid and dashed curves denote z of the equilibrium liquids above and below T_g (hypothetical), respectively. As shown in Fig. 2-4, z of the equilibrium liquid approaches 1 at high temperatures as it should and diverges at T_0. The magnitude of z is ~ 4 at T_g. This result means that a cooperative domain contains at most first nearest-neighbor molecules even at T_g. This is consistent with the fact that domain structure has never been found in glassy states by small angle diffraction experiments.

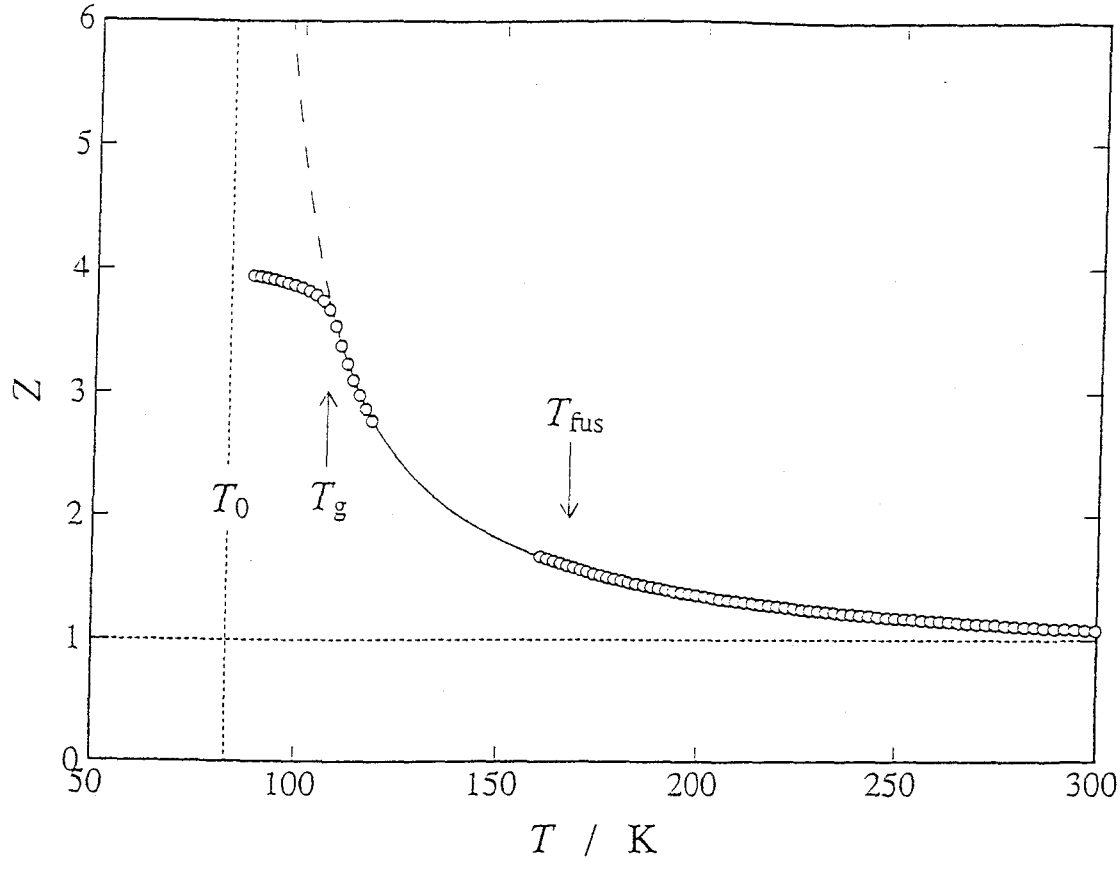

Fig. 2-4. Temperature dependence of the number (z) of molecules in a cooperative domain. The solid and dashed curves represent z of the equilibrium liquids above and below T_g (hypothetical), respectively.

References to Chapter 2

[1] Relaxations in Complex Systems; K.L. Ngai, E. Riande and G. B. Wright , Eds.; J. Non-Cryst. Solids 172-174 (1994).; Relaxations in Complex Systems; K. L. Ngai and G. B. Wright, Eds.; ibid 131-133 (1991).

[2] C. A. Angell, Relaxations in Complex Systems; K. L. Ngai and G. B. Wright, Eds.; National Technical Information Service, US Department of Commerce, Springfield, VA, (1985); p 1.

[3] Liquids, Freezing and Glass Transition; J. P. Hansen, D. Levesque and J. Zinn-Justin Eds.; North-Holland; Amsterdam, (1989).

[4] G. H. Fredrickson, Ann. Rev. Phys. Chem. 39 (1988) 149.

[5] M. I. Klinger, Phys. Rep. 165 (1988) 275.

[6] S. Brawer, Relaxation in Viscous Liquids and Glasses; Am. Ceram. Soc. Inc.: Columbus, (1985).

[7] G. Adam and J. H. Gibbs, J. Chem. Phys. 43 (1965) 139.

[8] W. Kauzmann, Chem. Rev. 43 (1948) 219.

[9] C. A. Angell, J. Non-Cryst. Solids 131-133 (1991) 13.

[10] C. A. Angell and W. Sichina, Ann. New York Acad. Sci. 279 (1976) 53.

[11] C. T. Moynihan and S. J. Cantor, Chem. Phys. 48 (1968) 115.

[12] R. J. Greet and D. J. Turnbull, Chem. Phys. 47 (1967) 2185.

[13] J. H. Magill, J. Chem. Phys. 47 (1967) 2802.

[14] A. A. Miller, J. Chem. Phys. 49 (1968) 1393.

[15] W. T. Laughlin and D. R. Uhlmann, J. Phys. Chem. 76 (1972) 2317.

[16], M. Naoki and T. Nose, J. Polym. Sci. Polym. Phys. Ed. 13 (1975) 1747.

[17] S. Takahara, O. Yamamuro and H. Suga, J. Non-Cryst. Solids 171 (1994) 259.

[18] S. Matsuoka and X. Quan, J. Non-Cryst. Solids 131-133 (1991) 293.

[19] J. G. Berberian and R. H. Cole, J. Chem. Phys. 84 (1986) 6921.

[20] A. Abe, R. L. Jernigan and P. J. Flory, J. Am. Chem. Soc. 88 (1966) 631.

[21] O. Yamamuro, M. Oguni, T. Matsuo and H. Suga, Bull. Chem. Soc. Jpn. 60 (1987) 1269.

[22] R. N. Goldberg and R. D. Weir, Pure Appl. Chem. 64 (1992) 1545.

[23] G. A. Crowder and M. Iwunze, Can. J. Chem. 55 (1977) 3413.

[24] C. G. Opaskar and S. Krimm, Spectrochim. Acta 23A (1967) 2261.

[25] J. H. Schachtschneider and R. G. Snyder, Spectrochim. Acta 19 (1963) 117.

Chapter 3

Heat Capacities of 3-Methylpentane and 1-Propanol under High Pressure: Pressure Dependence of the Configurational Entropy and Glass Transition Temperature

3-1 Introduction

The non-Arrhenius temperature dependence of the structural relaxation time is one of the important properties of the structural relaxation in the undercooled liquid [1]. In 1950s, two important theories were proposed to explain this property from the thermodynamic point of view. They are called the "entropy theory" [2-6] and the "free-volume theory" [7-9]. A number of experiments have been performed to investigate their validity but no clear conclusion has been obtained to date.

The entropy theory states that the relaxation time, τ, for the configurational change in the undercooled liquid is determined by the configurational entropy. Bestul and Chang [5] proposed a relation for τ

$$\tau = A \exp (B / S_C), \qquad (3\text{-}1)$$

where A and B are temperature- and pressure-independent constants, and S_C is the configurational entropy defined as the entropy component of the liquid other than those arising from the intra- and intermolecular vibrations. The value of S_C can be obtained

from the entropy of fusion and the heat capacity difference between the glass and undercooled liquid. The configurational entropy thus determined vanishes at a temperature below the glass transition temperature, T_g. This predicts divergence of τ and is consistent with experimental observation represented by the Vogel-Tammann-Fulcher (VTF) equation [10,11]. The temperature where S_c tends to zero is called the Kauzmann temperature [12].

Adam and Gibbs [6] proposed a .more advanced form of the entropy theory based on a model. In their theory,

$$\tau = A \exp (B / TS_c), \qquad (3\text{-}2)$$

Here, A is a pressure- and temperature-independent constant. B contains a term of activation free energy and, in general, depends on both pressure and temperature. In the undercooled regime, however, pressure- and temperature-dependence of B are usually very small comparing with those of S_c and was neglected in the following discussion.

In the free volume theory [7], τ is related to the free volume V_f by the equation

$$\tau = A \exp (B / V_f), \qquad (3\text{-}3)$$

where A and B are constants independent of T and P. The free volume is defined as the space through which the configurational change of the liquid molecules can take place. It roughly corresponds to the volume difference between the liquid and the

crystal. The free volume also tends to zero at a temperature below T_g.

The main subject of this chapter is to examine these theories through the pressure dependence of T_g. A direct approach for this examination is to determine T_g at various pressures where S_c and V_f can be obtained experimentally. If eq. 3-1, 3-2, or 3-3 is valid, the corresponding thermodynamic quantity S_c, TS_c, or V_f should be constant at T_g. However, the measurements of the absolute values of S_c and V_f, especially the former, are technically very difficult at high pressures. Many reports on the measurements of volume at high pressures have been published [13-16], while the relation between τ and V_f has never been discussed. The entropy determination under pressure has never been reported.

Another approach, though indirect, is to investigate the gradient of T_g curve on the P-T plane (dT_g/dP), which is usually constant in the low pressure region. The slope dT_g/dP can be related to the volume, V, configurational entropy, S_c, heat capacity gap, ΔC_p, thermal expansivity gap, $\Delta\alpha$, and isothermal compressibility gap, $\Delta\kappa$, at T_g under atmospheric pressure in different ways depending on the prediction of the different theories:

$$dT_g/dP = (\partial T/\partial P)_{Sc} = TV\,\Delta\alpha/\Delta C_p, \tag{3-4}$$

if eq. 3-1 is valid [4];

$$dT_g/dP = (\partial T/\partial P)_{TSc} = TV\,\Delta\alpha/(\Delta C_p + S_c), \tag{3-5}$$

if eq. 3-2 is valid [17,18];

$$dT_g/dP = (\partial T/\partial P)_{V_f} = \Delta\varkappa/\Delta\alpha \ , \qquad (3\text{-}6)$$

if eq. 3-3 is valid [4]. Here, the temperature and pressure dependences of A and B are assumed to be negligible.

Since the measurements of V, S_C, ΔC_p, $\Delta\alpha$, and $\Delta\varkappa$ under atmospheric pressure are much easier than those of S_C and V_f under pressure, most of the previous studies have been devoted to the check of the validities of eqs. 3-4 - 3-6. For many substances including 1-propanol [4,19-21], it has been pointed out that eq. 3-4 is more appropriate than eq. 3-6 and the relation

$$dT_g/dP \approx TV\,\Delta\alpha/\Delta C_p < \Delta\varkappa/\Delta\alpha \qquad (3\text{-}7)$$

holds in place of eq. 3-6. These observations indicate that the glass transition occurs at an iso-configurational-entropy state rather than an iso-free-volume state. Several authors [17,18,22,23] have discussed some quantitative test of eq. 3-5, but any definite conclusions have not been reached as to whether the glass transition point corresponds to iso-S_C or iso-TS_C condition.

The method using dT_g/dP data has several disadvantages. This method requires many thermodynamic parameters which should be determined in separate experiments and the accuracy of ΔC_p, $\Delta\alpha$ and $\Delta\varkappa$ are usually not high because they are derivatives of measured

quantities H and V. The experimental uncertainty involved in each quantity is accumulated in the application of eqs. 3-4 - 3-6 and this makes the test for the validity ambiguous. Uncertainty involved in the right-hand side of eqs. 3-4 - 3-6 is 10-20 % in the most reliable cases. This method becomes useless when dT_g/dP is strongly pressure-dependent in the low pressure region.

In the present study, the direct approach have been taken. The heat capacities of 1-propanol and 3-methylpentane were measured in the pressure range 0-200 MPa using an adiabatic high-pressure calorimeter to directly determine S_C under pressure. This method makes it possible to examine Eqs. 3.1 and 3.2 more clearly. The method based on eqs. 3-4 and 3-5, using newly obtained (dT_g/dP), ΔC_p, and S_C values, was useless because of the lack of the reliable values of $\Delta\alpha$ for both samples. We also determined the pressure dependence of the Kauzmann temperature T_0.

Both 1-propanol and 3-methylpentane are good glass-forming materials. At the same time they crystallize upon long annealing at temperatures above T_g. This property is very important because all the quantities including the entropy of fusion as well as the heat capacities of glass, undercooled liquid, and crystal are required for the determination of S_C as a function of temperature. The heat capacity of 1-propanol has already been measured at atmospheric pressure [24], and that of 3-methylpentane at atmospheric pressure [25,26] and at 108 MPa (for liquid state) [27]. The pressure dependence of T_g of 1-propanol has been estimated by a high-pressure dielectric measurement [28].

3-2 Experimental

3-2-1 Samples

Commercial reagents of 1-propanol and 3-methylpentane, which were claimed to be better than 99 mol% pure, were purchased from Tokyo Kasei Kogyo Co. Ltd. They were purified by the fractional distillation with a concentric type of rectifier HC-5500-F (Shibata Kagakukikai Kogyo Co. Ltd.). The distillate was carefully degassed and dehydrated with Molecular Sieves 3A 1/16 (Wako Pure Chemical Industries, Ltd.). The final product was distilled in vacuo with a home-made vacuum-line. The purities of the samples were investigated by a gas chromatograph (Perkin-Elmer F21). No trace of organic impurity was detected in either sample. A Karl-Fischer test was carried out for 1-propanol which is quite hygroscopic. The amount of water found in the calorimetric sample was determined to be 0.040 mol%. The quantity of the sample loaded in the calorimeter cell was 16.160 g (0.26889 mol) for 1-propanol and 12.851 g (0.14912 mol) for 3-methylpentane.

3-2-2 Heat Capacity Measurement

The heat capacity measurement was carried out by an intermittent heating mode with the adiabatic high-pressure calorimeter described elsewhere [29]. The heat capacities of the liquid, glassy and crystalline 1-propanol were measured in the temperature range 50-180 K at 0.1 MPa, 108.4 MPa, and 198.6 MPa. Those of 3-methylpentane were also measured in the temperature range 50-130 K at 0.1, 108.1 and 198.5 MPa. The glassy samples were formed by rapid cooling of the liquid sample under a prescribed constant

pressure. The cooling rates around T_g were 0.2-0.4 K min^{-1} for 1-propanol and 0.5-0.7 K min^{-1} for 3-methylpentane.

The temperature step of single heat-capacity determination was 1.0-2.0 K for the heating period of 200-1000 s. The time required for attaining the thermal equilibrium after each energy input increased from about 10 min at the lowest temperature to about 30 min at the highest temperature. The equilibration time was much longer than usual (5-10 min), reflecting very poor thermal conductivity of the present materials. The precision of the heat capacity was 0.5 % around the lowest temperatures and 1 % around the highest temperatures under high pressures.

As the sample temperature was increased from below T_g, spontaneous temperature drift of the sample was observed indicating that the structural relaxation rate became appreciable. The average drift rate around T_g was determined for a 10 min periods between 20 and 30 min after each energy input. The heat capacity datum was calculated by employing the temperatures extrapolated to the mid-point of each energizing period. Therefore, the quantity corresponded to "instantaneous" or "iso-configurational" heat capacity, which represents the vibrational heat capacity of the sample in glassy state.

In the present experimental set-up the helium gas is in contact with the sample in the sample cell. However, the amount of the dissolved helium was considered to be small enough to be neglected in this study. This is because the heat capacity of 3-methylpentane at 108 MPa agreed with the reliable literature data [27], which were determined by using 3-methylpentane as pressure-

transmitting medium. Also the heat capacity value of liquid 3-methylpentane obtained just after pressurization to 198.5 MPa was the same as for more than 1 month.

3-2-3 Calculation of Molar Heat Capacity under High Pressure

The molar heat capacity of the sample, $C_{p,m}$, was calculated from the equation [29]

$$C_{p,m} = [\ dQ/dT\ - C_e - C_H\ (\ V_e - nV_m\ )\ ]\ /\ n, \qquad (3\text{-}8)$$

where dQ/dT is the gross heat capacity determined experimentally, C_e is the heat capacity of the empty cell, C_H is the heat capacity of helium gas per unit volume, V_e is the inner volume of the empty cell, V_m is the molar volume of the sample, and n is the amount of the sample. The quantity C_e was measured with the present calorimeter at 0.1 MPa. Its pressure dependence (about 0.1 %) was neglected. The numerical value of C_H at 198 MPa was also measured with the present calorimeter and C_H at 108 MPa was estimated by extrapolation of the data obtained in the pressure range 0-100 MPa [32]. The accuracy of C_H was estimated to be ± 0.5 %. The quantity V_e at room temperature was measured by a gravimetric method with degassed water and its temperature and pressure dependences were estimated by using the thermal expansion [33] and mechanical data [34] of the copper-beryllium alloy. The uncertainty in the estimation of V_e at 198 MPa was < 0.2 %. The magnitude V_m of liquid 1-propanol was obtained by extrapolation of the literature values for the pressure range 0-100 MPa and

temperature range 130-300 K [28]. The value of V_m for liquid 3-methylpentane at 198 MPa was estimated by using the data measured in the pressure range 0-108 MPa and 110-300 K [27]. The uncertainty involved in the calculations of the data at 108 MPa and 198 MPa was about ±0.5 % and 2 %, respectively. For both samples, V_m of crystalline state was estimated using the present dT_{fus}/dP and $\Delta_{fus}S$ data in conjunction with the Clausius-Clapeyron equation and thermal expansivity of 1×10^{-4} K^{-1} which is typical for organic solids at atmospheric pressure. The magnitude of V_m for glassy state, which is continuous at T_g, was also estimated by using the thermal expansion of the crystalline state. The probable error in V_m is estimated to be ±1.5 % at 108 MPa and ±3 % at 198 MPa. Consequently, the accuracy of heat capacity determined in the present experiment was about ±0.5 % at 0.1 MPa, ±1 % (liquid) and ±4 % (glass and crystal) at 108 MPa, and ±2 % (liquid) and ±6 % (glass and crystal) at 198 MPa.

3-3 Results and Discussion

3-3-1 Heat Capacity

Tables 3-1 and 3-2 collect the molar heat capacities of 1-propanol and 3-methylpentane, respectively, as a function of temperature in their glassy, liquid, and crystalline states under the three pressures. The data for the glassy and liquid states are plotted in Fig. 3-1 for both substances. The heat capacity curves of 3-methylpentane are shifted by 30 $JK^{-1}mol^{-1}$ for the sake

Table 3-1. Heat capacities of 1-propanol.

T / K	C_p / J K^{-1}mol^{-1}	T / K	C_p / J K^{-1}mol^{-1}	T / K	C_p / J K^{-1}mol^{-1}	T / K	C_p / J K^{-1}mol^{-1}	T / K	C_p / J K^{-1}mol^{-1}	T / K	C_p / J K^{-1}mol^{-1}	T / K	C_p / J K^{-1}mol^{-1}
		133.65	69.30	149.62	106.4	114.53	61.44	110.57	110.4	89.46	51.39	67.40	46.39
0.1 MPa		135.29	70.18	151.25	106.5	116.02	62.73	111.97	110.3	90.74	51.92	68.62	47.02
		136.93	71.00	152.89	106.6	117.52	62.75	113.37	110.0	92.04	52.37	69.85	47.83
crystal		138.59	71.96	154.54	106.8	119.04	63.47	114.79	109.5	93.35	52.92	71.09	48.57
		140.25	72.88	156.21	106.8	120.56	63.84	116.22	109.2	94.66	53.53	72.34	49.20
54.08	33.77	141.93	73.77	157.68	107.1	122.10	64.38	150.09	108.2	95.99	54.07	73.59	49.97
55.09	34.16	143.62	74.89	159.38	107.2	123.64	65.07	151.62	107.5	97.33	54.52	74.85	50.68
56.09	34.87			161.10	107.2	125.20	65.69	153.16	108.7	98.68	55.05	76.12	51.35
57.10	35.49	glass and liquid		162.84	107.6	126.76	65.83	154.71	108.0	100.03	55.42	77.39	52.07
58.14	36.01			164.58	107.6	128.34	66.66	156.27	108.4	101.40	55.93	78.68	52.64
59.19	36.71	60.27	40.10	166.34	107.9	129.93	67.54	157.84	108.1	102.78	56.38	79.97	53.26
61.30	37.79	61.39	40.83	168.11	108.1	131.53	67.83	159.41	108.5	104.17	56.97	81.27	54.00
62.40	38.31	62.52	41.55	169.89	108.5	133.14	68.03	161.00	108.7	105.57	57.51	82.58	54.70
63.51	38.90	63.65	42.27			134.76	69.41	162.60	108.4	106.98	58.05	83.89	55.55
64.63	39.43	64.82	43.05			136.39	69.39	164.21	108.8	108.40	58.58	85.22	56.14
65.77	40.00	66.06	43.84	108.4 MPa		138.03	70.04	165.82	108.6	109.84	58.90	86.55	56.93
66.91	40.70	67.33	44.76			139.68	71.05	167.45	109.1	111.28	59.62	87.89	57.64
68.07	41.37	68.61	45.61	crystal		141.35	71.80	169.09	109.6	112.73	60.13	89.24	58.48
69.24	41.91	69.90	46.40			143.02	71.79	170.73	109.7	114.39	60.55	90.60	59.16
70.42	42.41	71.19	47.23	59.34	39.90	144.70	71.48	172.39	109.2	115.87	61.20	91.96	59.78
71.61	42.89	72.49	48.03	60.34	40.65	146.34	72.43	174.05	109.2	117.35	61.63	93.34	60.51
72.81	43.46	73.80	48.75	61.35	41.17	147.99	73.03	175.73	109.3	118.85	62.26	94.72	61.38
74.02	44.01	75.11	49.60	62.37	41.37	149.65	72.58	177.41	109.9	120.35	62.75	96.11	62.09
75.24	44.52	76.42	50.44	63.41	42.12	151.33	74.07	179.10	109.6	121.87	63.15	97.51	63.07
76.47	45.10	77.74	51.29	64.47	42.56	153.01	75.23	180.81	109.4	123.39	63.79	98.92	64.00
77.71	45.65	79.07	52.12	65.54	43.05					124.93	64.19	100.34	64.84
78.96	46.23	80.41	53.02	65.54	43.06	glass and liquid				126.48	64.74	101.77	65.81
80.22	46.76	81.75	53.98	66.62	43.51			198.6 MPa		128.04	65.41	103.20	67.13
81.49	47.39	83.10	54.95	67.72	44.01	64.86	46.95			129.61	66.06	104.65	68.77
82.77	47.95	84.45	56.01	68.83	44.55	65.94	47.39	crystal		131.19	66.63	106.11	70.69
84.06	48.57	85.82	57.13	69.95	45.02	67.05	48.09			132.78	67.04	107.57	73.60
85.36	49.07	87.19	58.36	71.09	45.64	68.17	48.70	52.74	32.89	134.38	67.40	109.03	79.16
86.66	49.65	88.56	59.68	72.24	46.10	69.30	49.38	53.66	33.37	135.99	67.73	110.47	92.47
87.98	50.26	89.95	60.91	73.39	46.48	70.45	49.95	54.60	34.05	137.62	68.61	111.88	111.5
89.31	50.73	91.34	63.03	74.56	47.07	71.60	50.62	55.55	34.73	139.25	69.13	113.31	111.0
90.64	51.31	92.74	65.29	75.74	47.43	72.77	51.31	56.53	35.23	140.90	69.91	114.75	111.3
91.99	51.74	94.15	68.09	76.94	48.06	73.94	51.86	57.53	35.88	142.55	70.52	116.20	111.6
93.35	52.31	95.22	70.38	78.14	48.53	75.13	52.52	58.54	36.45	144.22	71.14	117.66	111.7
94.71	52.91	95.94	72.61	79.35	49.26	76.33	53.16	59.57	36.95	145.90	71.53	119.13	111.6
96.09	53.46	96.68	76.41	80.58	49.51	77.54	53.74	60.61	37.48	147.59	72.32	120.61	111.5
97.47	54.00	97.42	83.48	81.81	50.17	78.76	54.10	61.66	38.11	149.29	72.81	122.11	111.4
98.86	54.63	98.50	106.0	83.06	50.38	79.99	54.87	62.73	38.77	151.00	73.51	123.61	111.2
100.27	55.13	100.45	107.3	84.31	51.15	81.22	55.66	63.82	39.29	152.73	74.26	125.13	111.0
101.68	55.66	101.80	107.3	85.58	51.05	82.47	56.36	64.91	39.81	154.46	74.96	126.66	111.2
103.10	56.23	103.17	107.2	86.85	52.40	83.73	56.94	66.02	40.66	156.20	75.70	128.20	110.8
104.54	56.84	104.54	107.0	88.14	52.02	85.00	57.50	67.12	41.05	160.94	78.02	158.21	110.5
105.98	57.39	105.93	106.9	89.44	52.78	86.27	58.23	68.21	41.63	162.71	79.15	159.57	110.6
107.43	58.05	107.33	106.7	90.74	53.73	87.56	59.05	69.29	42.15			160.94	110.5
108.89	58.61	108.74	106.6	92.06	53.56	88.86	59.71	70.38	42.63	glass and liquid		162.32	110.7
110.36	59.27	110.16	106.5	93.39	54.07	90.16	60.43	71.48	43.12			163.72	110.9
111.85	60.01	111.60	106.4	94.73	55.31	91.48	61.14	72.60	43.84	52.23	37.11	165.13	110.9
113.34	60.43	113.04	106.3	96.07	55.28	92.81	62.13	73.73	44.53	52.89	37.59	166.56	111.0
114.84	61.03	114.50	106.3	97.43	55.63	94.14	62.94	74.87	44.83	53.85	38.14	168.00	111.2
116.35	61.92	115.97	106.2	98.80	56.62	95.49	63.84	76.03	45.43	54.87	38.86	169.46	111.2
117.87	62.35	117.45	106.2	100.18	56.26	96.85	64.47	77.19	45.96	55.91	39.68	170.93	111.4
119.41	62.98	118.94	106.1	101.57	57.48	98.21	66.42	78.37	46.53	56.98	40.20	172.41	111.6
120.95	63.73	120.44	106.0	102.97	57.77	99.58	67.67	79.56	47.33	58.08	40.90	173.91	111.7
122.50	64.34	121.96	106.0	104.37	57.85	100.97	68.71	80.76	47.65	59.20	41.57	175.42	111.9
124.06	65.04	140.11	105.9	105.79	58.88	102.36	72.28	81.97	48.15	60.32	42.13	176.94	111.6
125.64	65.71	141.66	106.0	107.22	58.75	103.76	76.67	83.19	48.72	61.46	42.84	178.48	111.6
127.22	66.42	143.23	105.9	108.66	59.86	105.13	89.45	84.42	49.12	62.61	43.57		
128.81	67.09	144.81	106.0	110.11	60.40	106.47	110.9	85.67	49.58	63.78	44.14		
130.42	67.79	146.40	106.1	111.57	60.53	107.82	110.2	86.92	50.35	64.98	44.95		
132.03	68.58	148.00	106.2	113.05	61.72	109.19	110.2	88.18	50.79	66.19	45.69		

Table 3-2. Heat capacities of 3-methylpentane.

T / K	C_p / J K^{-1}mol^{-1}	T / K	C_p / J K^{-1}mol^{-1}	T / K	C_p / J K^{-1}mol^{-1}	T / K	C_p / J K^{-1}mol^{-1}	T / K	C_p / J K^{-1}mol^{-1}	T / K	C_p / J K^{-1}mol^{-1}	T / K	C_p / J K^{-1}mol^{-1}
		58.15	56.17	107.19	143.6	92.81	77.30	73.88	69.84	128.32	148.0	86.24	79.31
0.1 MPa		59.23	57.17	108.57	143.4	94.14	78.84	75.14	71.66	129.89	149.1	87.57	81.77
		60.32	58.01	109.97	144.4	95.48	78.55	76.41	72.72			88.91	84.97
glass and liquid		61.40	58.87	111.37	143.6	96.83	80.65	77.69	73.95			90.26	89.09
		63.56	60.92	112.78	143.3	98.19	81.21	78.98	75.90	198.5 MPa		91.30	92.08
23.29	20.48	64.65	61.77	114.20	143.5	99.56	81.84	80.28	77.72			92.05	99.22
23.95	21.37	65.76	62.90	115.63	144.5	100.94	82.01	81.59	79.80	glass and liquid		93.08	123.4
24.67	22.32	66.87	64.27	117.07	145.1	102.33	82.89	82.91	83.42			94.37	144.6
25.47	23.35	67.99	65.55	118.51	144.7	103.74	84.66	84.23	88.94	48.81	46.52	95.68	145.6
26.34	24.40	69.13	66.81			105.15	85.87	85.13	94.51	49.76	47.35	97.00	145.2
27.27	25.52	70.27	68.23			106.57	85.06	85.75	105.9	50.76	48.19	98.34	145.8
28.22	26.64	71.42	70.14	108.1 MPa		108.01	86.56	86.76	141.5	51.77	49.07	99.68	146.0
29.13	27.72	72.58	71.84			109.45	88.28	88.03	144.7	52.80	49.93	101.04	145.6
30.07	28.88	73.75	74.29	crystal		110.91	89.22	89.31	143.8	53.85	50.91	102.41	146.2
31.04	29.94	74.93	77.91			112.37	90.64	90.61	143.6	54.91	51.76	103.79	146.4
31.96	30.99	76.11	82.97	61.31	59.37	113.85	91.80	91.91	144.2	55.98	52.70	105.19	145.7
32.92	32.02	77.28	96.17	62.49	60.27			93.24	143.6	57.07	53.51	106.59	146.6
33.90	33.17	78.40	133.5	63.67	61.02	glass and liquid		94.56	144.2	58.17	54.43	108.00	146.2
34.90	34.22	79.52	139.5	64.87	61.59			95.90	143.8	59.28	55.21	109.43	146.3
35.93	35.28	80.65	140.7	66.07	62.57	48.68	52.15	97.26	144.2	60.40	56.03	110.87	147.4
36.95	36.37	81.79	140.8	67.29	63.45	49.68	52.99	98.62	143.6	61.54	57.17	112.31	147.6
37.96	37.47	82.95	141.0	68.51	64.01	50.71	53.79	99.99	144.5	62.68	57.82	113.77	147.8
38.96	38.47	84.11	140.9	69.74	64.71	51.75	54.58	101.38	144.6	63.84	58.64	115.24	147.6
39.99	39.50	85.29	141.6	70.98	64.93	52.81	55.26	102.77	143.6	65.00	59.55	116.73	147.6
41.04	40.62	86.46	142.1	72.23	65.72	53.89	56.22	104.18	144.9	66.18	60.48	118.22	148.2
42.07	41.61	87.63	141.7	73.48	66.87	54.98	56.89	105.60	144.3	67.36	61.56	119.73	148.7
43.10	42.46	88.82	141.5	74.75	67.06	56.08	57.94	107.02	145.9	68.56	62.50	121.24	147.9
44.14	43.60	90.01	142.1	76.01	68.07	57.20	58.50	108.47	145.1	69.76	63.42	122.78	147.3
45.19	44.63	91.25	142.1	77.26	68.68	58.32	59.14	109.92	144.1	70.97	64.35	124.32	147.8
46.24	45.59	92.53	142.2	78.52	68.97	59.46	60.02	111.38	144.9	72.20	64.89	125.87	149.0
47.30	46.59	93.82	142.0	79.79	69.16	60.61	60.74	112.85	146.6	73.43	66.03	127.44	149.1
48.36	47.44	95.11	142.5	81.08	70.18	61.77	61.54	114.33	146.4	74.67	66.96	129.01	149.7
49.42	48.48	96.41	142.4	82.37	71.51	62.94	62.39	115.83	146.4	75.92	68.34		
50.49	49.44	97.72	143.9	83.67	72.28	64.12	62.95	117.33	146.5	77.17	68.85		
51.57	50.46	99.05	143.1	84.98	72.34	65.30	63.87	118.85	147.9	78.44	70.26		
52.65	51.21	100.38	142.3	86.28	73.26	66.50	64.48	120.38	147.2	79.72	71.85		
53.74	52.48	101.73	143.0	87.59	74.64	67.71	65.34	121.92	147.8	81.00	72.48		
54.85	53.39	103.08	143.3	88.89	75.92	70.15	67.38	123.47	147.8	82.30	74.12		
55.95	54.29	104.44	143.4	90.18	75.59	71.38	68.14	125.03	147.9	83.60	75.70		
57.05	55.17	105.81	143.2	91.49	77.06	72.63	68.96	126.75	148.3	84.91	77.30		

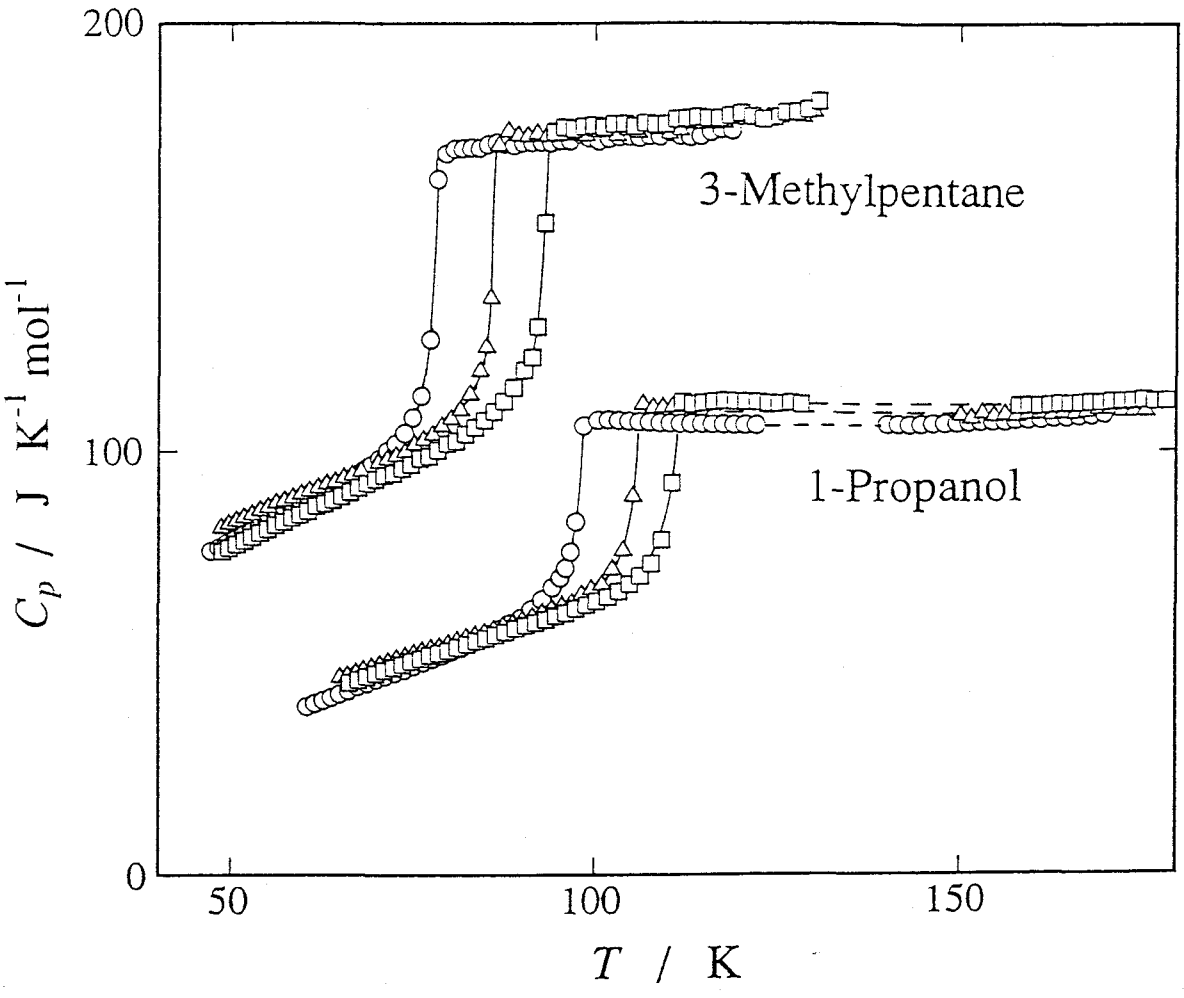

Fig. 3-1. Heat capacities of glassy and liquid states of 1-propanol at 0.1 (circles), 108.4 (triangles), and 198.6 MPa (squares) and those of 3-methylpentane at 0.1 (circles), 108.1 (triangles), and 198.5 MPa (squares). The heat capacity curves of 3-methylpentane are shifted by every 30 $JK^{-1}mol^{-1}$ for clarity. The data of 1-propanol are missing owing to irreversible crystallization in the temperature range shown by the dashed line.

of clarity. A large heat-capacity jump due to the glass transition occurred in all curves. The heat capacity values and glass transition temperatures of both samples at 0.1 MPa agreed well with the literature values [24,26]. Agreement with the previous high-pressure data [27] was also satisfactory (with ±1 %).

The crystallization of 1-propanol occurred spontaneously when the undercooled liquid was warmed in the course of the heat capacity measurement. Thus C_p data are missing in the temperature region shown by the dashed lines in Fig. 3-1. The interpolation in this region was performed in terms of second order polynomials in T. The crystallization took about 12 h for the completion. The heat capacities of crystalline 1-propanol were then measured at 0.1, 108.4 and 198.5 MPa. The crystallization of 3-methylpentane has been reported to be extremely sluggish [26]. In the present study, however, the 3-methylpentane sample crystallized by chance in the course of the measurement. This occurred when the sample which had been kept at 108.1 MPa and depressuized to 0.1 MPa at 50 K was warmed to 88 K. Completion of crystallization required about 6 days. The crystalline sample was then pressurized to 108.1 MPa, and the heat capacity was measured from 50 K. Curiously, crystallization of 3-methylpentane never occurred again after this measurement; thus the heat capacities of crystalline 3-methylpentane at 0.1 MPa and 198.5 MPa are missing in the present study.

Figs. 3-2 and 3-3 show the heat capacities of glass-liquid and crystalline 1-propanol at 108.4 MPa and 3-methylpentane at 108.1

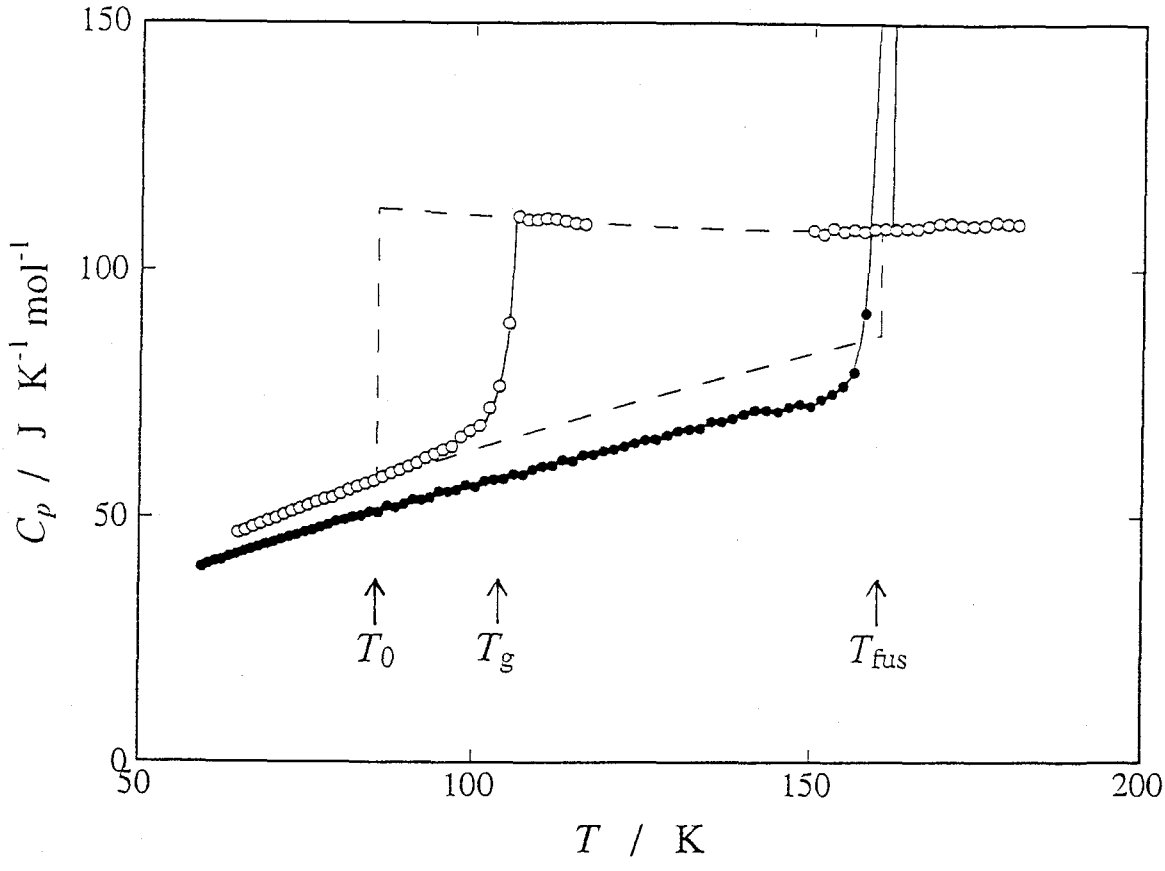

Fig. 3-2. Heat capacities of glassy-liquid (open circles), and crystalline (closed circles) states of 1-propanol at 108.4 MPa. The dashed lines represent the extrapolation of the heat capacities determined by the least-squares method (see text for the details).

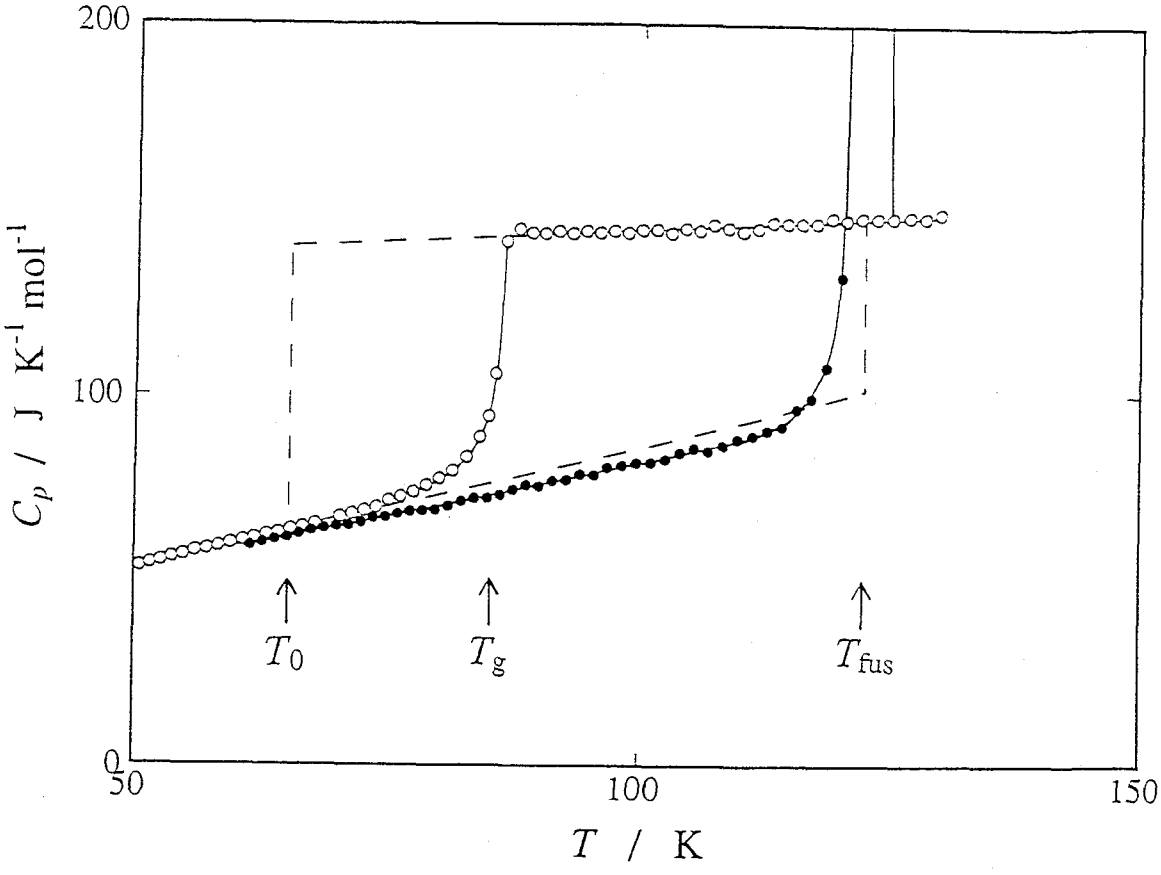

Fig. 3-3. Heat capacities of glassy-liquid (open circles) and crystalline (closed circles) states of 3-methylpentane at 108.1 MPa. The dashed lines represent the extrapolation of the heat capacities determined by the least-squares method (see text for the details).

MPa, respectively. The heat capacities of the crystalline states, especially of 1-propanol, were smaller than those of the glassy states as usually observed at ambient pressure. A large heat capacity peak was observed at fusion temperature, T_{fus}, for both samples.

In Figs. 3-2 and 3-3, the dashed curves represent the extrapolations of the heat capacities, which were used for the estimation of S_C. The heat capacity of the glass was extrapolated by the following method so as to minimize the ambiguity of the process. First, the heat capacities of the crystal at each pressure were fitted by the second order polynomials:

$$C_p(\mathrm{cr}) = A + BT + CT^2. \tag{3-9}$$

Then, the heat capacities of the glass at temperatures between T_g-20 K and T_g-15 K were fitted by the equation

$$C_p(\mathrm{gl}) = A + B(fT) + C(fT)^2. \tag{3-10}$$

Here, the temperature dependence of the heat capacity of the glass was assumed to be given by the same equation as that of the crystal with the temperature rescaled by a factor f. The scaling factor f was left as an adjustable parameter to be optimized by the least-squares fitting. The heat capacity of 3-methylpentane at 198.5 MPa, which was missing in this study, was substituted from literature data at 0.1 MPa [26]. The liquid heat capacity was extrapolated by the linear least-squares fit of the data at

temperatures between T_g+5 K and T_g+15 K. The error introduced by this method will not be very serious because the heat capacity depends on the temperature only weakly in this region and the lowest temperature of the extrapolation (Kauzmann temperature T_0) was not far from T_g (about 20 K below T_g).

3-3-2 Pressure Dependences of Glass Transition and Fusion

Table 3-3 gives the thermodynamic quantities associated with glass transition and fusion at different pressures. The temperature and entropy of fusion for 3-methylpentane at 198.5 MPa, where the crystalline state could not be obtained, were estimated by a linear extrapolation of the data at 0.1 and 108.1 MPa. This extrapolation could be a good approximation in view of the fact that T_{fus} vs. P and $\Delta_{fus}S$ vs. P data can be reproduced well by straight lines in the pressure range 0-200 MPa for 1-propanol. The glass transition temperature, T_g, was determined as that at which the temperature drift rate became zero, i.e., the sample enthalpy was apparently on the equilibrium value during the course of heat-capacity measurements. The T_g value determined in this way corresponds roughly to the time scale of 1 ks. The determination of the Kauzmann temperature T_0 will be described in section 3-4-1.

Fig. 3-4 shows the pressure dependence of T_{fus}, T_g, and T_0 for 1-propanol and 3-methylpentane. The dashed lines for 3-methylpentane represent the extrapolation of the data taken at 0.1 and 108.1 MPa as described above. All the quantities linearly increased with pressure in the present pressure range 0-200 MPa.

Table 3-3. Thermodynamic quantities associated with the glass transition and the fusion at each pressure.

1-propanol

P / MPa	T_{fus} / K	$\Delta_{fus}H$ / $Jmol^{-1}$	$\Delta_{fus}S$ / $JK^{-1}mol^{-1}$	T_g / K	ΔC_p / $JK^{-1}mol^{-1}$	T_0 / K
0.1	148.81	5399	36.25	96.2	47.0	78.4
108.4	160.52	5663	35.30	103.8	45.4	85.4
198.6	168.76	5878	34.83	109.1	45.4	92.1

3-methylpentane

P / MPa	T_{fus} / K	$\Delta_{fus}H$ / $Jmol^{-1}$	$\Delta_{fus}S$ / $JK^{-1}mol^{-1}$	T_g / K	ΔC_p / $JK^{-1}mol^{-1}$	T_0 / K
0.1	110.25[a]	5303[a]	48.12[a]	77.0	69.4	58.4
108.1	122.35	5598	45.80	85.3	66.2	65.1
198.5	132.47[b]	——	43.85[b]	91.8	65.3	72.2

[a] Obtained by Finke et al. [26].

[b] Estimated by the extrapolation which is described in the text.

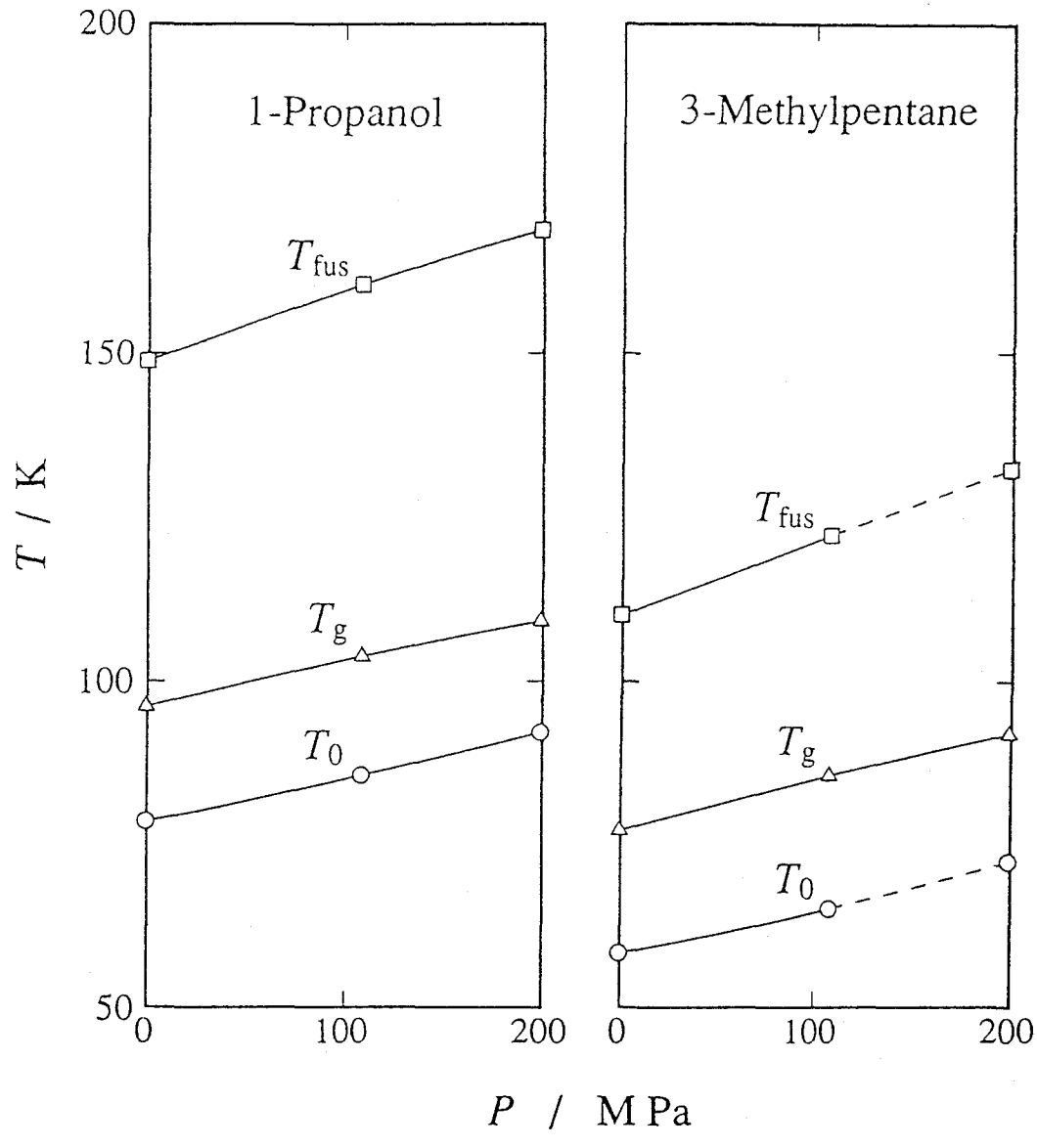

Fig. 3-4. Pressure dependence of the temperatures of fusion (squares), glass transition (triangles) and Kauzmann temperature (circles) of 1-propanol and 3-methylpentane. The curves were drawn by the least squares methods. For 3-methylpentane, the value of T_{fus} at 198.5 MPa was determined by the extrapolation shown by the dashed line, and T_0 at 198.5 MPa was calculated using the extrapolated quantities (see text for the details).

The gradients of T_g vs. P lines for 1-propanol and 3-methylpentane were 65 and 75 K GPa^{-1}, respectively. The former value agreed with that estimated by high-pressure dielectric measurement (70 K GPa^{-1}) [28].

3-3-3 Configurational Entropy

The configurational entropy as a function of temperature was calculated from the experimental data by

$$S_C = \Delta_{fus}S - \int_0^{T_{fus}} [C_p(g) - C_p(cr)]/T \, dT - \int_T^{T_{fus}} [C_p(l) - C_p(g)]/T \, dT, \quad (3\text{-}11)$$

where $C_p(l)$, $C_p(g)$, and $C_p(cr)$ are the heat capacities of liquid, glass, and crystal, respectively.

The first and third terms in the right-hand side of eq. 3-11 were obtained with high accuracy from the present data at each pressure. The quantity $C_p(l)$-$C_p(g)$ was obtained for the first time by the present adiabatic method while the previous calorimetric study under high pressure [35,36] employed mainly hot-wire and AC methods, both being unsuitable for determination of accurate heat capacities. The extrapolations of $C_p(l)$ to T_0 and $C_p(g)$ to T_{fus} were performed as described before.

The second term of eq. 3-11 represents the correction for the difference in vibrational entropies at T_{fus} between the glassy and crystalline states. Unfortunately, it was not easy to estimate this term from our data, because the lowest temperature of measurement was about 50 K for every pressure. Hence, this term was evaluated by using the data at atmospheric pressure [24,26]

neglecting their pressure dependence. The correction was less than 1 % of the total heat capacity in the case of 3-methylpentane [27]. The estimated value of the second term at 108 MPa was 11.0 $JK^{-1}mol^{-1}$ for 1-propanol and 5.98 JK-1mol-1 for 3-methylpentane. These values correspond to 31 % and 13 % of the $\Delta_{fus}S$, respectively. The vibrational correction to the determination of configurational entropy has usually been neglected.

The Kauzmann temperature, T_0, was determined as the temperature at which S_C vanishes. The value thus obtained at each pressure is tabulated in the last columns of Table 3-3 and is graphically shown in Fig. 3.4. The gradients of T_0 vs. P lines for 1-propanol and 3-methylpentane were both 69 K GPa^{-1}. The pressure dependence of T_0 was determined for the first time.

3-3-4 Examination of the Entropy Theory

In order to examine the validity of the entropy theory (eqs. 3-2 and 3-3), the temperature dependence of S_C at each pressure was calculated in terms of eq. 3-11. Fig. 3-5 shows the temperature dependence of S_C for 1-propanol and 3-methylpentane. The numerical value of S_C at T_{fus} corresponds to the first and second terms of eq. 3-11, which can be evaluated accurately. The decrease in S_C below T_{fus} corresponds to the third term of eq. 3-11, which is obtained by using extrapolations of the C_p data shown in Figs. 3-2 and 3-3. The decrease in S_C between T_{fus} and T_g and that between T_g and T_0 are shown by solid and broken curves, respectively. The magnitude of S_C at T_0 was taken to be zero according to the definition. The value of S_C at T_g decreased

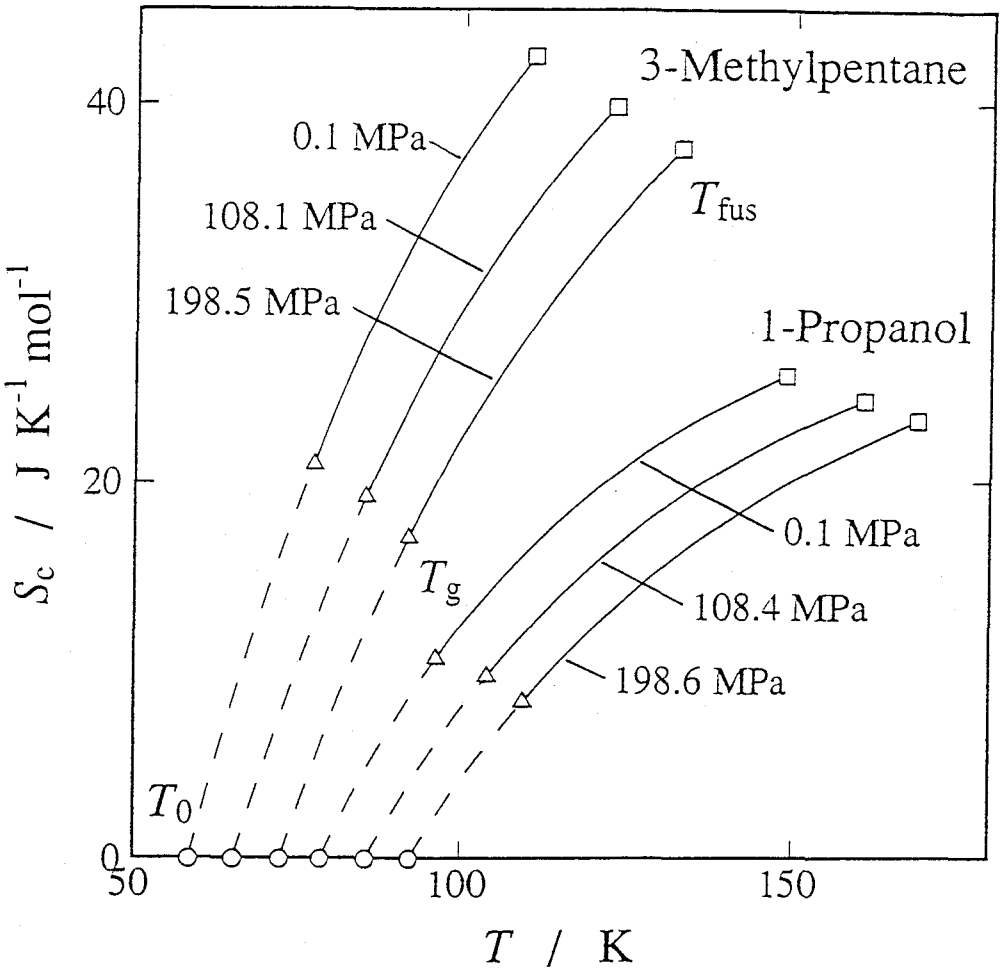

Fig. 3-5. Temperature dependence of the configurational entropy of 1-propanol at 0.1, 108.4, and 198.6 MPa and that of 3-methylpentane at 0.1, 108.1, and 198.5 MPa. The quantities at T_{fus}, T_g, and T_0 are represented by squares, triangles, and circles, respectively. See text for the procedure to obtain the solid and dashed curves.

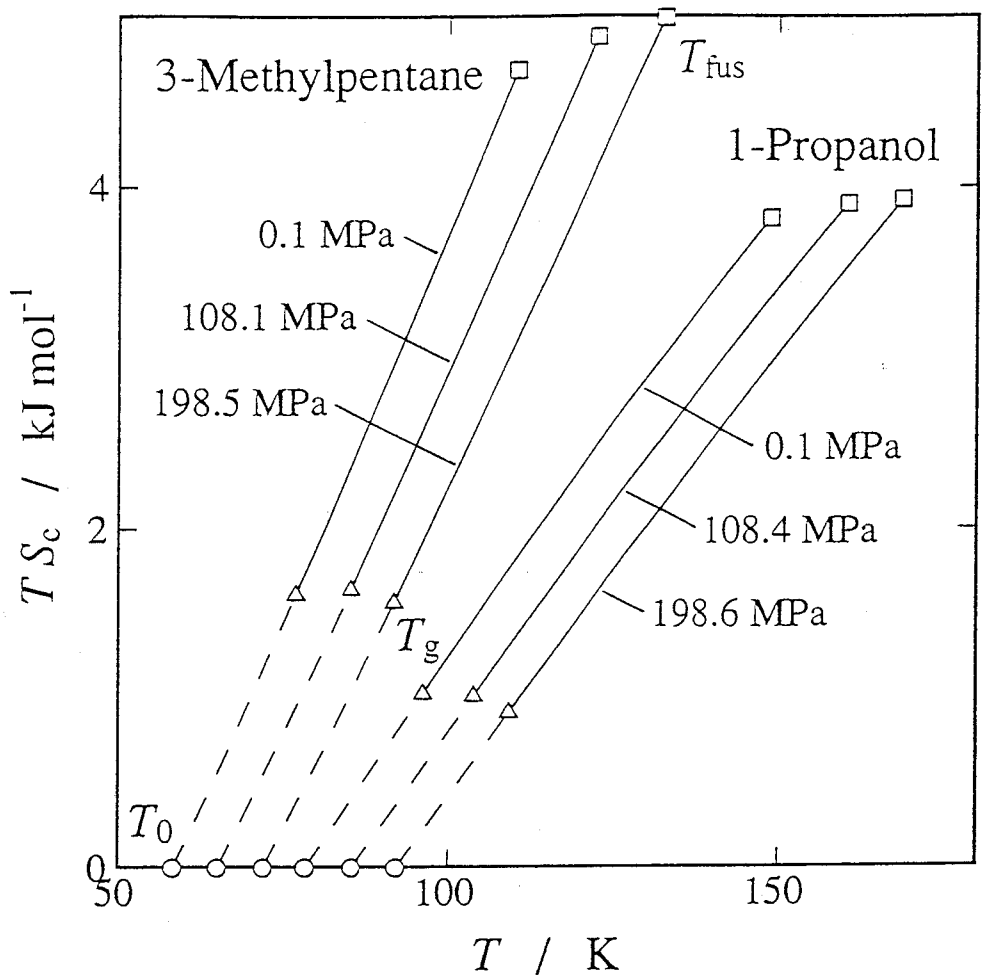

Fig. 3-6. Temperature dependence of the configurational entropy multiplied by the temperature for 1-propanol at 0.1, 108.4, and 198.6 MPa and that for 3-methylpentane at 0.1, 108.1, and 198.5 MPa. The quantities at T_{fus}, T_g, and T_0 are represented by squares, triangles, and circles, respectively. See text for the procedure to obtain the solid and dashed curves.

systematically with increasing pressure against the prediction from eq. 3-1.

Fig. 3-6 shows the temperature dependence of TS_C at three pressure for 1-propanol and 3-methylpentane. The procedures of the calculation were similar to those of Fig. 3-5. It was shown that TS_C at each pressure is almost constant at the corresponding T_g. This clearly indicates that the Adam-Gibbs theory (eq. 3-2) is valid within the accuracy of the present experiment and it reproduces the experimental data better than the simple entropy theory (eq. 3-1) does both for 1-propanol and 3-methylpentane. Thus the glass transition can be regarded to occur at constant TS_C rather than at constant S_C in both cases.

In the Adam-Gibbs theory, the configurational entropy, S_C, is related to the size of the "domain" in which the molecules are able to change their configurations cooperatively. The larger the domain size, the smaller the configurational entropy is. In the case of molecular liquids such as 1-propanol and 3-methylpentane, it is considered that a decrease in S_C is readily achieved by applying pressure as well as by lowering temperature. This is because the applied pressure decreases the intermolecular distance and increases intermolecular interaction, causing stronger cooperativity both for the segmental (methyl and methylene) and overall rotations of the molecules and resulting in formation of larger domains. The decrease in S_C due to the pressure increase to 198 MPa around T_g was quite large both for 1-propanol (8 JK^{-1} mol^{-1} at 109 K) and 3-methylpentane (15 $JK^{-1}mol^{-1}$ at 92 K). These magnitudes correspond to the S_C changes due to the temperature

decreases of 17 K and 19 K, respectively. The large pressure dependence of S_C reflects the large pressure dependence of T_g; 65 K GPa^{-1} for 1-propanol and 75 K GPa^{-1} for 3-methylpentane.

References to Chapter 3

[1] K.L. Ngai, E. Riande and G.B. Wright, eds., "Relaxations in Complex Systems", J. Non-Cryst. Solids 172-174 (1994); K.L. Ngai, and G.B. Wright, eds., "Relaxations in Complex Systems", J. Non-Cryst. Solids 131-133 (1991).

[2] J.H. Gibbs and E.A. DiMarzio, J. Chem. Phys. 28 (1958) 373.

[3] E.A. DiMarzio and J.H. Gibbs, J. Chem. Phys. 28 (1958) 807.

[4] M. Goldstein, J. Chem. Phys. 39 (1963) 3369.

[5] A.B. Bestul and S.S. Chang, J. Chem. Phys. 40 (1964) 3731.

[6] G. Adam and J.H. Gibbs, J. Chem. Phys. 43 (1965) 139.

[7] A.K. Doolittle, J. Appl. Phys. 22 (1951) 1471.

[8] M.H. Cohen and D.Turnbull, J. Chem. Phys. 31 (1959) 1164.

[9] D. Turnbull and M.H. Cohen, J. Chem. Phys. 34 (1961) 120.

[10] H. Vogel, Z. Physik 22 (1921) 645.

[11] G. Tammann and G. Hesse, Z. Anorg. Allg. Chem. 156 (1926) 245.

[12] W. Kauzmann, Chem. Rev. 43 (1948) 219.

[13] A. Quach and R. Simha, J. Appl. Phys. 42 (1971) 4592.

[14] J.I. Berg and R. Simha, J. Non-Cryst. Solids 22 (1976) 1.

[15] H.J. Oels and G. Rehage, Macromolecules 10 (1977) 1036.

[16] P.Zoller, J. Poly. Sci. Poly. Phys. Ed. 20 (1982) 1453.

[17] T. Nose, Polymer J. 2 (1971) 445.

[18] C.A. Angell, E. Williams, K.J. Rao and J.C. Tucker, J. Phys. Chem. 81 (1977) 238.

[19] R.O. Davies and G.O. Jones, Adv. Phys. 2 (1953) 370.

[20] J.M. O'Reilly, J. Polym. Sci. 57 (1962) 429.

[21] M. Goldstein, J. Phys. Chem. 77 (1973) 667.

[22] M. Naoki and T. Nose, J. Polym. Sci. Polym. Phys. Ed. 13 (1975) 1747.

[23] T. Atake and C.A. Angell, J. Phys. Chem. 83 (1979) 3218.

[24] J.F. Counsell, E.B. Lees and J.F. Martin, J. Chem. Soc. A (1968) 1819.

[25] D.R. Douslin and H.M. Huffman, J. Am. Chem. Soc. 68 (1946) 1704.

[26] H.L. Finke and J.F. Messerly, J. Chem. Thermodyn. 5 (1973) 247.

[27] M. Oguni, K. Watanabe, T. Matsuo, H. Suga and S. Seki, Bull. Chem. Soc. Jpn. 55 (1982) 77.

[28] A. Gilchrist, J.E. Earley, and R.H. Cole, J. Chem. Phys. 26 (1957) 196.

[29] O. Yamamuro, M. Oguni, T. Matsuo and H. Suga, Bull. Chem. Soc. Jpn. 60 (1987) 1269.

[30] O. Yamamuro, M. Oguni, T. Matsuo and H. Suga, J. Chem. Phys. 86 (1987) 5137.

[31] O. Yamamuro, M. Oguni, T. Matsuo and H. Suga, J. Phys. Chem. Solids 48 (1987) 935.

[32] R.D. McCarty, J. Phys. Chem. Ref. Data, 2 (1973) 923.

[33] E.S. Itskevich, A.N. Voronovskii, A.F. Gavrilov and V.A. Sukhoparonov, Instrum. Exp. Tech. (USSR) 6 (1966) 1452.

[34] Sumitomo Special Metal Co. Ltd., Catalog No. E6101 (1987).

[35] B. Sundqvist, O. Sandberg and G. Bäckström, J. Phys. D10 (1977) 1397.

[36] N.O. Birge and S.R. Nagel, Phys. Rev. Lett. 54 (1985) 2674; N.O. Birge, Phys. Rev. B34 (1986) 1631.

Chapter 4

Development of an Adiabatic Calorimeter for Simultaneous Measurement of Enthalpy and Volume under High Pressure

4-1 Introduction

The Gibbs energy (G) surface against temperature (T) and pressure (P) contains all the information about the thermodynamic properties of a substance. This surface can be constructed from the experimental data of the heat capacity, thermal expansivity and compressibility as functions of T and P. Hence, calorimetry (enthalpy measurement) and dilatometry (volume measurement) under pressure are the most important experiment methods in the equilibrium thermodynamic study.

The enthalpy (H) and volume (V) measurements under pressure provide important information also for the non-equilibrium problems. When the external parameters such as T and P of the liquid are changed rapidly, the structural relaxation is observed to a new equilibrium one. It is of interest to observe such relaxation phenomena in the two different thermodynamic quantities H and V as functions of time (t). The relaxation process can be characterized by a locus in the three dimensional space (H - V - t). A simultaneous measurement of H and V is a potent method of investigation of non-equilibrium processes since the same non-equilibrium state can not be realized in separate experiments. High-resolution experiments are also required when the magnitude

of the relaxation in H and V is very small near the equilibrium state.

At atmospheric pressure, H and V are measured separately with high precision over a wide temperature range. The V measurements [1-6] have been extended to high pressures but only a few apparatus [7,8] have been reported for the precise H measurements under high pressure. An apparatus for simultaneous measurement of H and V was reported by Oguni *et al.* [7]. This apparatus worked under adiabatic condition at hydrostatic constant pressures up to 110 MPa and in the temperature range between 100 and 370 K. The imprecisions of the measurements were 0.5 % in the heat capacity and 0.01 % in the volume, the compared with those of the separate measurements, 0.1-0.2 % in the heat capacity and ca. 10^{-3} % in the volume.

In the present study, an adiabatic calorimeter was constructed for simultaneous and high-precision measurements of H and V under high pressure. The basic design of the present apparatus follows that of the previous calorimeter by Oguni *et al.* but a great improvement was attained for the dilatometric measurement. The precision of the present V measurement is ca. 10^{-5} %, which is ca. 10^{+3} times better than those of the previous one. The increased precision made it possible to investigate the structural relaxation with small volume change as described in Chapter 6.

The design and construction of the apparatus, calculation of H and V from the raw data, and calibration and test experiments will be described in sections 4-2, 4-3, 4-4, respectively. The calibration and test experiments were performed at atmospheric

pressure since the pressure dependence of the calibration data is negligible or easily calculated as described in the experiments of polystyrene in Chapters 5 and 6.

4-2 Construction of the Apparatus

4-2-1 Principle

The calorimetric measurement is based on the adiabatic method. The heat capacity (C_p) is measured by determining the temperature increment (ΔT) of the sample caused by electrically supplied energy (ΔE) under adiabatic condition; *i.e.*, $C_p = \Delta E/\Delta T$. Enthalpy relaxation ($\Delta H(t)$) is measured by monitoring the spontaneous temperature change ($\Delta T(t)$) of the cell as a function of time (t) under adiabatic condition; *i.e.*, $\Delta H(t) = C_p \Delta T(t)$.

The sample is pressurized hydrostatically using pressure transmitting liquids (PTL). The applied pressure is regulated at a constant value by permitting the flow of PTL into or out of the cell through the pressure transmitting tube connecting the sample cell and the pressure control system. The effect of PTL on the calorimetric measurement is corrected for as described below.

The dilatometric measurement is performed by a method similar to that of Quach and Simha [1]. Their method was based on the traditional Bridgman's bellows method [9]. The liquid sample or the solid sample with PTL is confined in the cell capped with the flexible metal bellows which is exposed to external hydrostatic pressure from the high-pressure system. The bellows expands or

contract so as to balance the pressure of the sample with the applied pressure. The volume change is obtained from magnetic detection of the change in length of the bellows. Each part of the apparatus will be described in the following sections.

4-2-2 Cryostat and Adiabatic Control System

Fig. 4-1 shows a schematic drawing of the cryostat. It is based on the principle of adiabatic calorimetry with provisions for measurement under high pressure. These are pressure transmitting tubes C1-C3 and the volume measurement system A. The pressure transmitting tubes connect the inner space of the cell N and the high pressure system. They are made of stainless steel and have the size of 2.1 mm I.D. and 6.4 mm O.D. C3 is joined to C2 by the couplings (H1, H2) and the thermal anchor G2. They are made of copper-beryllium alloy which has high thermal conductivity and sufficient mechanical strength. The cell N is dismountable at H2.

Adiabatic condition between the cell and its environment is achieved by evacuating the space inside the vacuum jacket P to 10^{-4} Pa and by regulating the temperatures of the parts surrounding the cell. The inner adiabatic shield M and the tube C3 are controlled at the same temperature as the cell. The outer adiabatic shield J and the thermal anchor G2 are held a few kelvins lower than the cell to assist the control of M and C3. The temperature of the tube C2 is usually kept slightly higher than that of G2. The tube C1 is controlled at around the room temperature. The adiabatic shield E for the tube C2 is controlled

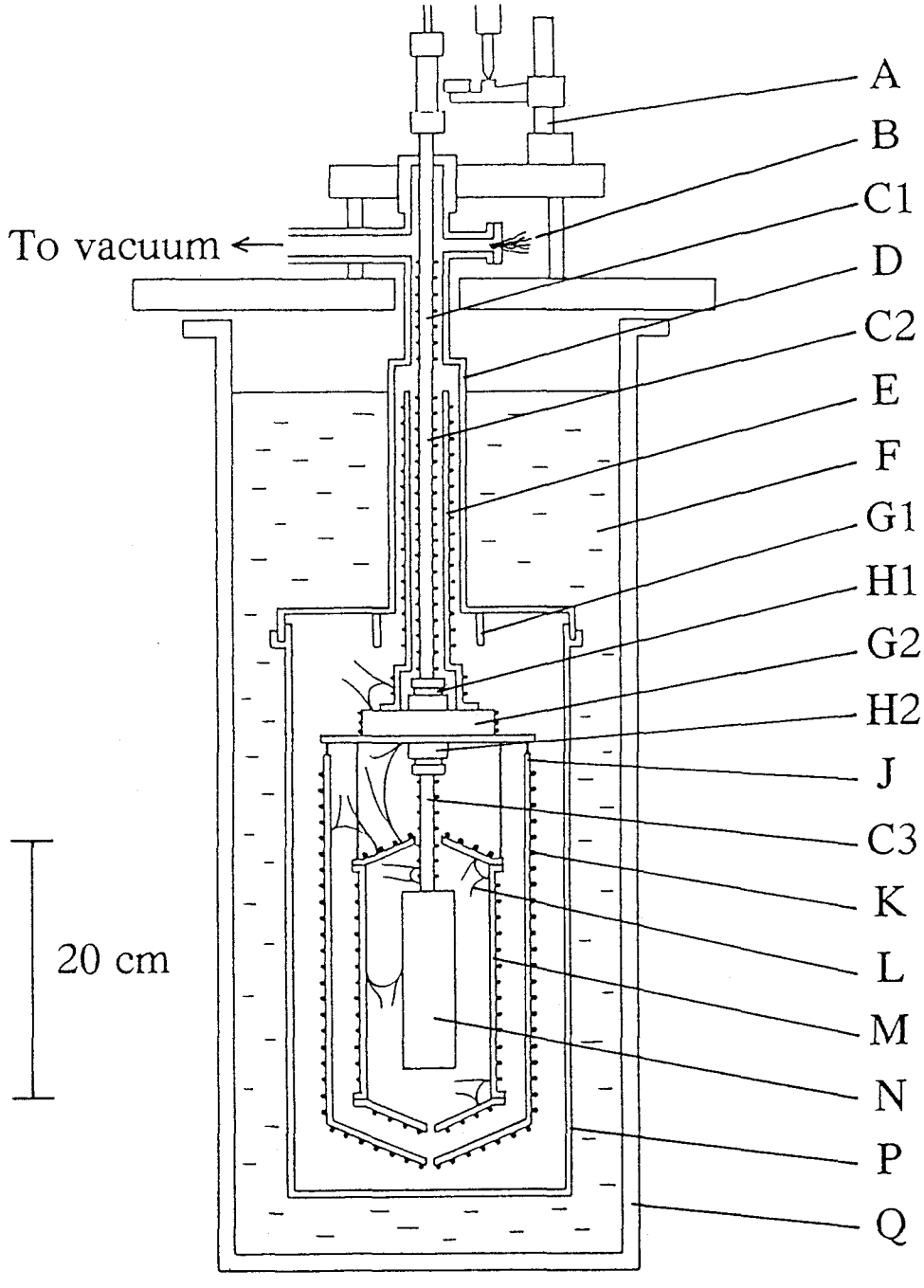

Fig. 4-1. Schematic drawing of the cryostat. (A) Volume measurement system, (B) flange for lead wires, (C1-C3) pressure transmitting tubes, (D) pumping tube, (E) adiabatic shield for the tube C2, (F) refrigerant, (G1,G2) thermal anchors, (H1,H2) couplings, (J) outer adiabatic shield, (K) heater wires, (L) thermocouples, (M) inner adiabatic shield, (N) sample cell, (P) vacuum jacket, (Q) Dewar flask.

at the same temperature as G2 to reduce the temperature distribution in C2. All of the adiabatic shields are made of copper for its high thermal conductivity. The temperature controls described above are performed by negative-feedback circuits using the temperature difference signals from the Chromel-Constantan thermocouples L and the heater wires K placed on the surface of the regulated parts. The heater wires are wound pair-wise to reduce inductive interference. The leads of the thermocouples and the heater wires are wound around the inner adiabatic shield M and thermal anchors G1 and G2 for heat exchange and taken out of the cryostat through the flange B. The vacuum seal between the leads and the flange B is made by epoxy-resin (Araldite, Chiba-Geigy). The cryostat is immersed in the refrigerant (liquid nitrogen or ice water) F filled in the Dewar flask Q. The sample cell is cooled with the help of He gas of about 10 kPa introduced into the jacket P. The cryostat, the volume measurement system, and the high-pressure system are all located in a room whose temperature is kept constant within ±0.5 °C.

4-2-3 Sample cell

Fig. 4-2 shows a sectional drawing of the sample cell. The main parts of the cell (D1-D3, E2, E3 and F) are made of copper-beryllium alloy. The surface of the cell is gold-plated for the reduction of radiative heat transfer and for protection against corrosion. The cell was designed so as to withstand the applied pressure up to 100 MPa, resulting in the increase of mass of the

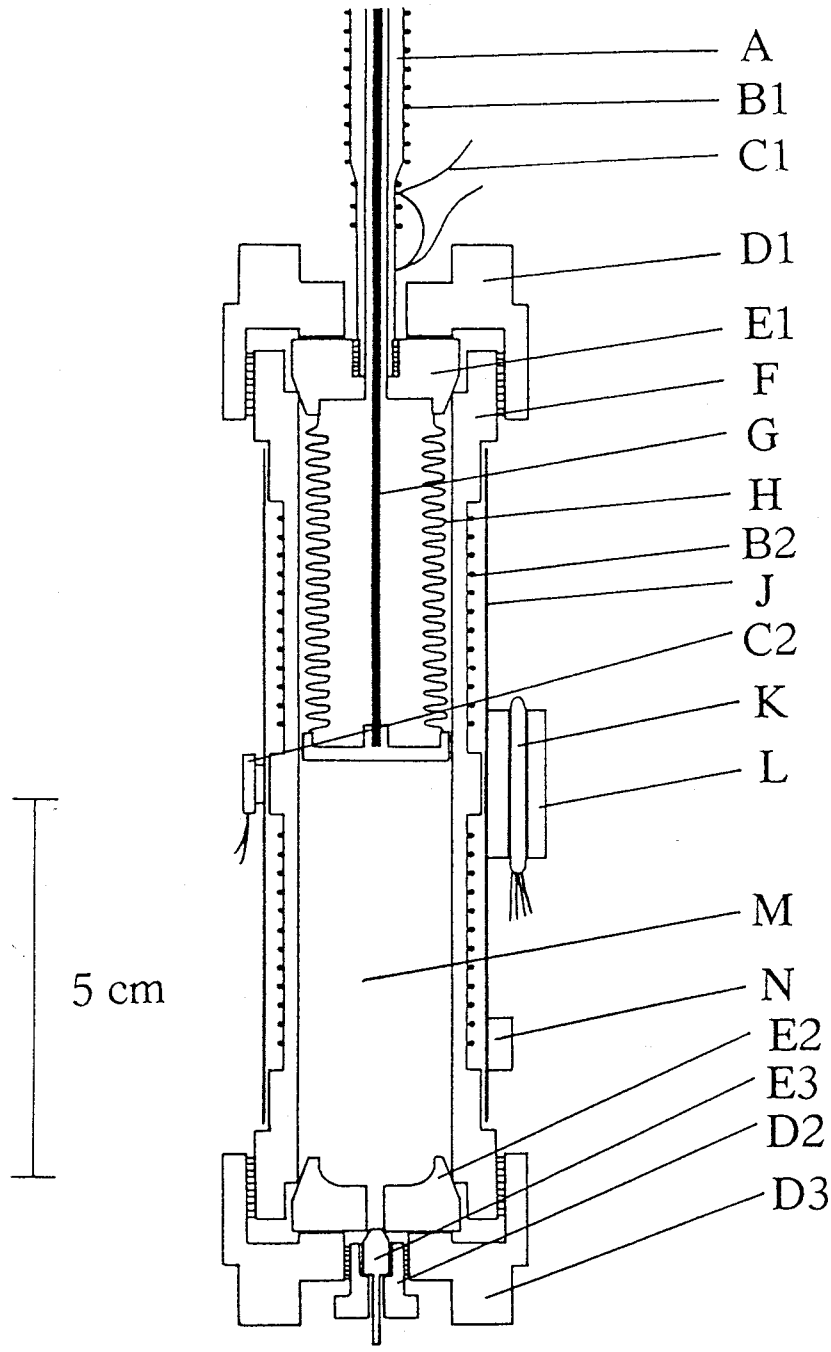

Fig. 4-2. Sectional drawing of the sample cell. (A) Pressure transmitting tube, (B) heater wires, (C) thermocouples, (D) gland nuts, (E) plugs, (F) main body of the cell, (G) displacement transmitting rod, (H) bellows, (J) cell cover, (K) Rh-Fe resistance thermometer, (L) thermometer holder, (M) sample room, (N) thermal anchor.

cell (651.46 g) and decrease in the ratio of the sample heat capacity to that of the empty cell (SE ratio). The small SE ratio makes the imprecision of the calorimetric measurement larger than that of a conventional adiabatic calorimeter. The maximum pressure can be increased up to 200 MPa by increasing the thickness of F at the expense of the SE ratio.

The pressure transmitting tube A is connected to the stainless steel plug E1 by screw and silver soldered. The cylindrical body F (20 mm I.D., 24-28 mm O.D.) of the cell is closed on the both ends by the plugs E1-E3 and the gland nuts D1-D3. The plugs E1 and E2 are pressed against the both edges of the inner wall of J by driving the screw of the gland nuts D1 and D2, respectively. The plug E3 is pressed against the edge of the hole (1.2 mmϕ) drilled at the center of E2 by driving the screw of the gland nut D3. The pressure inside the cell is sealed by these metallic cone connections. This sealing method is the same as those used in the adiabatic high-pressure calorimeter reported by Yamamuro *et al.* [8], is superior to the traditional Bridgman method in that it does not require any packing material, thus avoiding complicated pressure and temperature dependence of the cell volume due to shrinkage of the packing.

The phosphorus-copper bellows H fixed to E1 with silver solder divides the inner space of the cell into two. The liquid sample or the solid sample with PTL is placed in the sample room M (ca. 22 cm^3). The solid sample is usually shaped into a rod and loaded in M after removing the plug E2. The liquid sample or PTL for the solid sample is introduced through the hole of E2 by pouring in

vacuo and then sealed with the plug E3 and the gland nut D3. The inner space of the bellows (ca. 10 cm^3) and the pressure transmitting tube A are filled with PTL. The bellows expands or contracts by pressure difference of less than 0.1 MPa. The inner wall of the body F is fitted well to the bellows and plays a role of the guide for the movement of the bellows. The stainless steel rod G is soldered to the closed end of the bellows to transmit the displacement of the bellows to the outside of the cryostat. The rod G passes through inside the tube A and reaches to the volume measurement system described in the next section.

The PTL in the sample room and the PTL in the bellows are selected taking the fusion temperature and the solubility of the sample into consideration. For low temperature experiments, 3-methylpentane or 1-propanol have usually been used as PTL, because they are liquid at room temperature and undergo neither crystallization nor glass transition down to 100 K. If the sample is dissolved in PTL, it must be confined in a thin plastic cup which can deform accommodating the volume change. For high temperature experiments, various type of materials (water, silicone oil, Hg etc.) have been used as PTL. In the present study, 1-butanol ($184 < T/K < 390$) and Fluorinert ($170 < T/K < 400$) were used as PTL. Fluorinert (Sumitomo 3M Co. Ltd.) is a mixture completely fluorinated alkanes and so it is chemically inert and dissolves in neither water nor hydrocarbon oils.

Electrical energy is supplied into the cell by the manganin heater wire B2. The thin cell-cover J made of copper is installed to minimize heat leak by radiation from B2. The thermocouple C2

for the temperature control between the cell and the inner shield, the holder L for the Rh-Fe resistance thermometer K and the thermal anchor N for the heater wire B2 are all soldered on the outer surface of J.

4-2-4 Volume Measurement System

Fig. 4-3 shows a schematic drawing of the volume measurement system. The strong and discoidal magnet F (Coremax, Sumitomo Special Metal Co. Ltd.) is fixed on the top of the rod J which is connected to the bellows inside the cell. The magnet moves up and down smoothly in the cylinder E made of diamagnetic stainless steel (SUS310S). The inner bore of E is fitted well to the magnet F so as to prevent its horizontal shift. The I.D. and O.D. of E are 5.7 and 10 mm, respectively. E is connected to the pressure transmitting tubes A1 and A2 by using the gland nuts B1 and B2 and plug C1 and C2, respectively. The pressure seal of these parts are similar to that in the sample cell. The total length of the rod J is so long (ca. 60 cm) that its temperature dependence is considerable in magnitude (ca. 8 μm/K). However, this effect is canceled by the temperature dependence of the pressure transmitting tubes since the material (stainless steel) and the temperature of J and A2 are same.

The displacement of the magnet F is measured with the Magnesensors G and the Magnescale M (Sony Magnescale Inc.). The two Magnesensors G are fixed symmetrically on the supporting arm H which can be moved up and down by manual operation of the cathetometer P. The Magnesensors measure the vertical

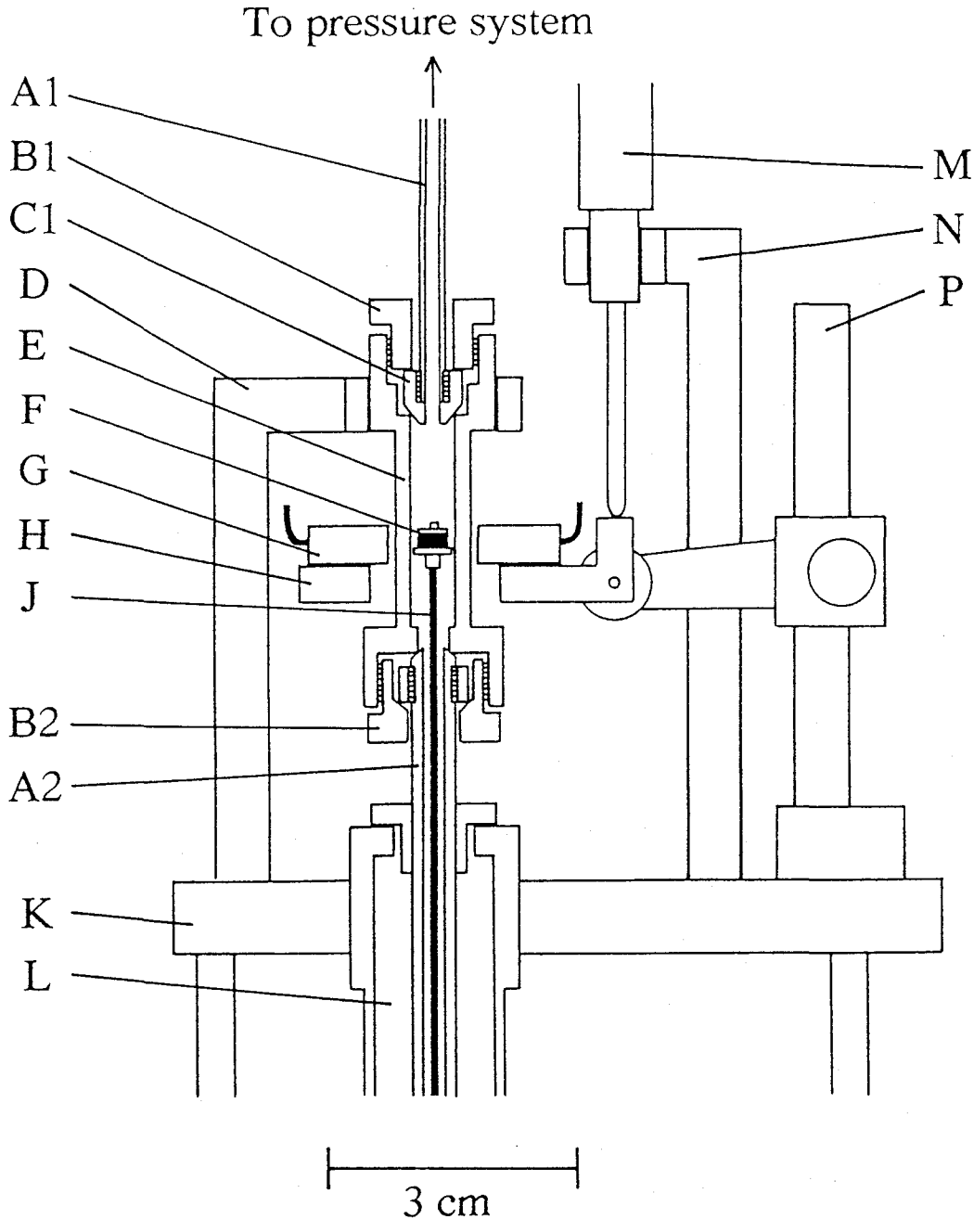

Fig. 4-3. Schematic drawing of the volume measurement system. (A) Pressure transmitting tubes, (B) gland nuts, (C) plugs, (D) supporting arm, (E) diamagnetic cylinder, (F) magnet, (G) Magnesensors, (H) Magnesensor holder, (J) displacement transmitting rod, (K) volume measurement stage, (L) cryostat, (M) Magnescale, (N) Magnescale holder, (P) cathetometer.

displacement of the center of the magnet against the center of the Magnesensor by use of the magnetic field from the magnet. The output signal of Magnesensor (electrical potential) is proportional to the displacement of the magnet in the range of ±0.2 mm. The imprecision of the displacement measurement was ca. ±0.01 μm (see section 4-3-5). The height of the Magnesensors is measured by the Magnescale M which has a precision of ± 1 μm.

There are two modes with different resolution to measure the displacement of the magnet. The low resolution mode is used for large volume change of the sample such as that due to the large temperature change. In this mode, the Magnesensor is used as the zero-point detector and its height is read with the Magnescale. The high resolution mode is used for small volume change such as that due to an isothermal structural relaxation of the sample. In this mode, the height of the Magnesensors is fixed, and their output signal is recorded with the digital multimeter (Keithley 195A). The precision of the measurement with the high resolution mode is estimated to be ca. 10^{-5} % of the sample volume, which is much better than that of the conventional dilatometer (ca. 10^{-3} %).

4-2-5 Calorimetric System

The electrical energy supply and the temperature measurement are carried out with the calorimetric measurement system which has been constructed before [8]. The temperature of the cell is measured with a Rh-Fe resistance thermometer (27 Ω at 273 K; Oxford Instrument Ltd.) calibrated on the temperature scale EPT76

(T < 30 K) and IPTS68 (30 < T < 300 K). For the temperature range 300 - 380 K, the calibration was made by the present author against the standard platinum resistance thermometer (R800-0, Chino Corp.), which had been calibrated to the IPTS68. The heat capacity difference caused by the conversion to the new temperature scale ITS90 [10] was estimated to be smaller than 0.05 % over the temperature range 100 - 380 K.

4-2-6 High-Pressure System

The high-pressure system of the previous calorimeter [7] was modified for the present purpose. Fig. 4-4 shows the block diagram of the system. Two PTL's in the high-pressure system are separated by the flexible metal bellows in the pressure media separator F. The pressure generation side (right-hand side) of F is filled with liquid kerosene, while the cryostat side (left-hand side) with liquid 3-methylpentane or 1-butanol. The liquid 3-methylpentane or butanol in the glass bulb D is charged into the high pressure system through the valve G1 by pouring in vacuum. Liquid kerosene is also charged by the same manner through the valve G5.

The pressure generator H can generate pressure up to 200 MPa. The applied pressure can be regulated within ±100 kPa by the method developed by Oguni et al [7]. The deviation from the preset pressure is detected as the change in resistance of the stain-free Manganin coil L in the vessel K. This is converted to an electrical signal by the Wheatstone Bridge and used for the negative-feedback circuit M to control the current of the heater

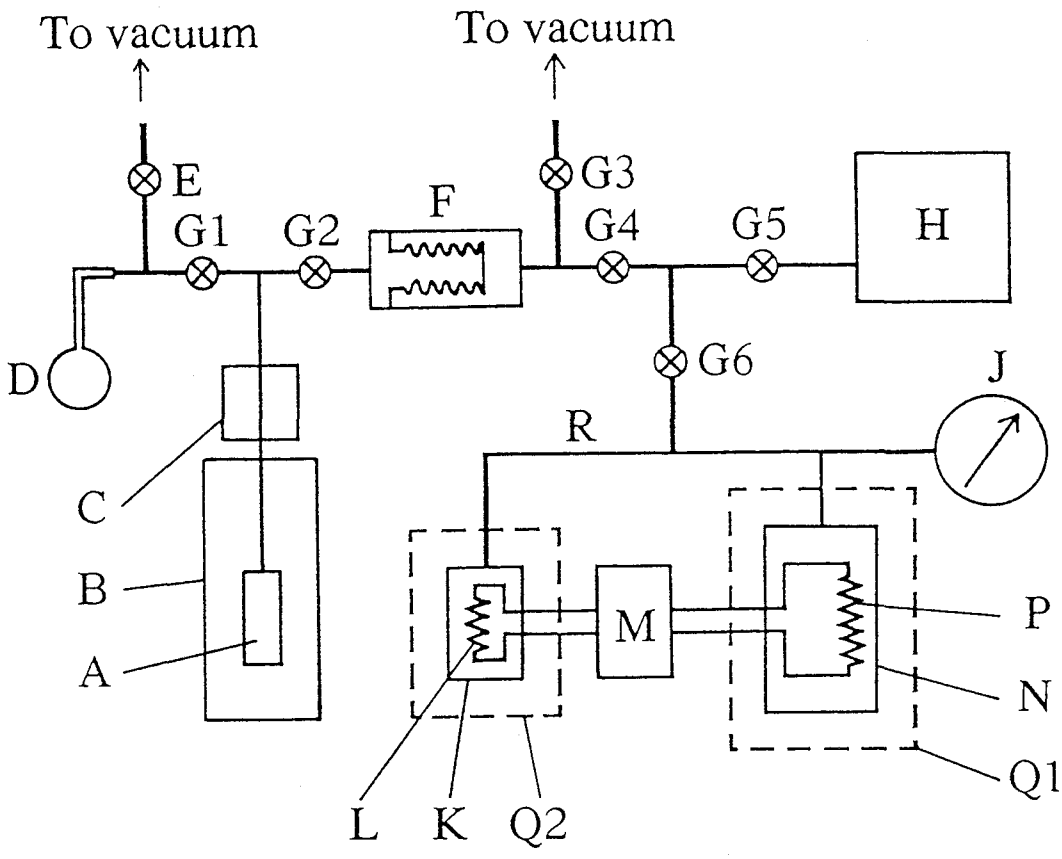

Fig. 4-4. Block diagram of the high pressure system. (A) Sample cell, (B) cryostat, (C) volume measurement system, (D) glass bulb, (E) PTFE cock, (F) pressure-transmitting-liquid separator, (G) high-pressure valves, (H) pressure generator, (J) Heise pressure gauge, (K) pressure sensor vessel, (L) Manganin pressure sensor, (M) pressure control circuit, (N) kerosene reservoir, (P) heater wire, (Q) thermostats, (R) pressure transmitting tubes.

wire P in the kerosene reservoir N. The pressure deviation is thus compensated by the temperature change of the kerosene in N. To reduce the fluctuation due to the temperature change, both K and N are placed in the thermostats Q1 and Q2, respectively. The pressure is read with the Heise gauge J calibrated within the error of ±0.1 MPa. The pressure can also be determined with high precision (±10 kPa) by measuring the resistance of the Manganin coil with the high-precision a.c. resistance bridge (ASL. F17). In this method, the calibration function for the transformation from resistance to pressure is determined by using the Heise gauge and so the accuracy of the pressure is the same as that of the Heise gauge.

4-3 Determination of Thermodynamic Quantities

4-3-1 Volume

The volume of the sample is derived from the displacement L of the magnet measured by Magnesensor and Magnescale. L is given by the sum of two terms,

$$L = L_{SC} + E_{Se}(dL/dE) \qquad (4\text{-}1)$$

where, L_{SC} and E_{Se} represent the digital reading of the displacement by Magnescale and the analog output signal by Magnesensor, respectively. (dL/dE) is the sensitivity coefficient relating E_{Se} to L and was evaluated to be 0.125 μm/mV from a

calibration experiment. In the high resolution mode, L is determined from eq. 4-1 for a fixed L_{SC}. The resolution in this modes is 10 nm corresponding to 2×10^{-6} cm^3. The region where (dL/dE) is constant is ±1.5 V corresponding to ±200 μm and so the high resolution mode was used for determination of small volume changes accompanying isothermal was structural relaxation. In the low resolution mode, the dial of the cathetmeter is adjusted so as to make the second term of eq. 4.1 zero and the displacement of the Magnesenser is read by Magnescale. The resolution is therefore that of the Magnescale (1 μm) but a larger displacement (upto 25 mm) can be measured in this mode. It has to be pointed out that the accuracy of the L measurement depends on that of L_{SC} in both modes.

The molar volume of the sample V_S is related to the sample room V_{Sr} by

$$V_S(T,P) = [V_{Sr}(T,P) - n_{ptls}V_{ptls}(T,P)] / n_S \qquad (4\text{-}2)$$

where V_{ptls} is the volume of the PTL in the sample room. The pressure transmitting liquid in the bellows (PLSb) may be different from PTLS (the pressure transmitting liquid in the sample room). n_{ptls} and n_S are the amounts of PTL and the sample, respectively. The symbols in the parentheses represent independent variables; T is the temperature of the cell and P the pressure inside the cell. V_{Sr} is related to the experimental data $L(T,P)$ by the equation

$$V_{sr}(T,P) = V_{sr}(T_0,P_0) + \int_{L(T_0,P_0)}^{L(T,P)} A(L)\, dL + \Delta V_{cor}(T,P) \qquad (4\text{-}3)$$

where A is the effective cross-sectional area of the bellows in the cell. T_0 and P_0 represent the reference points of temperature and pressure; T_0 = 30 °C and P_0 = 0.1 MPa. ΔV_{cor} represents the correction term for the temperature and pressure dependence of the volume of the sample room. $V_{sr}(T_0,P_0)$ is determined from the values of V_s and V_{ptls} at (T_0,P_0) which is individually determined by other dilatometers for absolute volume measurement (picnometer etc.). The difference in thermal expansivities between the stainless steel rod and the phosphorus-copper bellows gives rise to the error of $(L-L_0)$, which is estimated to be less than 0.5 %.

ΔV_{cor} is given by

$$\Delta V_{cor}(T,P) = \int_{T_0}^{T} \alpha_e(T) \left[V_{sr}(T_0,P_0) + \int_{L(T_0,P_0)}^{L(T,P)} A(L)\, dL \right] dT + \Delta V_{cor}(P,T_0) \qquad (4\text{-}4)$$

where, α_e is the thermal expansivity of the cell, which is effectively equal to that of copper at atmospheric pressure. The second term corresponds the expansion of the cell owing to the inside pressure and so should be zero at atmospheric pressure.

Consequently, $A(L)$, $\Delta V_{cor}(P,T_0)$ and $V_{ptls}(T,P)$ should be determined by the calibration experiments where only a standard reference liquid or PTL are confined in the sample room. $A(L)$ is evaluated from the volume measurement of a standard liquid at

atmospheric pressure using eqs. 4-2 - 4-4 without the terms of $V_{ptls}(T,P)$ and $\Delta V_{cor}(P,T_0)$. The thermal expansivity of the standard liquid should be large and known as a function of temperature to allow determination of $A(L)$ for a large change of L. $\Delta V_{cor}(P,T_0)$ can be determined from the volume measurement of the liquid, whose volume is known as a function of pressure at 30 °C, at various pressures and 30 °C by using eqs. 4-2 - 4-4 with $A(L)$ determined above. $V_{ptls}(T,P)$ should be determined in the P and T ranges of interest for the present study.

4-3-2 Heat Capacity

The molar heat capacity of the sample at constant pressures (C_s) is obtained from the equation

$$C_s(T,P) = [C_{tot}(T,P) - C_e(T,L) - n_{ptls}C_{ptls}(T,P) - V_b\{L(T,P)\}C_{ptlb}(T,P)] / n_s. \quad (4\text{-}5)$$

Here, C_{tot} is the gross heat capacity. C_e, C_{ptls} and C_{ptlb} denote the heat capacities of the empty cell, a mole of PTL (in the sample room), and a unit volume of PTL (in the bellows), respectively. V_b represents the volume of the inside space of bellows. C_e, C_{cl}, C_{tr} and V_b should be determined by the following calibration experiments.

The stainless-steel rod inside the bellows is included in C_e. $C_e(T,L)$ is therefore determined from experimental data of the empty cell corrected for the heat capacity of the rod. Pressure

dependence of C_e is given by $(\partial C_e/\partial P)_T$ / C_e ~ 10^{-5} MPa^{-1}, which is negligible in the present pressure range (ca. 10^2 MPa).

$V_b(L)$ can be obtained from two series of heat capacity measurements of 1-butanol. The inside space of the bellows is empty in the first series while it is filled with 1-butanol in the second one; the sample room is filled with 1-butanol in both series. $V_b(L)$ was calculated from the difference between the total heat capacities of the two series. The molar heat capacity of 1-butanol was in advance measured at atmospheric pressure with a conventional type of adiabatic calorimeter as described in Section 4-4-5. The volume data of 1-butanol were taken from ref. [11]. $V_b(L)$ thus determined is as follows:

$$V_b/cm^3 = 8.642 + \int_{1.8532}^{L/cm} A(L)/cm^2 \, dL. \qquad (4\text{-}6)$$

$C_{ptlb}(T,P)$ can be obtained by the heat capacity and volume measurement under high pressure in which both sample room and bellows are filled with the same PTL.

4-4 Calibration and Test Experiments

4-4-1 Heat Capacity of the Empty Cell

The heat capacity of the empty cell was measured in the temperature range 280-370 K at atmospheric pressure. Both of the sample room and the inner space of the bellows were filled with

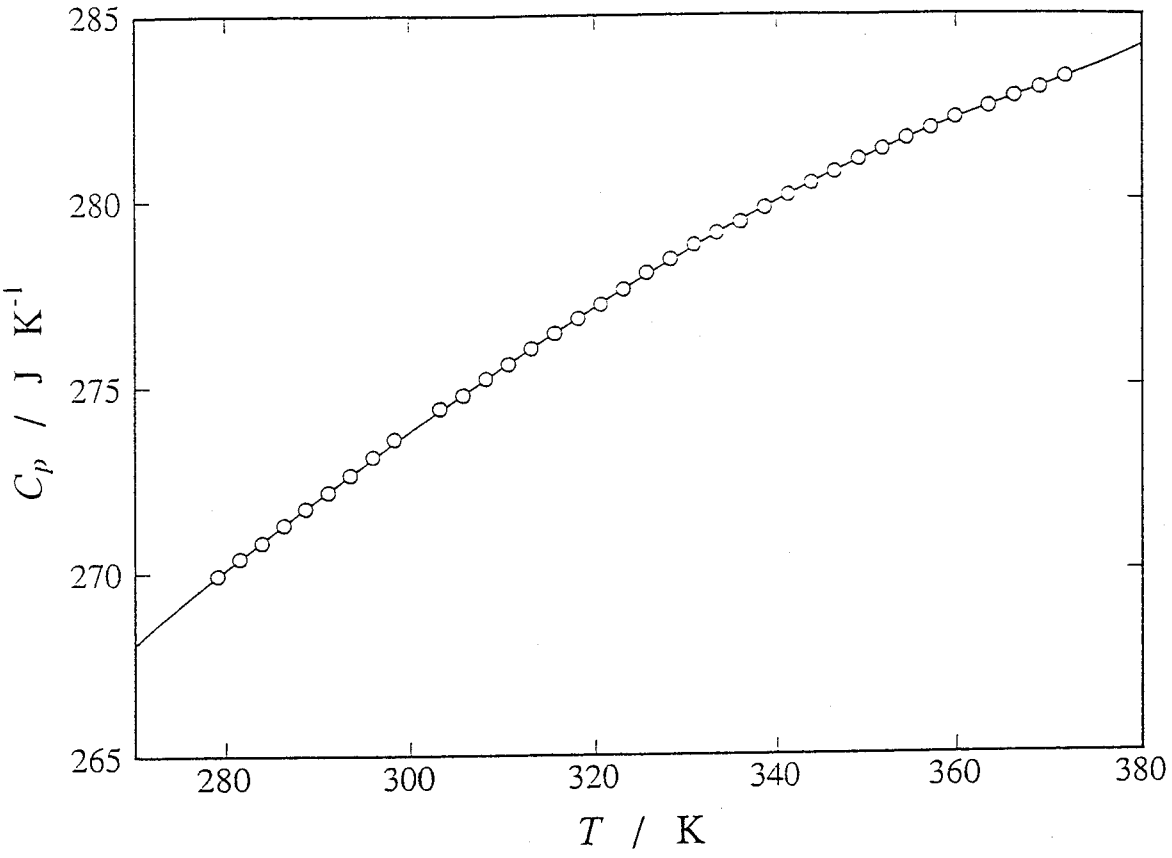

Fig. 4-5. Heat capacity of the empty cell. Solid line represents the curve smoothed by the least-squares fit.

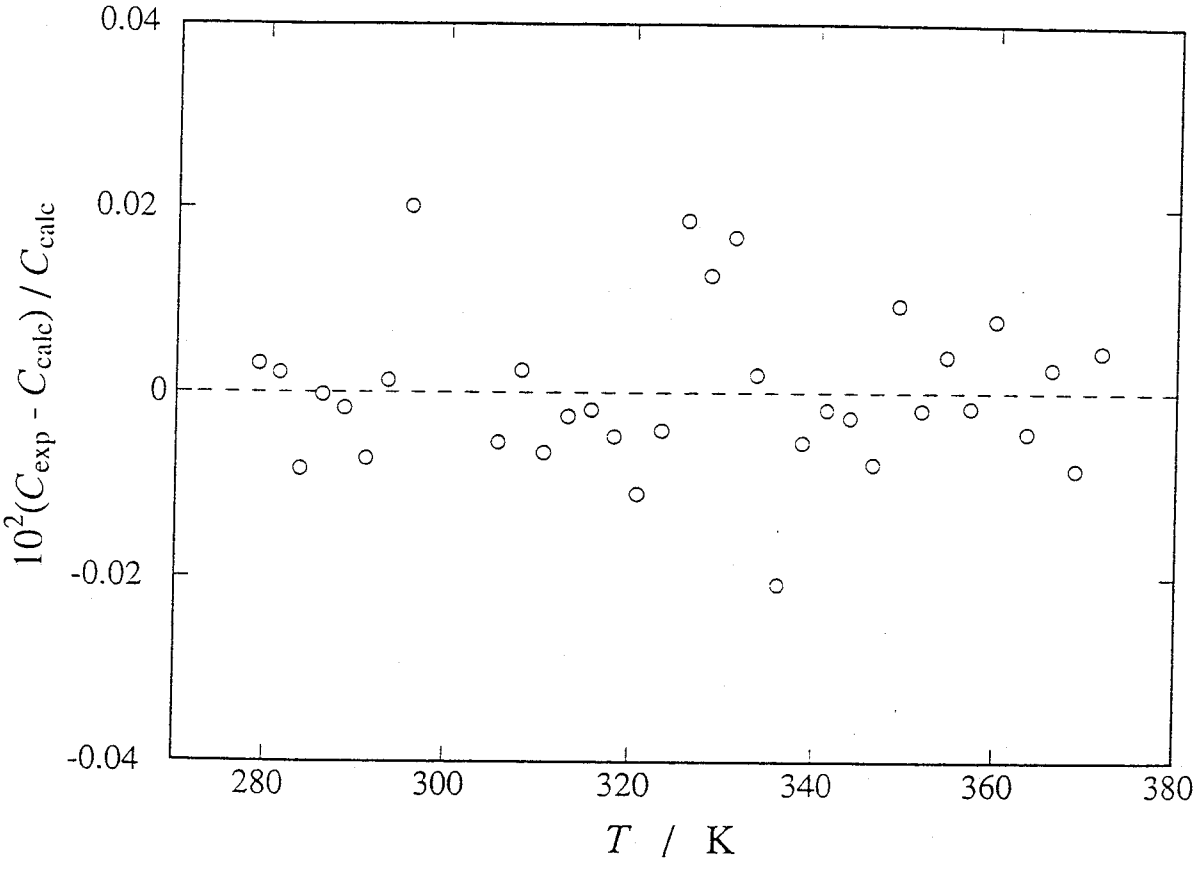

Fig. 4-6. Deviation plot of the observed heat capacities of the empty cell.

air at atmospheric pressure. The heat capacity contribution from the air is small (0.01 % of the total heat capacity) and neglected. The temperature step of a cycle of the heat capacity measurement was about 2.5 K with a heating period of 1500-2000 s. The time required for thermal equilibration after each energy input was about 5 min. The displacement of the magnet was stationary to within 0.2 mm all through the experiment.

The experimental data are plotted in Fig. 4-5. The smoothed curve (see a curve in Fig. 4-5) was obtained by fitting the data to a 6th order polynomial. Fig. 4-6 gives the percent deviation plot from the smoothed curve. The deviations are within ±0.02 % over the whole temperature range. This result is satisfactory considering the massive and complicated structure of the cell.

4-4-2 Calibration Experiment Using Toluene

The heat capacity and volume of toluene were measured simultaneously in the temperature range between 280 and 370 K at atmospheric pressure. The purpose of this measurement was to evaluate the effective cross-sectional area of the bellows in the cell using the literature volume data of toluene [12]. The precision of the volume measurement is also discussed.

Commercial reagent of toluene, whose purity was claimed to be better than 99 mol%, was purchased from Tokyo Kasei Kogyo Co. Ltd. The sample was purified by the fractional distillation with a concentric type of rectifier HC-5500-F (Shibata Kagakukikai Kogyo Co. Ltd.). The final purity of the sample was checked by gas chromatography (Perkin-Elmer F21) and no trace of organic impurity

was detected. After repeated degassing, the main distillate was poured into the sample room of the cell in vacuo. The mass of the sample loaded was 18.544 g (0.20126 mol). The inner space of the bellows was filled with air at atmospheric pressure.

The displacement of the magnet (L) was measured in the low resolution mode. The temperature step of a cycle of the heat capacity measurement was about 2.5 K with heating period of 1500-2000 s. The time required for thermal equilibration after each energy input was about 10 min. The longer equilibration time (compared with that of the empty cell) is aneffect of the sample heat capacity.

The experimental heat capacities of toluene are summarized in Table 4-1 and plotted in Fig. 4-7. The observed values of L are also plotted in Fig. 4-8. The solid curve in Fig. 4-8 is the best-fit 5th order polynomial in T. The corresponding deviation plot are shown in Fig. 4-9. Over the whole temperature range, the deviations were within ±2 μm corresponding to ±0.02 % of the maximum $L-L_0$ (ca. 10 mm) value. This uncertainty of L corresponds to an error of $\pm 4\times10^{-4}$ cm^3 ($\pm 2\times10^{-3}$ % of the total sample volume) in the volume measurement.

Fig. 4-10 shows the L dependence of the effective cross-sectional area of the bellows A, in which each point was calculated from the two adjacent V vs. L data using eq. 4-3. A second order polynomial was fitted to these data. The optimum function was

Table 4-1. Molar heat capacity of toluene.

T	$C_{p,m}$	T	$C_{p,m}$	T	$C_{p,m}$
K	$JK^{-1}mol^{-1}$	K	$JK^{-1}mol^{-1}$	K	$JK^{-1}mol^{-1}$
277.92	152.0	310.78	160.3	342.48	170.6
280.23	152.5	313.17	160.8	344.99	171.6
282.55	153.0	315.57	161.3	347.50	172.6
284.86	153.4	317.98	161.9	350.02	174.0
287.18	153.8	320.39	162.6	352.55	174.8
289.51	154.3	322.81	163.3	355.09	175.8
291.85	154.7	325.23	163.8	357.64	176.3
294.20	156.1	327.67	164.7	360.20	178.2
296.55	156.8	330.12	165.7	362.76	179.0
298.90	157.1	332.58	166.4	365.34	180.3
303.64	158.3	335.03	167.7	367.92	181.7
306.02	158.9	337.50	168.4	370.51	182.2
308.39	159.6	339.99	169.2	373.10	182.9

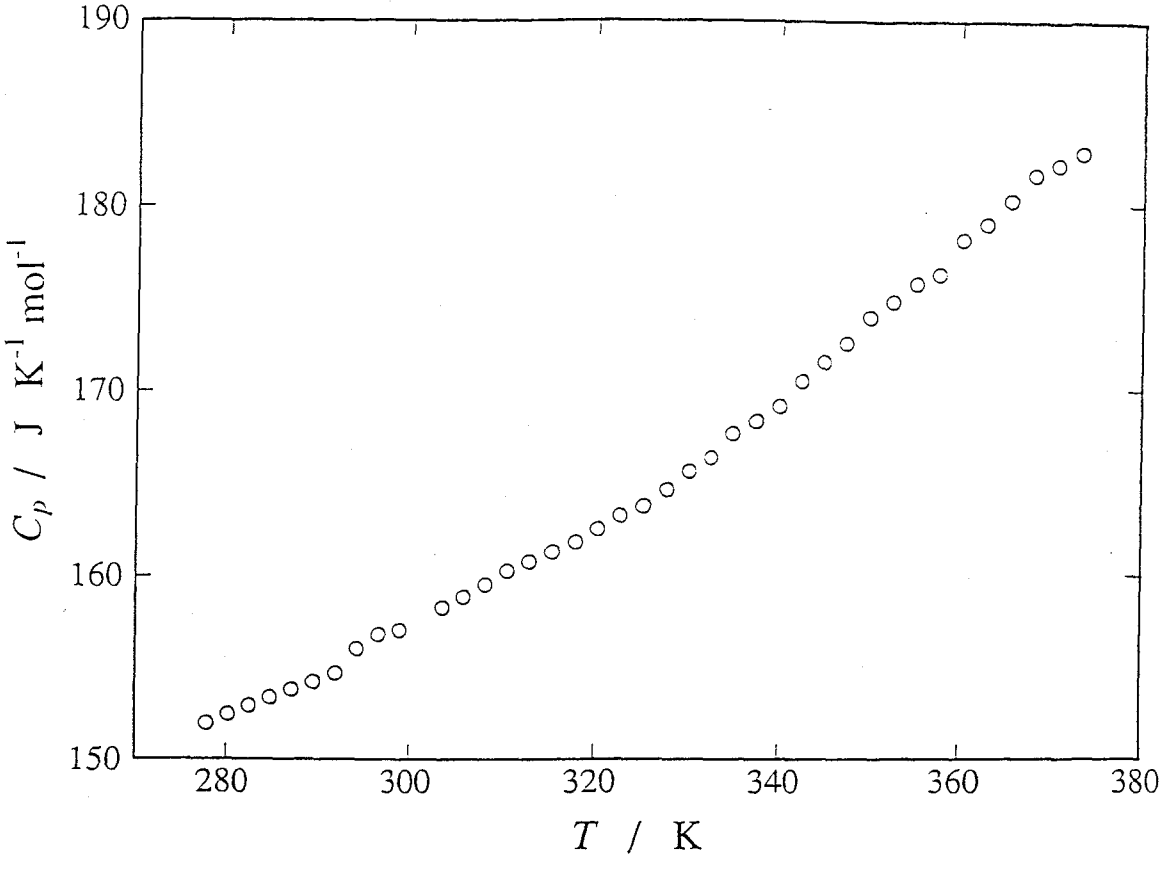

Fig. 4-7. Molar heat capacity of toluene.

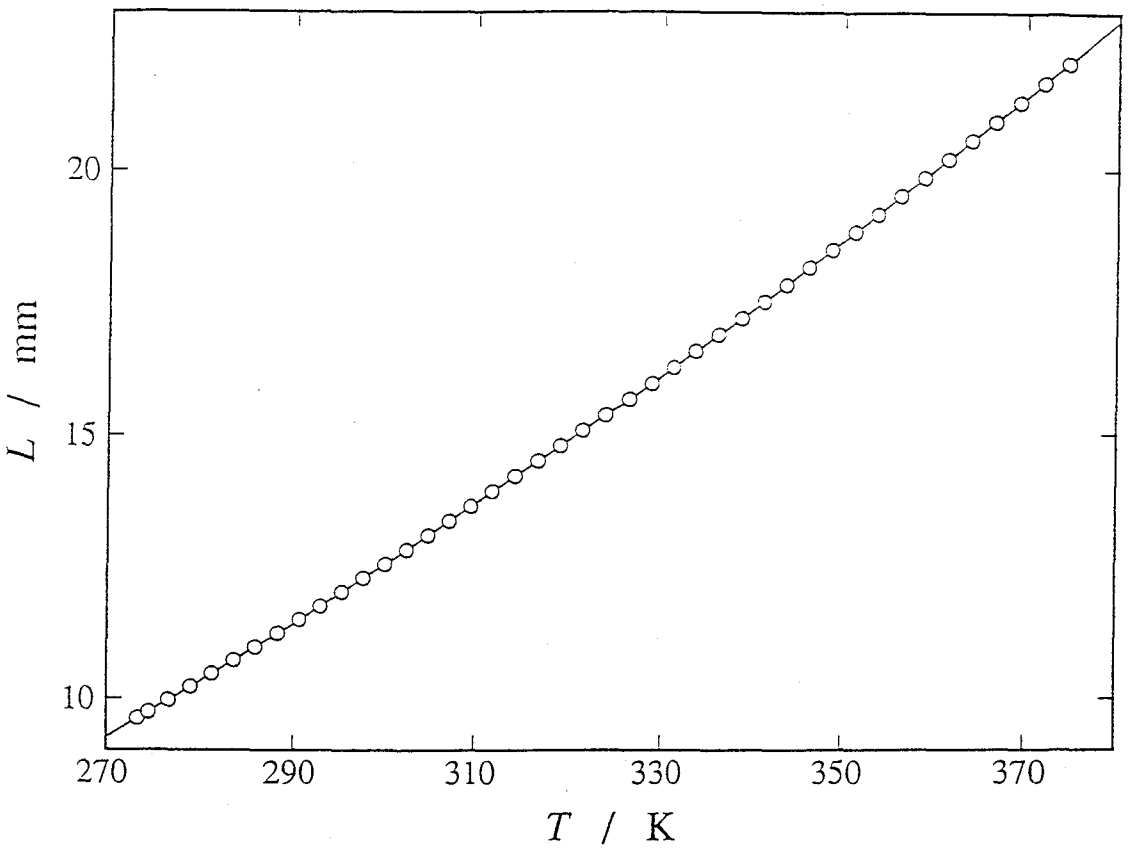

Fig. 4-8. Temperature dependence of the displacement of the bellows in the volume measurement of toluene.

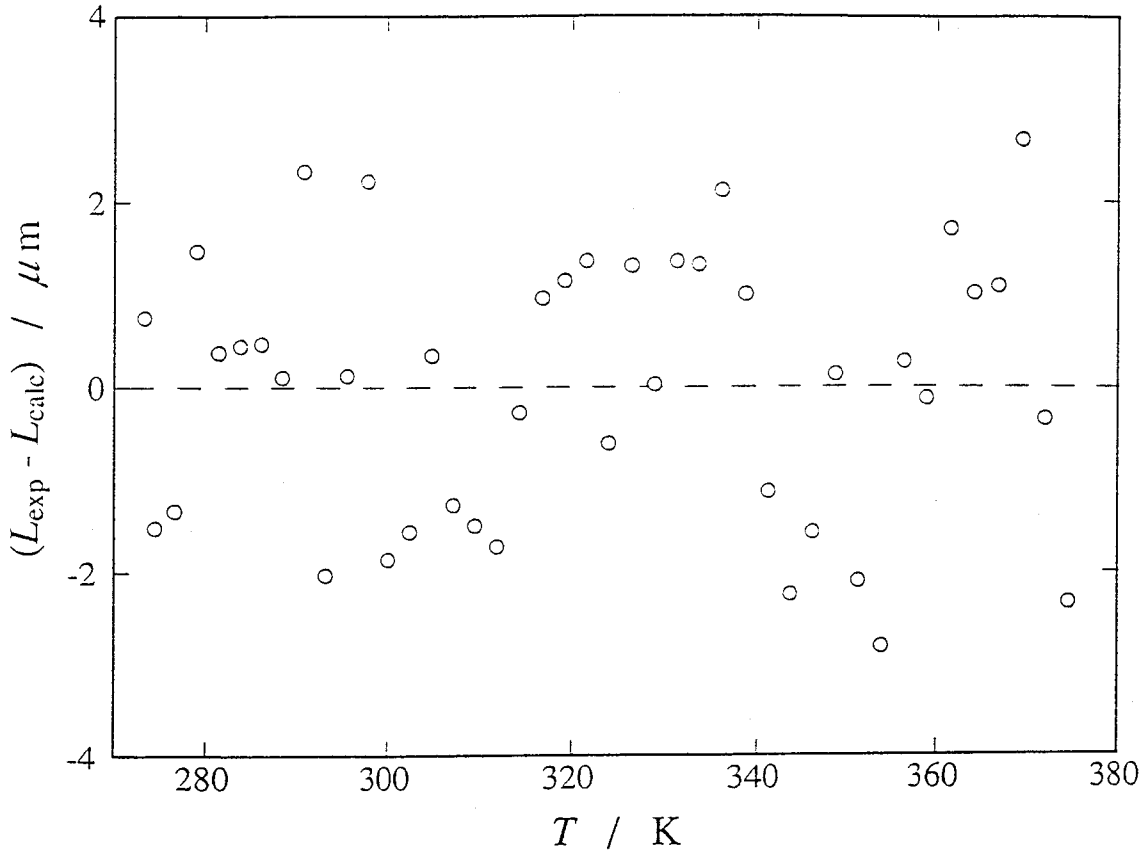

Fig. 4-9. Deviation plot of the displacement of the bellows in the volume measurement of toluene.

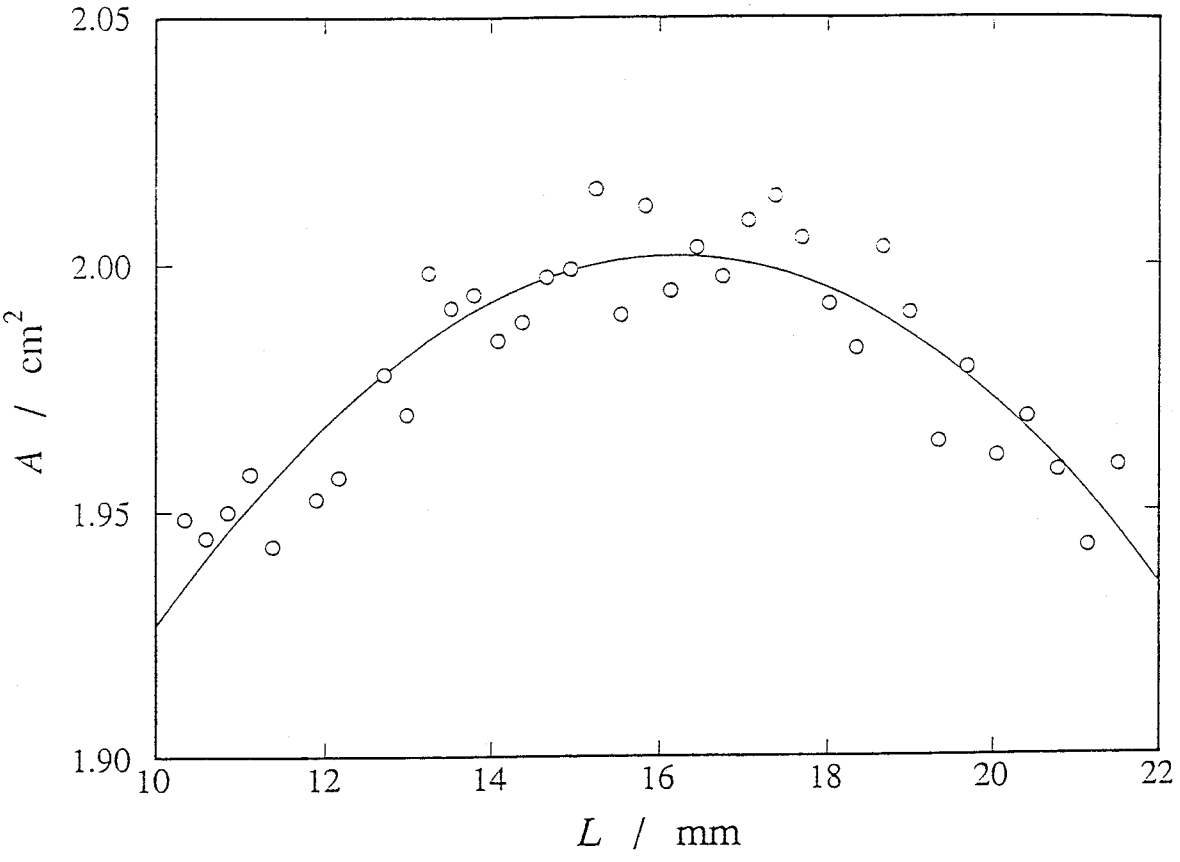

Fig. 4-10. Effective cross-sectional area of the bellows against its displacement.

$$A(L)/\mathrm{cm}^2 = 1.486 + 6.385\times10^{-2}\ (L/\mathrm{mm}) - 1.974\times10^{-3}\ (L/\mathrm{mm})^2, \quad (4\text{-}7)$$

which is shown by the solid line in Fig. 4-10. The deviations of the experimental values from this function were within ±0.015 cm^2 (±0.8 % of A).

4-4-3 Heat Capacity and Thermal Expansivity of Water

The heat capacity and volume of water were measured simultaneously in the temperature range 280-370 K at atmospheric pressure. The accuracy of the heat capacity and volume measurement is discussed using the literature values of the heat capacity [13] and volume [14] of water.

Water was purified by distillation followed by deionization. The resistivity of the purified sample was 18.3 $\mathrm{M\Omega^{-1}\ cm^{-1}}$. After repeated degassing, the purified water was introduced into the sample room in vacuo. The mass of the sample loaded was 21.449 g (1.1906 mol). The inner space of the bellows was filled with air at atmospheric pressure. The procedure of the measurement was the same as that for toluene.

The experimental heat capacities of water are tabulated in Table 4-2 and plotted in Fig. 4-11. The solid line in Fig. 4-11 represents the literature value [13]. The deviations of the experimental values from the literature curve were within ±0.2 % over the whole temperature range. This accuracy of the heat capacity measurement is as good as that of the ordinary adiabatic calorimeters. This result is rather amazingly good considering

Table 4-2. Molar heat capacites of water.

T	$C_{p,m}$	T	$C_{p,m}$	T	$C_{p,m}$
K	J K^{-1} mol^{-1}	K	J K^{-1} mol^{-1}	K	J K^{-1} mol^{-1}
		Series 1			
278.92	75.55	312.51	75.13	344.12	75.42
281.26	75.54	314.41	75.18	346.69	75.49
283.61	75.40	316.33	75.29	349.28	75.54
285.97	75.35	318.81	75.24	351.87	75.57
288.33	75.39	321.31	75.23	354.48	75.58
290.71	75.36	323.81	75.19	357.08	75.72
293.10	75.30	326.32	75.19	359.70	75.76
295.49	75.22	328.83	75.18	362.33	75.92
297.89	75.17	331.36	75.17	364.97	75.99
300.31	75.28	333.90	75.25	367.61	76.03
305.17	75.15	336.44	75.32	370.26	76.04
307.60	75.11	338.99	75.35	372.93	76.06
310.05	75.07	341.55	75.40		
		Series 2			
278.31	75.63	311.91	75.14	344.63	75.37
280.65	75.47	314.38	75.13	347.20	75.47
283.00	75.42	316.85	75.08	349.79	75.61
285.36	75.39	319.34	75.13	352.38	75.68
287.73	75.30	321.83	75.08	354.98	75.72
290.11	75.26	324.33	75.10	357.59	75.75
292.49	75.21	326.83	75.11	360.21	75.83
294.89	75.19	329.35	75.11	362.84	75.97
297.29	75.16	331.87	75.18	365.47	76.03
299.71	75.21	334.41	75.18	368.12	76.10
304.57	75.13	336.95	75.22	370.77	76.16
307.01	75.15	339.50	75.30		
309.46	75.18	342.06	75.34		

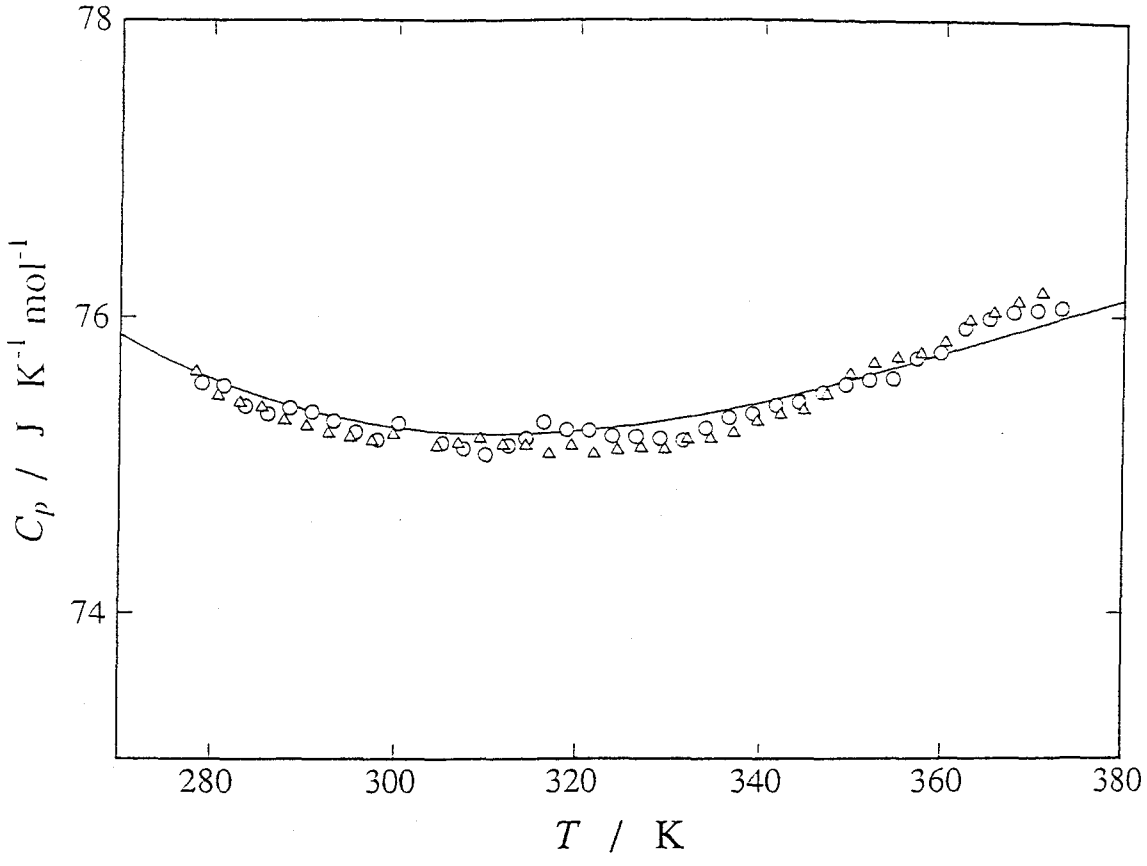

Fig. 4-11. Molar heat capacities of water. Circles and triangles denote the data in series 1 and 2, respectively. The solid line represents the literature smoothed curve [13].

Table 4-3. Molar volume of water. V_m / cm^3mol^{-1} = 18.0940 + ΔV / cm^3mol^{-1}.

T	ΔV	T	ΔV	T	ΔV
K	cm^3mol^{-1}	K	cm^3mol^{-1}	K	cm^3mol^{-1}
		Series 1			
275.43	-0.0799	306.38	0.0192	340.27	0.3053
277.76	-0.0803	308.83	0.0343	342.83	0.3327
280.09	-0.0792	311.28	0.0507	347.98	0.3905
282.43	-0.0766	313.74	0.0679	350.57	0.4202
287.15	-0.0666	315.10	0.0782	353.17	0.4510
289.52	-0.0600	317.57	0.0969	355.78	0.4828
291.90	-0.0523	320.06	0.1164	358.39	0.5152
294.29	-0.0427	325.06	0.1584	361.02	0.5486
296.69	-0.0329	327.57	0.1806	363.65	0.5828
299.10	-0.0211	332.63	0.2282	368.93	0.6539
301.51	-0.0092	335.17	0.2529	371.59	0.6907
303.95	0.0044	337.71	0.2789	374.26	0.7284
		Series 2			
275.39	-0.0798	308.23	0.0305	343.34	0.3389
277.14	-0.0804	310.68	0.0465	345.91	0.3669
279.48	-0.0795	313.14	0.0638	348.49	0.3966
281.82	-0.0774	315.61	0.0820	351.08	0.4263
284.18	-0.0736	318.09	0.1010	353.68	0.4572
286.54	-0.0686	320.58	0.1208	356.28	0.4895
288.92	-0.0617	323.08	0.1414	358.90	0.5225
291.30	-0.0542	325.58	0.1630	361.52	0.5558
293.69	-0.0453	328.08	0.1854	366.79	0.6252
296.09	-0.0352	330.61	0.2089	369.44	0.6612
298.50	-0.0244	333.14	0.2333	372.09	0.6984
300.92	-0.0120	335.68	0.2581	374.76	0.7365
303.35	0.0015	338.22	0.2845		
305.79	0.0152	340.78	0.3107		

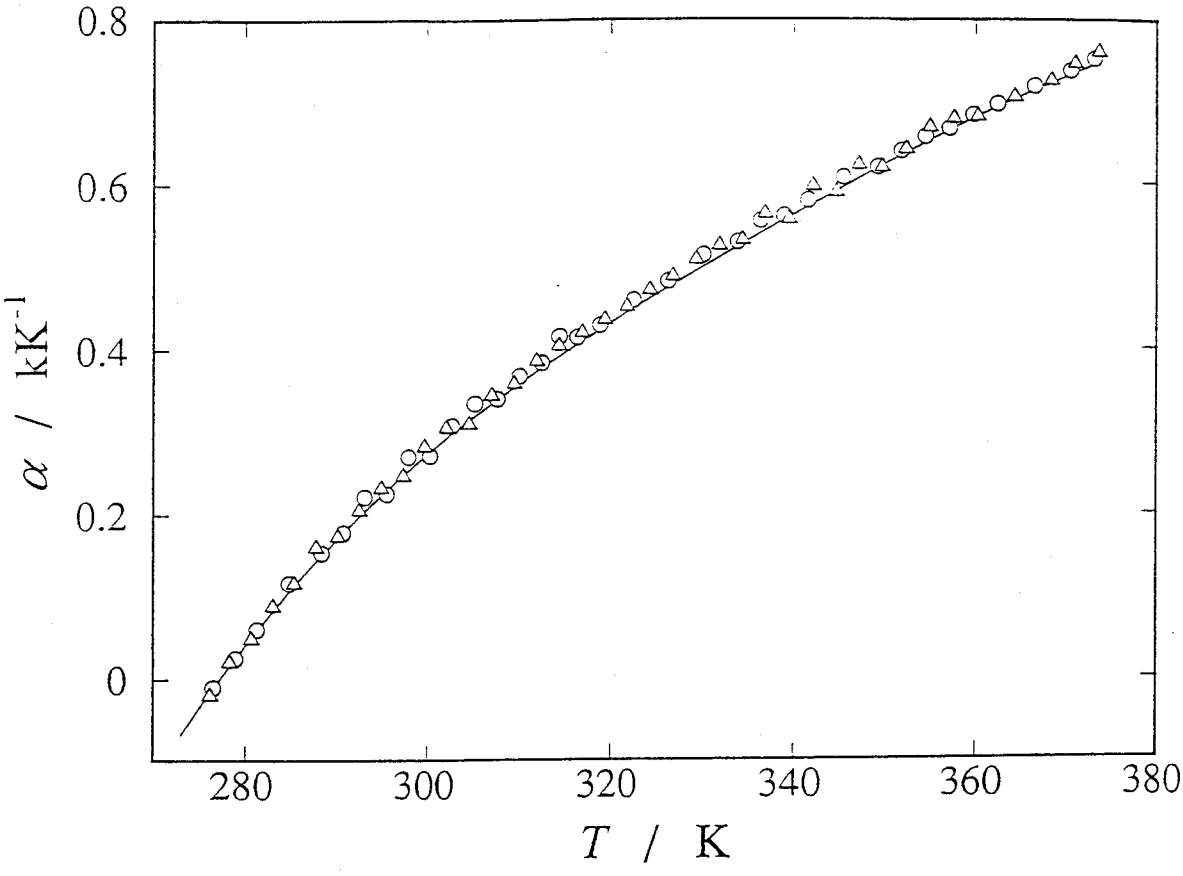

Fig. 4-12. Thermal expansivities of water. Circles and triangles denote the data in series 1 and 2, respectively. The solid line was calculated from the literature volume data [14].

the fact that the SE ratio (see section 4-3-2) of the present calorimeter is about 10 times less favorable than that of the ordinary calorimeters.

The experimental molar volumes of water are tabulated in Table 4-3. The literature value of 18.0940 cm^3 mol^{-1} [14] was used as the molar volume at the reference point (30 °C, 0.1 MPa). The thermal expansivities of water calculated from the volume data in Table 4-3 are plotted in Fig. 4-12. The solid line in Fig. 4-12 represents the value calculated from the literature data [14]. The deviations of the experimental values from the literature curve were within $\pm 2 \times 10^{-5}$ K^{-1} over the measured temperature range. This result indicate that the volumetric part of the present apparatus is as good as the best dilatometers even in the low resolution mode.

4-4-4 Heat Capacity and Thermal Expansivity of Fluorinert

The heat capacity and the volume of Fluorinert (Sumitomo 3M Co. Ltd., FC-40) were simultaneously measured in the temperature range between 280 and 370 K. This material was used as PTL for the sample room in the experiments of polystyrene described in Chapters 5 and 6.

In this measurement, the sample room of the cell was filled with Fluorinert and a copper rod because, writtn only Fluorinert filled in the cell, the volume would exceed the calibrated range of the bellows owing to the large thermal expansivity of the liquid. The copper rod whose purity was claimed to be 99.994 mol%, was purchased from Nilaco Co. The size of the rod loaded

Table 4-4. Heat capacity of Fluorinert FC40.

T	C_p	T	C_p	T	C_p
K	J $K^{-1}g^{-1}$	K	J K^{-1} g^{-1}	K	J K^{-1} g^{-1}
277.86	1.009	308.52	1.052	346.20	1.110
280.10	1.014	311.40	1.055	349.32	1.116
282.35	1.016	314.29	1.058	351.99	1.121
284.60	1.020	317.18	1.063	354.24	1.128
286.87	1.023	320.09	1.067	356.94	1.134
289.18	1.028	323.00	1.070	360.07	1.141
291.53	1.028	325.92	1.072	363.21	1.147
294.19	1.035	329.43	1.080	366.34	1.152
297.05	1.038	336.89	1.092	369.49	1.154
299.91	1.039	339.99	1.098	372.63	1.162
305.65	1.048	343.09	1.104		

Table 4-5. Volume of Fluorinert FC40. $V / cm^3g^{-1} = 0.53839 + \Delta V / cm^3g^{-1}$.

T	ΔV	T	ΔV	T	ΔV
K	cm^3g^{-1}	K	cm^3g^{-1}	K	cm^3g^{-1}
275.17	-0.01795	301.34	-0.00119	341.54	0.02751
275.56	-0.01770	304.21	0.00071	344.64	0.02994
276.75	-0.01697	307.08	0.00265	347.75	0.03236
278.98	-0.01558	309.96	0.00459	350.88	0.03486
281.22	-0.01418	312.84	0.00658	353.76	0.03717
283.47	-0.01276	318.63	0.01063	356.70	0.03959
285.73	-0.01134	321.54	0.01269	359.84	0.04220
288.01	-0.00990	324.45	0.01479	362.99	0.04483
290.35	-0.00840	327.38	0.01690	365.84	0.04724
292.71	-0.00688	327.45	0.01696	368.74	0.04975
295.62	-0.00499	330.95	0.01952	371.68	0.05232
298.48	-0.00310	338.44	0.02514	374.64	0.05494

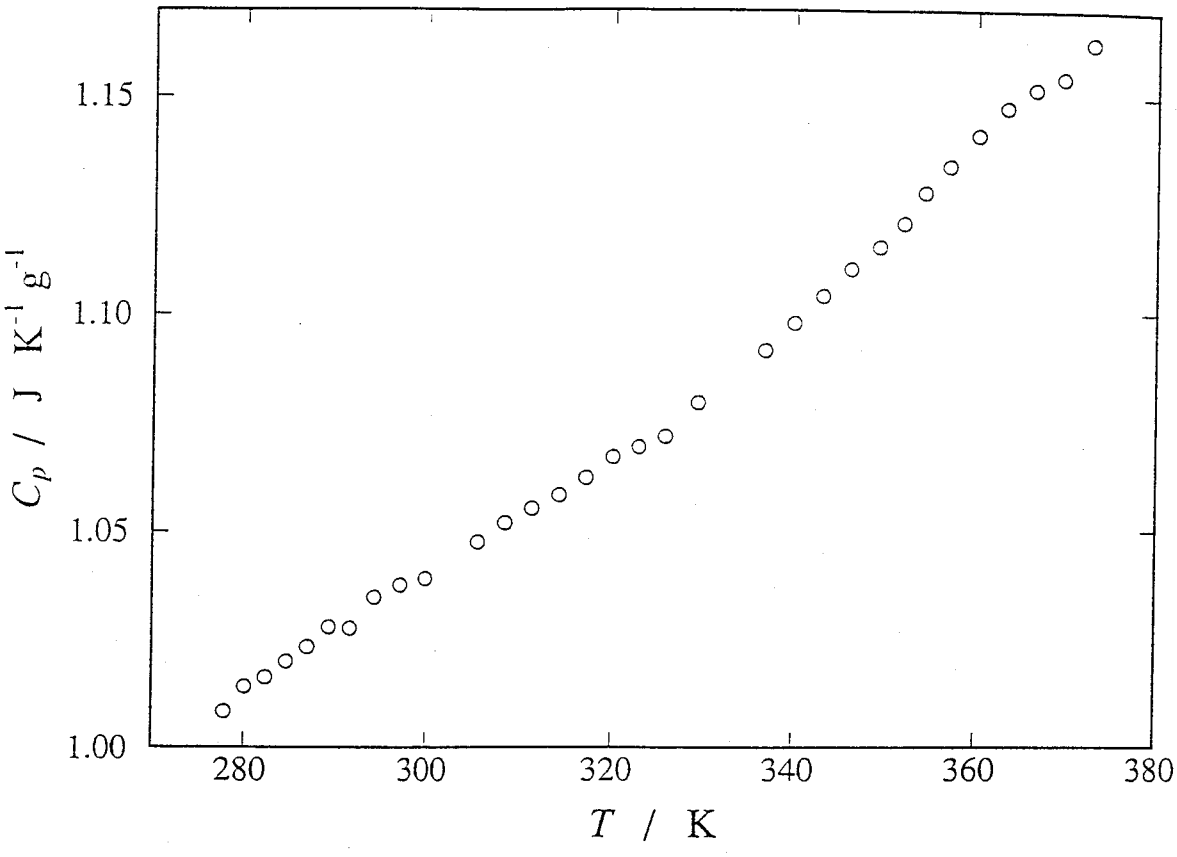

Fig. 4-13. Heat capacity of Fluorinert FC40.

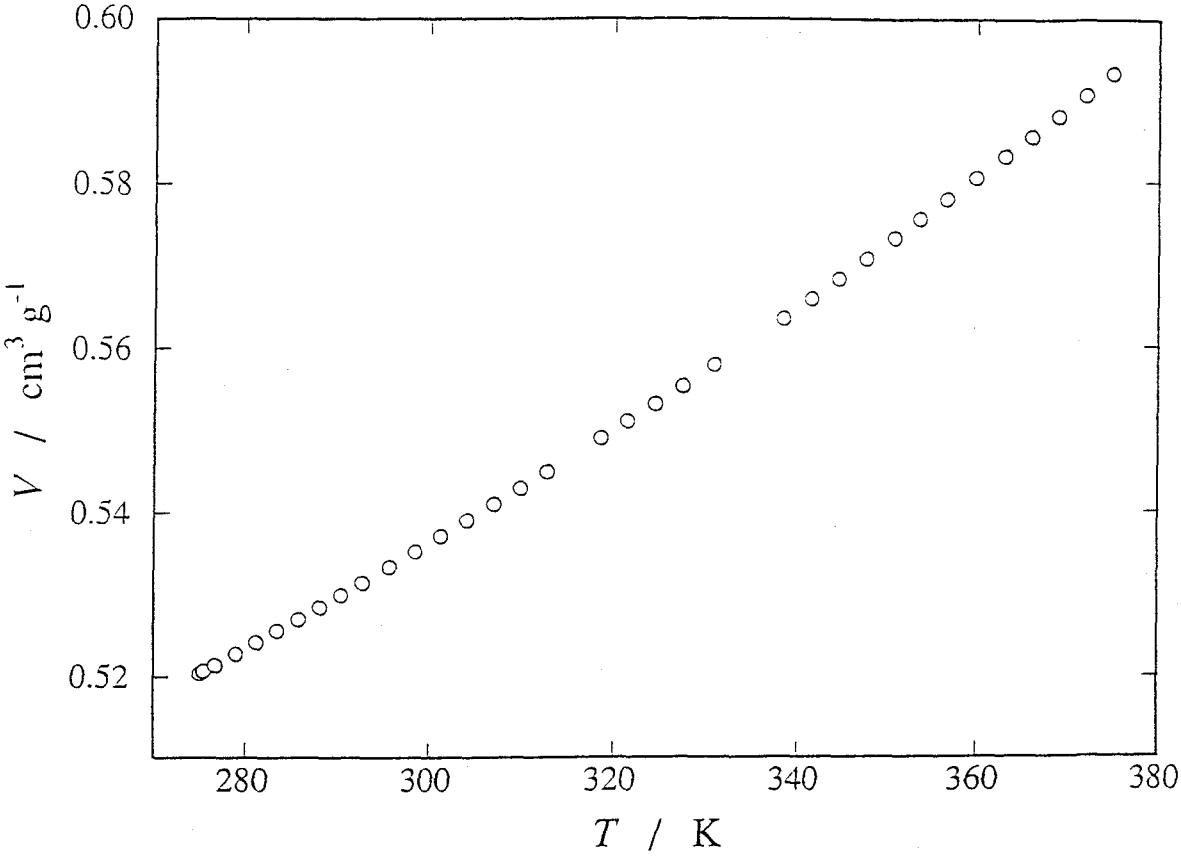

Fig. 4-14. Volume of Fluorinert FC40.

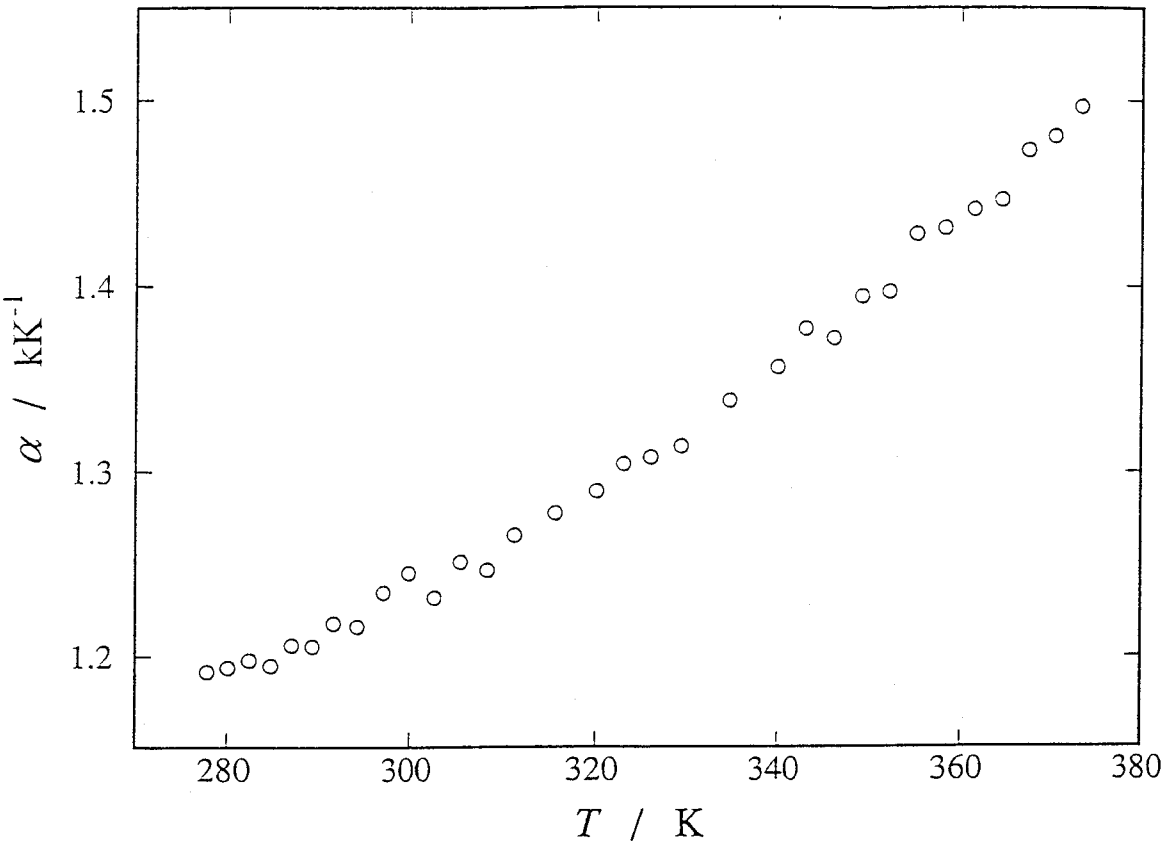

Fig. 4-15. Thermal expansivity of Fluorinert FC40.

was 12.7 mmϕ × 41.6 mm and its mass was 47.031 g. The effects of the rod were subtracted by using the literature data of the heat capacity [15] and volume [16] of copper. Fluorinert was degassed and poured into the sample room in vacuo. The mass of the Fluorinert was 30.514 g. The specific volume of Fluorinert at the reference point (30 °C, 0.1 MPa) was determined to be 0.53839±0.00003 cm^3g^{-1} with a pycnometer of the Lipkin-Davison type which was calibrated in advance by water. The inner space of the bellows was filled with air at atmospheric pressure. The procedure of the measurement was the same as that for toluene.

The experimental heat capacities and volumes of Fluorinert are tabulated in Tables 4-4 and 4-5, respectively. They are plotted in Figs. 4-13 and 4-14, respectively. The thermal expansivity of the Fluorinert calculated from the volume data is also plotted in Fig. 4-15.

4-4-5 Heat Capacity of 1-Butanol

The heat capacity of 1-butanol was measured in the temperature range 280-370 K with an adiabatic calorimeter described elsewhere [17]. This materiel was used as PTL in the experiments of polystyrene described in Chapter 5. The heat capacity of 1-butanol has already been measured in the temperature range 90-294 K [18]. The pressure of the present measurement was to extend the temperature region of the data. The volume of 1-butanol has already been reported in the temperature range 279-381 K [11].

Commercial reagent of 1-butanol, whose purity was claimed to be better than 99 mol%, was purchased from Tokyo Kasei Kogyo Co.

Table 4-6. Molar heat capacity of 1-butanol.

T	$C_{p,m}$	T	$C_{p,m}$	T	$C_{p,m}$
K	$JK^{-1}mol^{-1}$	K	$JK^{-1}mol^{-1}$	K	$JK^{-1}mol^{-1}$
275.67	163.3	309.91	185.8	345.26	215.5
278.12	164.5	312.78	188.0	348.24	218.1
281.41	166.5	315.65	190.3	351.21	220.6
284.46	168.4	318.56	192.6	354.23	223.2
287.25	170.0	321.53	195.1	357.28	225.8
290.05	171.9	324.48	197.6	360.32	228.4
292.84	173.6	327.43	200.0	363.36	230.8
295.62	175.4	330.36	202.6	366.38	233.3
298.40	177.3	333.28	205.1	369.39	235.8
301.24	179.4	336.25	207.6	372.45	238.2
304.14	181.5	339.27	210.2		
307.03	183.5	342.27	212.9		

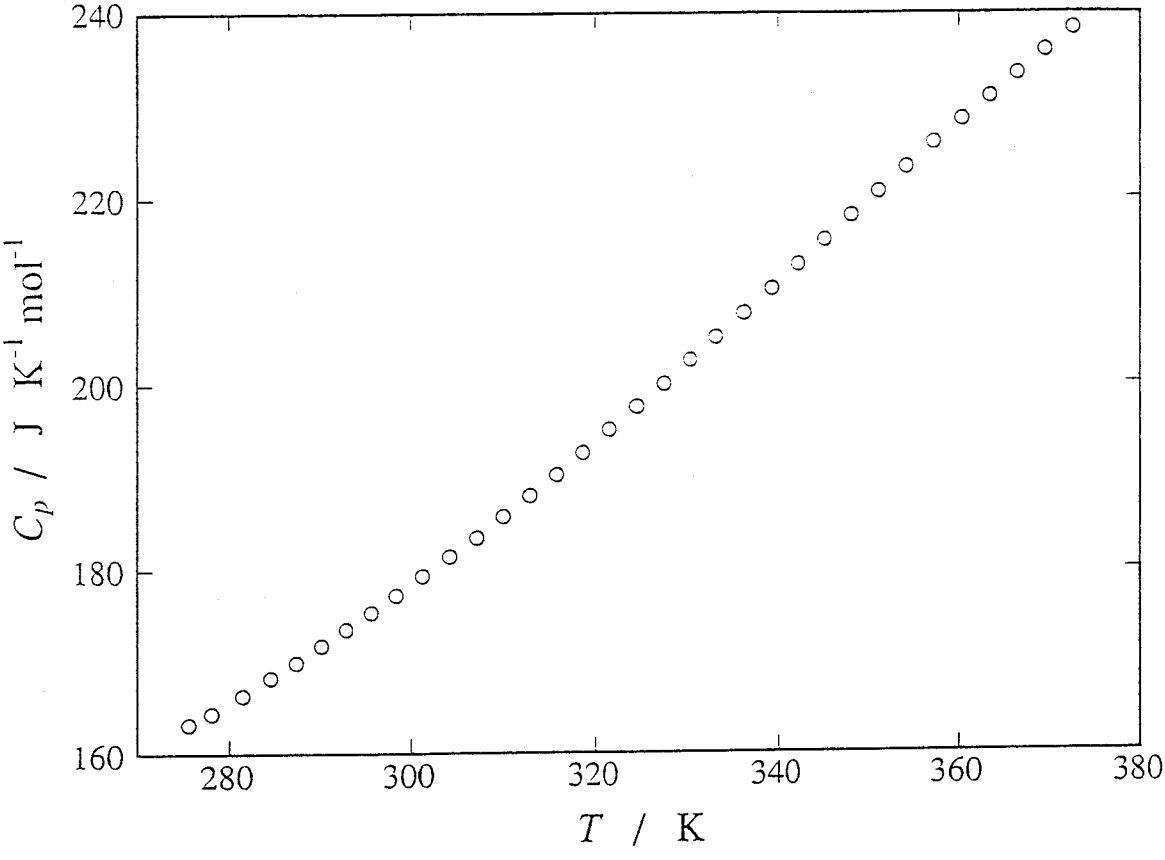

Fig. 4-16. Molar heat capacity of 1-butanol.

Ltd. The sample was purified by the fractional distillation with a concentric type of rectifier HC-5500-F (Shibata Kagakukikai Kogyo Co. Ltd.). The main distillate of 3.3081 g (4.4630×10^{-2} mol) was loaded in the calorimeter cell. Helium gas was charged into the dead space (0.92 cm^3) of the calorimeter cell to enhance the thermal equilibration between the sample and the cell. The heat capacity was measured by an intermittent heating mode. The temperature step of a cycle of the heat capacity measurement was ca. 3 K with a heating period of ca. 1000 s. The time required for thermal equilibration after each energy input was about 7 min.

The experimental heat capacities of 1-butanol are tabulated in Table 4-6 and plotted in Fig. 4-16. The heat capacities obtained in this experiment coincided with the literature values [18] around 275 K within the probable error of the previous experiment (0.2 %).

4-4-6 Volume Measurement in the High Resolution Mode

To test the precision of the volume measurement in the high resolution mode, the small volume change accompanying thermal equilibration after each energy input was monitored in the course of the experiment of water described above.

Fig. 4-17 shows the output signal of Magnesensor E_{se} (the upper panel) and the temperature of the cell T (the lower panel) after energy input. During this measurement, L_{sc} was fixed to 12.390 mm corresponding to 21.5187 cm^3 of water volume. The abscissa of Fig. 4-17 is the time t and its origin is the time at which the energy input was finished. The times required for the

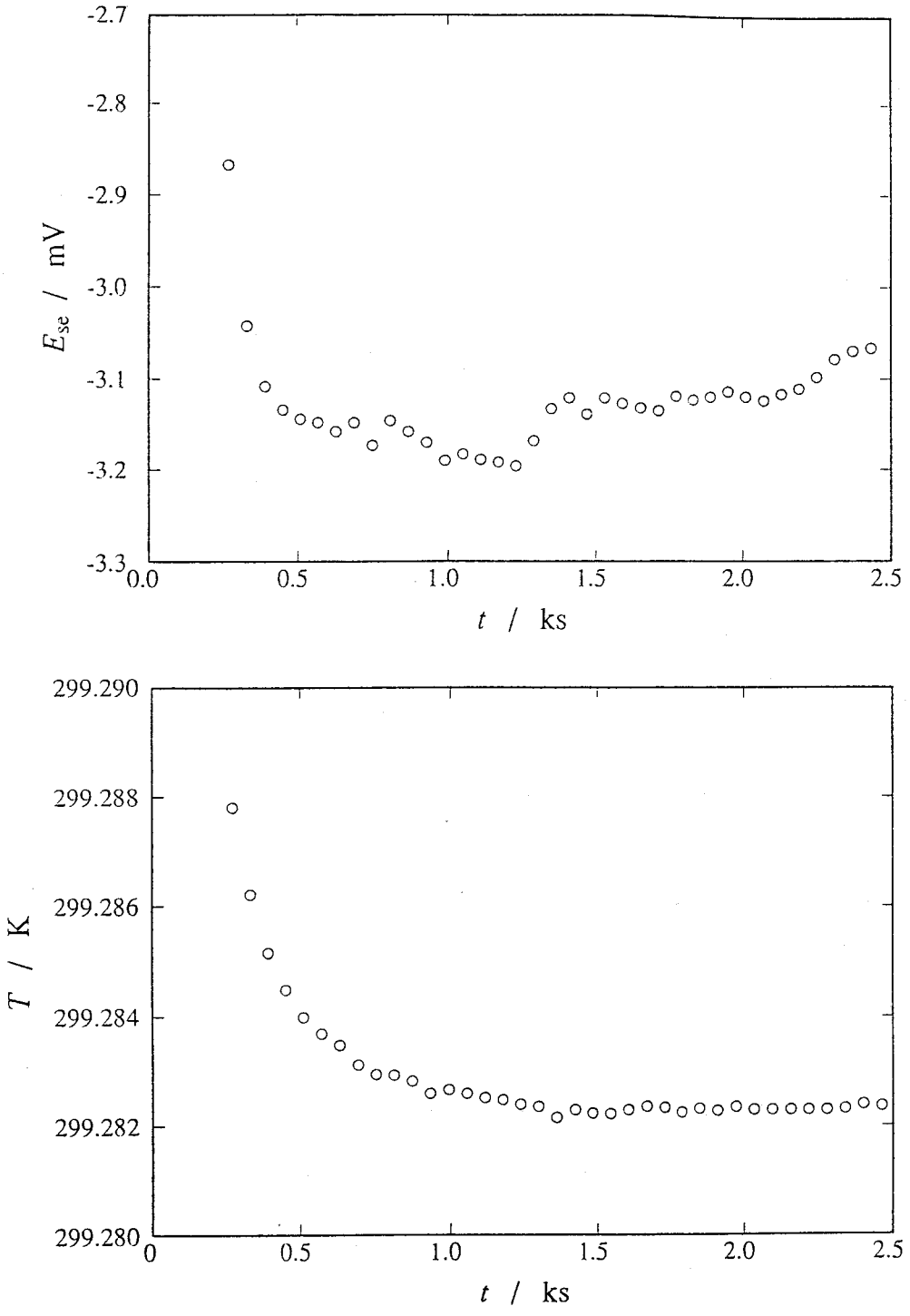

Fig. 4-17 Output signal of Magnesensor (upper) and the temperature of the cell (lower) measured after the energy input for the heat capacity and volume measurement.

thermal equilibration were ca. 10 min for E_{se} and ca. 20 min for T, respectively. From these data, the precision of E_{se} was estimated to be ±0.1 mV corresponding to ca. ±10 nm in L and $\pm 2\times10^{-6}$ cm^3 ($\pm10^{-5}$ % of total) in the volume. On the other hand, the precision of T was estimated to be ±100 μK. These precisions are good enough for the apparatus to be employed for the investigation of the structural relaxation with small volume change as described in Chapter 6. The resolution of the volume measurement attained by the apparatus is more than 10 times important over that of the best previous dilatometer.

References to Chapter 4

[1] A. Quach and R. Simha, J. Appl. Phys. 42 (1971) 4592.

[2] J.I. Berg and R. Simha, J. Non-Cryst. Solids 22 (1976) 1.

[3] H.J. Oels and G. Rehage, Macromolecules 10 (1977) 1036.

[4] P. Zoller, J. Poly. Sci. Poly. Phys. Ed. 20 (1982) 1453.

[5] M. S. Benson, P. S. Snyder and J. Winnick, J. Chem. Thermody. 3 (1971) 891.

[6] R. Landau and A. Wurflinger, Rev. Sci. Instrum. 51 (1980) 533.

[7] M. Oguni, K. Watanabe, T. Matsuo, H. Suga and S. Seki, Bull. Chem. Soc. Jpn. 55 (1982) 77.

[8] O. Yamamuro, M. Oguni, T. Matsuo and H. Suga, Bull. Chem. Soc. Jpn. 60 (1987) 1269.

[9] P. W. Bridgman, Proc. Am. Acad. Arts Sci. 66 (1931) 185.

[10] R. N. Goldberg and R. D. Weir, Pure Appl. Chem. 64 (1992) 1545.

[11] A. Zander, Lieb. Ann. 214 (1882) 138.

[12] J. S. Burlew, J. Am, Chem. Soc. (1940) 696.

[13] Thermophysical Properties of Matter vol 6, TPRC Purdue Univ. (IFI/Plenum New York-Washington, 1970).

[14] P. H. Bigg, J. Appl. Phys. 18 (1967) 521.

[15] S. M. Dockerty, Can. J. Res. 9 (1933) 84.

[16] F. L. Uffelmann, Phil. Mag. 10 (1930) 633.

[17] M. Tastumi, T. Matsuo, H. Suga and S. Seki, Bull. Chem. Soc. Jpn. 48 (1975) 3060;
T. Matsuo and H. Suga, Thermochim. Acta 88 (1985) 149.

[18] G. S. Parks, J. Chem. Phys. 47 (1925) 338.

Chapter 5

Heat Capacity, Thermal Expansivity and Compressibility of Atactic Polystyrene around Glass Transition under Pressure

5-1 Introduction

As described in Chapters 1, 3 and 4, the enthalpy and volume measurements under pressure, especially the simultaneous measurement of these quantities, provides important information on the dynamics of the undercooled liquid and the glass transition. However, the simultaneous measurement has never been performed for any materials. In the study in this chapter, the enthalpy and volume of atactic polystyrene were measured simultaneously around the glass transitions at 0.1 MPa and 21 MPa with the apparatus described in Chapter 4. Polystyrene was chosen as sample material since it has a glass transition temperature at 350 K which is suitable for the present apparatus and it is completely insoluble into Fluorinert which was the present pressure transmitting liquid (PTL). So far, some reports have been published on the enthalpy and volume measurements (not simultaneous) of polystyrene with different molecular weight. However, the accuracy of the literature data are not so high and their values differ from each other.

The first aim of the study in this chapter is to precisely determine the heat capacity gap ΔC_p, thermal expansivity gap $\Delta\alpha$, the isothermal compressibility gap $\Delta\varkappa$ at T_g and the pressure

dependence of the glass transition temperature dT_g/dP. These quantities were used for the indirect method to examine the validity of the entropy and free volume theories (see Chapter 3). If the configurational entropy S_c is constant at T_g of deferent pressures then eq. 3-4 holds, while if the free volume V_f is constant then eq. 3-6 holds. The direct method described in Chapter 3 cannot be used in polystyrene because polystyrene does not crystallize and so S_c and V_f cannot be determined experimentally. ΔC_p, $\Delta\alpha$, and $\Delta\kappa$ are used also to evaluate the Prigogine-Defay ratio $\Pi \equiv \Delta C_p \Delta\kappa / TV(\Delta\alpha)^2$ [1]. This quantity gives the information for the number of the internal parameters required to specify the glassy state thermodynamically [1,2]; i.e., if Π = 1 then one internal parameter is sufficient, and if Π > 1 then more than two internal parameters are necessary.

The second aim of the study in this chapter is to compare the temperature dependence of the enthalpy and volume relaxation rates below T_g. As the temperature of a glass increases, the structural relaxation time becomes shorter and the glassy state relaxes to the equilibrium state. This relaxation is observed as the exothermic effect (enthalpy decrease) in the calorimetric measurement and volume contraction in the dilatometric measurement. The relaxation data thus obtained contain the informations about the structural relaxation at the state far from equilibrium. The comparison between the temperature dependences of these relaxations have not been performed before.

The third aims of the study in this chapter is to demonstrate the performance of the apparatus described in Chapter 4 and

accumulate the thermodynamic data which will be used in the data analysis in Chapter 6.

5-2 Experimental

5-2-1 Sample and Pressure Transmitting Liquid

Atactic polystyrene with low (M_w = 5.97×10^{-3}) and narrowly-distributed (M_w/M_n = 1.02) molecular weight was purchased from Tosoh Co. The sample (11.350 g) was dried under vacuum at 420 K for 36 h and molded in a cylindrical cup. This cup was made of poly(chloro-trifluoroethylene) (Neoflon; Daikin Kogyo Ltd.) and can deform allowing the sample to change its volume. The mass of the cup was 3.2231 g and the dimension was as follows; height: 47 mm, outer diameter: 19 mm, thickness: 0.3 mm. The cup filled with the sample was placed in the sample room of the cell together with PTL (Fluorinert). The mass of the Fluorinert was 17.330 g. The inner space of the bellows of the cell was filled with air in the experiments at atmospheric pressure and with 1-butanol in the experiments under high pressure. The methods to charge Fluorinert and butanol into the cell have been described in Chapter 4.

5-2-2 Heat Capacity and Thermal Expansivity

Heat capacity (C_p) and thermal expansivity (α) were measured simultaneously at atmospheric pressure (0.1 MPa) in the temperature range between 280 and 380 K and at 21 MPa between 320 and 380 K. The displacement of the magnet L, was measured in the

low resolution mode. The temperature step of a cycle of the heat capacity and thermal expansivity measurement was about 2.5 K with heating period of 1500-2000 s. The time required for thermal equilibration after each energy input was about 30 min.

The glassy sample were prepared by cooling the liquid rapidly (ca. 2 K min^{-1}) under the pressure at which the Cp and α were measured. Since the main interest of this study was the evaluation of T_g and ΔC_p and $\Delta\alpha$ at T_g, the applied pressure inside the cell was not controlled and so varied between 19.1 to 21.3 MPa during the measurement owing to the thermal expansion of the sample and the PTL's (Fluorinert and 1-butanol). At T_g (360.3 K), the pressure was 20.8 MPa. The heat capacity and thermal expansivity of the glassy state were calculated by assuming the temperature and volume drifts due to the structural relaxation as if they were due to the effects of heat leakage and employing the temperature and volume extrapolated to the mid-point of each energizing period. Therefore, the obtained quantities corresponded to "instantaneous" or "iso-configurational" heat capacity and thermal expansivity, respectively

The heat capacity and thermal expansivity of the sample were evaluated from the raw data by using the method described in Section 4-3. The specific volume of the polystyrene at the reference point (30 °C, 0.1 MPa) was determined to be 0.956±0.003 cm^3/g with a pycnometer which was in advance calibrated against the volume of water. The values tabulated in Tables 4-5 - 4-7 were used for the heat capacity and volume of Fluorinert and heat capacity of 1-butanol. The molar volume of 1-butanol was taken

from the literature [3]. The heat capacity and the thermal expansivity of the Neoflon were measured at atmospheric pressure with the present apparatus. The specific volume of Neoflon at the reference point (30 °C, 0.1 MPa) was determined to be 0.4673 cm^3 g^{-1} by measuring the dimensions and the mass of a Neoflon rod. The pressure dependences of the heat capacities and the thermal expansivities of PTL's and the sample cup was estimated from their volume and compressibility data at atmospheric pressure. The errors of the data of C_p and α at 21 MPa, which were caused by the uncertainties of the above estimations and the pressure change during the measurement, were estimated to be 2 % and 10 %, respectively.

The drift rates of the temperature and volume were measured simultaneously in the course of the measurement of the heat capacity and thermal expansivity. (dT/dt) and (dV/dt) were determined by least-squares fitting using the data between 30 and 45 min after each energy input. The rate of the change in the configurational enthalpy due to the structural relaxation was calculated by

$$dH_C/dt = C_{tot}[(dT/dt)-(dT/dt)_{nat}]/w, \qquad (5\text{-}2)$$

where C_{tot} is the total heat capacity excluding the configurational part of the sample, T the observed temperature of the cell, $(dT/dt)_{nat}$ the temperature-drift rate due to the slight incompleteness of the adiabatic control and w the mass of the

sample. The drift rate of the change in the configurational volume due to the structural relaxation was calculated by

$$dV_C/dt = (dV/dt)/w - (dT/dt)(dV_{sr}^*/dT)/w, \quad (5\text{-}3)$$

where V and V_{sr}^* are the observed volume of the sample room and the volume of the sample room excluding the configurational part of the sample, respectively. The second term in the right-hand side of eq. 5-3 corresponds to the correction for the thermal expansion caused by the temperature change due to the enthalpy relaxation. The magnitude of this term was ca. 10 % of the first term through the measurement.

5-2-3 Compressibility

The sample volume was measured isothermally at several pressures (ca. every 2 MPa) between 0.1 and 10 MPa at several temperatures between 320 and 380 K. The glassy sample was prepared by cooling the liquid rapidly (ca. 3 K min^{-1}) at atmospheric pressure. The values of $(\partial V/\partial P)_T$ were obtained as a function of pressure using the volume difference between each successive pressures. The values of $(\partial V/\partial P)_T$ at atmospheric pressure were determined by the extrapolation of these data. The data thus obtained contain the contributions from all of the materials inside the sample room (sample, Fluorinert, sample cup). The compressibility of the sample cannot be determined because of lack of the compressibility data of Fluorinert and sample cup. However, its gap ($\Delta\varkappa$) at T_g can be determined because the

compressibility of Fluorinert and sample cup change continuously with temperature.

5-3 Results and Discussion

5-3-1 Heat Capacity and Thermal Expansivity

The numerical data of the heat capacity and volume of polystyrene at 0.1 MPa are tabulated in Tables 5-1 and 5-2, respectively. Figures 5-1 and 5-2 show the plots of the heat capacities and thermal expansivities, respectively. In these figures, the data at 21 MPa are shifted upward by 0.5 $JK^{-1}g^{-1}$ (C_p) and 0.5 kK^{-1} (α) for the sake of clarity. At both pressures, the precisions of the heat capacity and thermal expansivity data were 0.3 % and 3 %, respectively. A large jump due to the glass transition occurred in all of the curves. The solid straight lines represent the extrapolations of the data, which were used for the estimation of ΔC_p and $\Delta\alpha$ at T_g. ΔC_p and $\Delta\alpha$ thus determined are tabulated in Table 5-3 with their probable error. These values at 0.1 MPa agreed satisfactory with the most reliable literature values [4] shown in the brackets in Table 5-3.

5-3-2 Compressibility Gap at T_g

Fig. 5-3 shows the temperature dependence of $(\partial V/\partial P)_T$ at 0.1 MPa. A jump due to the glass transition was observed at 353 K. The solid straight lines represent the extrapolations of the data used for the estimation of $\Delta\varkappa$ at T_g. The value of $\Delta\varkappa$ was

Table 5-1. Heat capacity of atactic polystyrene.

T	C_p	T	C_p	T	C_p
K	J K^{-1} g^{-1}	K	J K^{-1} g^{-1}	K	J K^{-1} g^{-1}
279.98	1.155	314.21	1.318	346.81	1.482
282.71	1.168	316.71	1.326	349.34	1.508
285.44	1.181	319.20	1.342	351.86	1.555
288.22	1.198	321.70	1.345	354.38	1.652
290.95	1.208	324.20	1.357	356.88	1.806
293.68	1.219	326.71	1.366	359.40	1.821
296.41	1.237	329.21	1.376	361.91	1.839
299.14	1.249	334.23	1.398	364.42	1.860
304.24	1.263	336.74	1.417	366.94	1.868
306.73	1.265	339.26	1.435	369.46	1.866
309.22	1.288	341.78	1.439	371.98	1.871
311.72	1.301	344.29	1.461		

Table 5-2. Volume of atactic polystyrene. $V / cm^3g^{-1} = 0.956 + \Delta V / cm^3g^{-1}$.

T	ΔV	T	ΔV	T	ΔV
K	cm^3g^{-1}	K	cm^3g^{-1}	K	cm^3g^{-1}
286.80	-0.00348	317.95	0.00334	348.07	0.01027
289.58	-0.00292	320.45	0.00388	350.60	0.01099
292.31	-0.00235	322.95	0.00450	353.12	0.01195
295.04	-0.00176	325.45	0.00504	355.64	0.01309
297.77	-0.00108	327.96	0.00554	358.14	0.01470
300.50	-0.00047	330.47	0.00606	360.65	0.01613
303.00	0.00007	332.98	0.00664	363.17	0.01758
305.48	0.00061	335.49	0.00723	365.68	0.01901
307.98	0.00116	338.00	0.00776	368.20	0.02046
310.47	0.00169	340.51	0.00832	370.72	0.02189
312.96	0.00223	343.03	0.00898	373.25	0.02334
315.46	0.00277	345.55	0.00951		

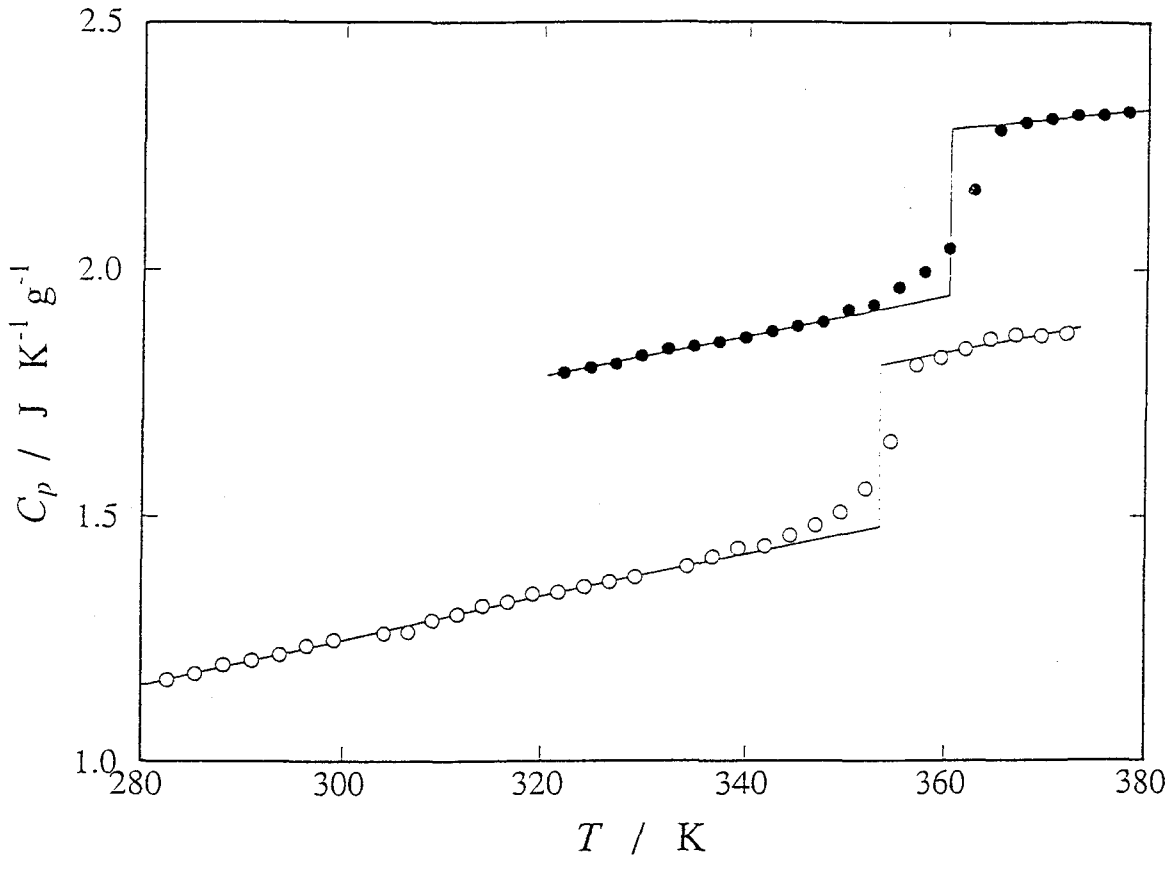

Fig. 5-1. Molar heat capacities of glassy and liquid atactic polystyrene at 0.1 MPa (open circles) and 21 MPa (closed circles). The data at 21 MPa are shifted upward by 0.5 $JK^{-1}g^{-1}$ for the sake of clarity. The solid straight lines represent the extrapolations of the data used for the determination of ΔC_p at T_g.

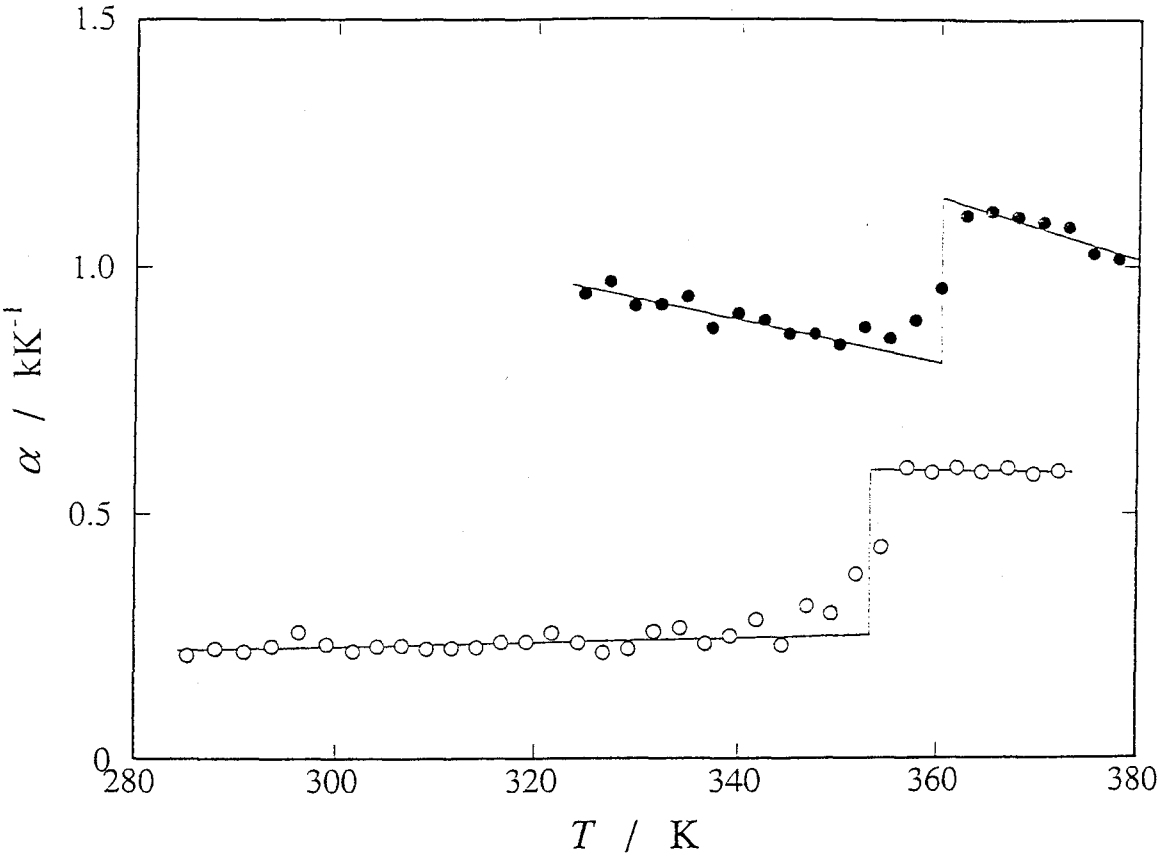

Fig. 5-2. Thermal expansivities of glassy and liquid atactic polystyrene at 0.1 MPa (open circles) and 21 MPa (closed circles). The data at 21 MPa are shifted upward by 0.5 kK^{-1} for the sake of clarity. The solid straight lines represent the extrapolations of the data used for the determination of $\Delta\alpha$ at T_g.

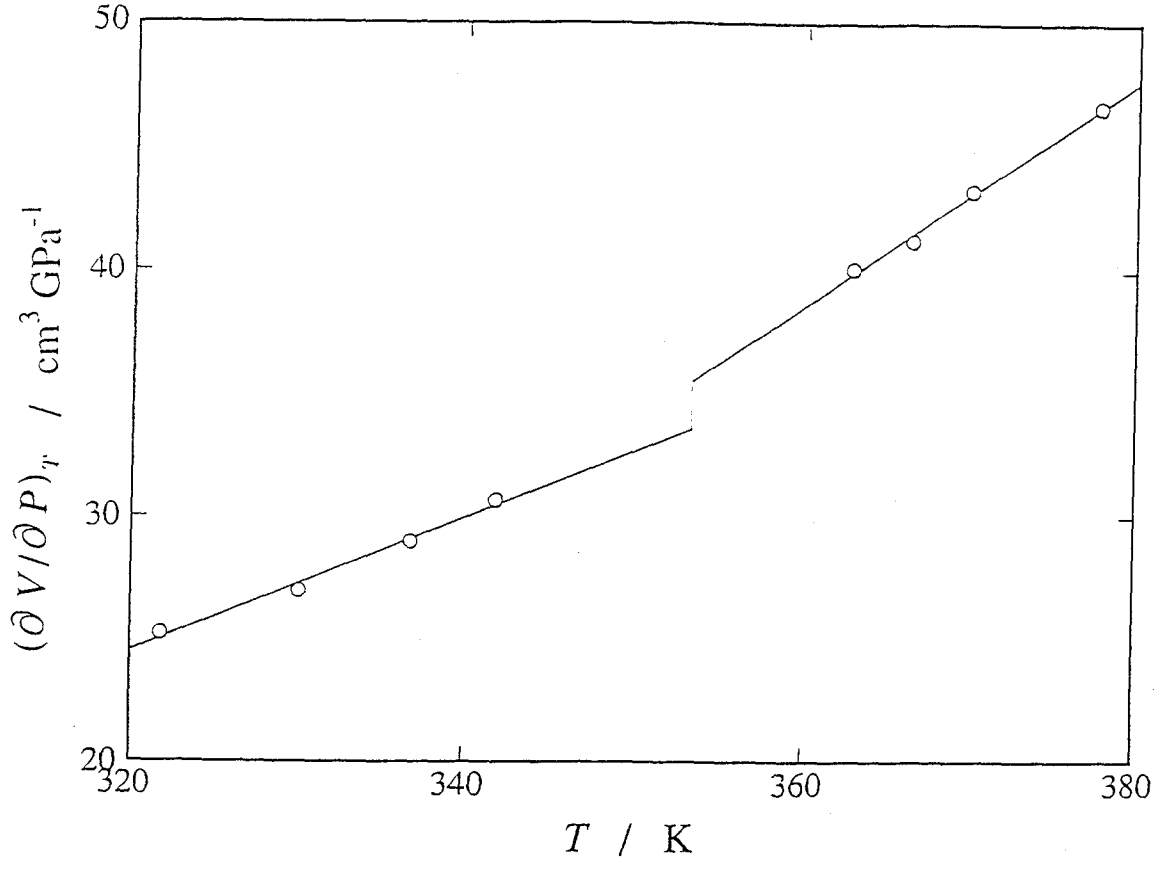

Fig. 5-3. Temperature dependence of $(\partial V/\partial P)_T$ of atactic polystyrene at 0.1 MPa. The data contain the contributions from the sample, Fluorinert and the sample cup. The solid straight lines represent the extrapolations of the data used for the determination of $\Delta\kappa$ at T_g.

Table 5-3. Thermodynamic quantities associated with the glass transition of atactic polystyrene.

P	T_g	ΔC_p	$\Delta\alpha$	$\Delta\varkappa$	V
MPa	K	$J\,K^{-1}g^{-1}$	kK^{-1}	GPa^{-1}	cm^3g^{-1}
0.1	353.3±0.3	0.33±0.03	0.34±0.02	017±0.10	0.968±0.003
		(0.30) [a]	(0.36) [a]	(0.19) [b]	
20.8±0.1	360.3±0.3	0.34±0.02	0.33±0.03	—	—

[a] The most reliable literature value [4].

[b] The most reliable literature value [5].

determined to be 0.17±0.10 GPa^{-1} by using the specific volume data shown in Table 5-1 (0.968 cm^3g^{-1} at T_g). Unexpected large temperature dependence of Fluorinert obstructed the precise extrapolation and made the uncertainty of $\Delta\kappa$ much larger than that of most reliable literature data [5]. Hence, the literature value of $\Delta\kappa$ (0.19 GPa^{-1}) was used in the discussion in Section 5-3-4.

5-3-3 Structural Relaxation below T_g

Fig. 5-4 shows the temperature dependence of the spontaneous temperature drift rates recorded during the heat capacity measurement at 0.1 and 21 MPa. The exothermic effect followed by endothermic one is a clear indication of the glass transition as described in Section 5-1. The glass transition temperatures (353.3 K and 360 K) were determined as the temperature at which the sign of the spontaneous temperature drift rate changed from positive to negative. The slope of the glass transition line (dT_g/dP) was 0.382 K MPa^{-1}.

Fig. 5-5 shows the rates of configurational enthalpy and volume change determined simultaneously at 0.1 MPa between 30 and 45 min. after the heating. The temperature dependence of the volume relaxation rates was measured for the first time. General temperature dependence of the two curves in Fig. 5-5 is similar, but they are different in finer details. This result indicates that the relaxation functions of the enthalpy and volume differ from each other at the state investigated here ,i.e., the state far from equilibrium. The direct comparison between the

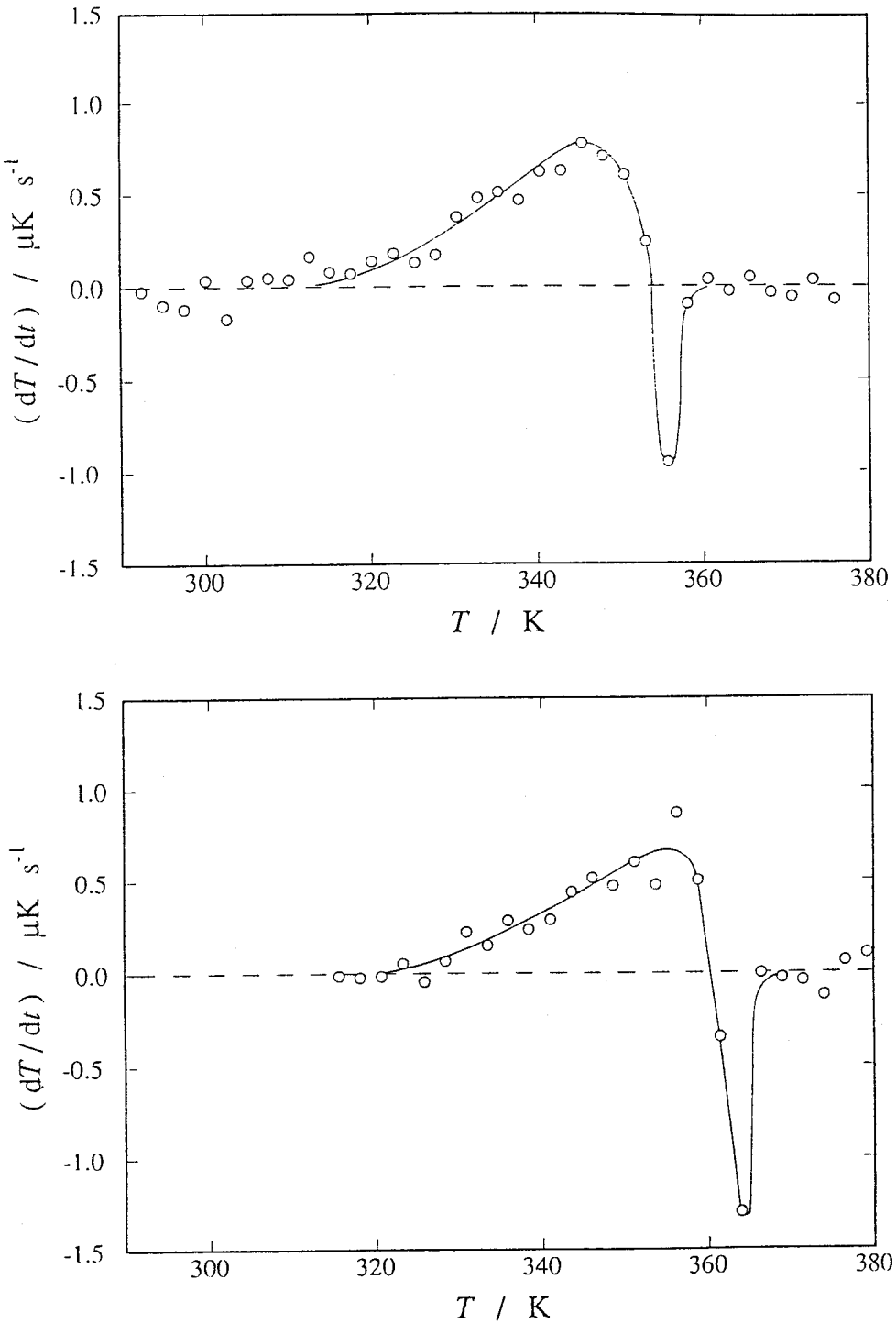

Fig. 5-4. Spontaneous temperature drift rates recorded during the heat capacity measurement of atactic polystyrene at 0.1 MPa (upper) and 21 MPa (lower).

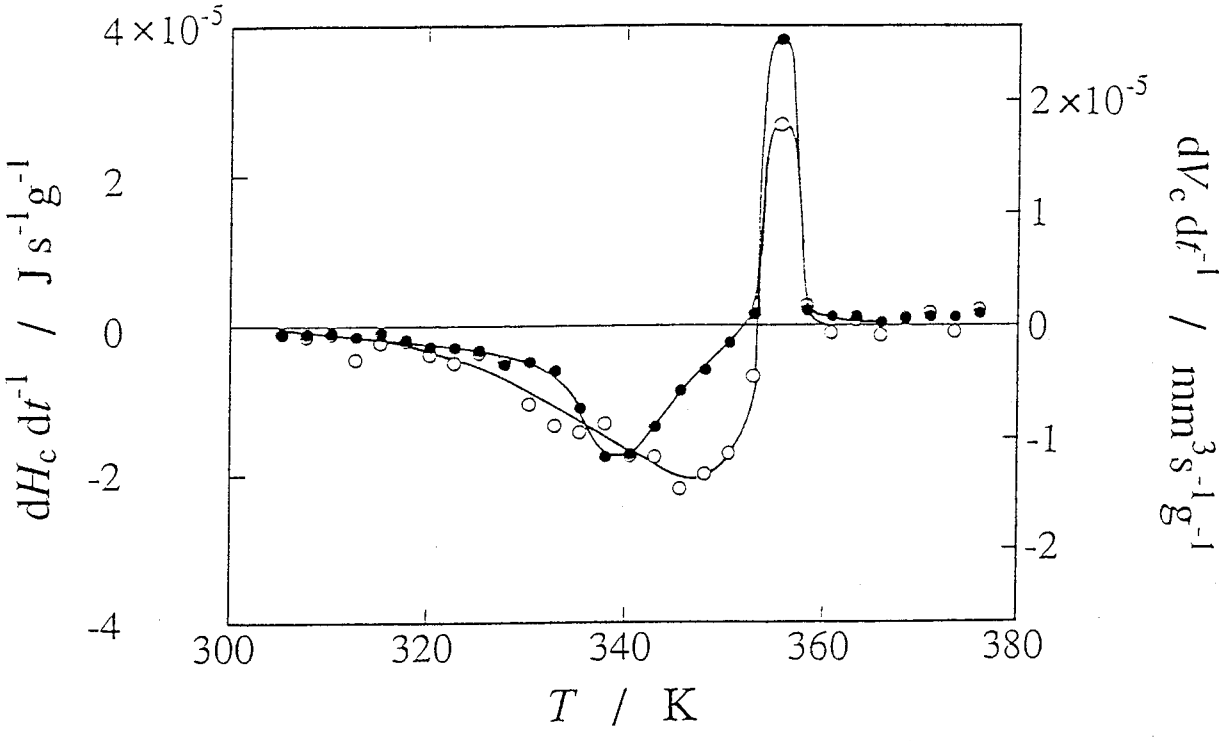

Fig. 5-5. Temperature dependence of the drift rates of configurational enthalpy (open circles) and volume (closed circles) in the simultaneous measurement of atactic polystyrene.

relaxation functions of the enthalpy and volume, though just near the equilibrium, will be performed in Chapter 6.

5-3-4 Pressure Dependence of T_g and Prigogine-Defay Ratio

To examine the validity of the entropy theory (eq. 3-4) and the free volume theory (eq. 3-6) through the pressure dependence of T_g, the quantities of $(TV\Delta\alpha/\Delta C_p)$ and $(\Delta\kappa/\Delta\alpha)$ at T_g at 0.1 MPa were calculated from the present experimental data shown in Table 5-3. They are summarized in Table 5-4 together with the experimental value of (dT_g/dP). The value of $(\Delta\kappa/\Delta\alpha)$ calculated by using the literature value for $\Delta\kappa$ and the present experimental value for $\Delta\alpha$ was also shown in the bracket in this table. It was found that $(TV\Delta\alpha/\Delta C_p)$ agreed with (dT_g/dP) within the experimental error. On the other hand, $(\Delta\kappa/\Delta\alpha)$ value calculated by using the literature value was larger than (dT_g/dP). These results indicate that the entropy theory is much better than the free volume theory to describe the pressure dependence of T_g.

The Prigogine-Defay ratio Π was calculated to be 1.6 by using the literature value for $\Delta\kappa$ and the present experimental data for other quantities. The present result ($\Pi > 1$) indicates that more than two internal parameters are required to describe the glassy state thermodynamically. This is consistent with the previous reports [2,6].

Table 5-4. The pressure dependence of the glass transition temperature, the quantities of the right-hand side of eqs. 3.4 and 3.6, and the Prigogine-Defay ratio calculated from the experimental data. the values in the brackets were calculated using the literature value for $\Delta\varkappa$..

dT_g/dP	$TV\Delta\alpha/\Delta C_p$	$\Delta\varkappa/\Delta\alpha$	Π
K MPa^{-1}	K MPa^{-1}	K MPa^{-1}	
0.34±0.02	0.35±0.03	0.5±0.3	1.5±1.0
		(0.56±0.03) [a]	(1.6±0.2) [a]

[a] The quantities calculated using the literature value [5] for $\Delta\varkappa$..

References to Chapter 5

[1] I. Prigogine and R. Defay, Chemical thermodynamics (Longmans Green, New York, 1954).

[2] P. K. Gupta and C. T. Moynihan, J. Chem. Phys. 65 (1976) 4136.

[3] A. Zander, Lieb. Ann. 214 (1882) 138.

[4] H.J. Oels and G. Rehage, Macromolecules 10 (1977) 1036.

[5] J.J. Tribone and J.M. O'Reilly, J. Polym. Sci. Polym. Phys. Ed., 27 (1989) 837.

[6] C. T. Moynihan and A. V. Lesikar, Ann. NY Acad. Sci. 371 (1981) 151

Chapter 6

Enthalpy and Volume Relaxation in Glassy Atactic Polystyrene

6-1 Introduction

As structural relaxation proceeds in a glass, its volume, enthalpy and other macroscopic properties change as functions of time. One can describe the kinetic process of a relaxing glass as a locus in a multi-dimensional space spanned by the axes representing these quantities as discussed briefly in Chapter 1.

Enthalpy H and volume V are basic thermodynamic quantities that can be measured with high accuracy and precision. There are many reports [1-6] on the enthalpy and the volume relaxations near the grass transition temperature T_g. In these reports, the relaxation functions for H and V were determined separately. However, it is obviously desirable to measure these quantities simultaneously as the relaxation proceeds. This allows accurate comparison of the relaxation functions to be made between the two quantities. Such comparison would be extremely difficult between two separately measured quantities, because two non-equilibrium states cannot be produced precisely in the same way in two apparatuses measuring two different quantities.

In the present study, the structural relaxation of polystyrene was investigated by the simultaneous measurement of H and V using the apparatus described in Chapter 4. The purpose of this study is to investigate the relaxation path in the H-V plane focusing

attention on the following two points: (I) the examination of the fictive temperature concept [7] and (II) the relation between the relaxation path and Gibbs free energy surface.

The fictive temperature is one of the traditional and important concepts on the glassy states. The fictive temperature of a glassy state is defined as the temperature at which the equilibrium liquid has the same configurational properties as that of the glassy state. If the fictive temperature concept is valid, i.e., if the fictive temperatures of different configurational properties (e.g. H and V) coincide with each other, one may regard the relaxation as taking place through the various configurations of the equilibrium liquid at atmospheric pressure.

The Gibbs free energy surface has information about the number of the microscopic states of the total system consisting of the sample and the heat bath in equilibrium. It plays an important role also in the non-equilibrium thermodynamics of systems close to the equilibrium state. In the present study, the relation between the relaxation path and the gradient of the Gibbs free energy surface was investigated based on the experimental data.

6-2 Experimental

The experiment was performed with the sample and apparatus described in Chapter 5. Before the relaxation experiment, the sample was warmed up to 373 K ($\approx T_g$ + 20 K) and then cooled rapidly down to 353 K ($\approx T_g$). The cooling rate was ca. 1.7 K

min^{-1}. The enthalpy and volume changes due to the structural relaxation were observed simultaneously as functions of time.

The enthalpy relaxation of the sample was measured as the exothermic spontaneous temperature-drift of the cell caused by the enthalpy released from the sample. The departure from the equilibrium configurational enthalpy at time t was calculated by

$$\Delta H_C(t) = [C_{tot}\{T(t_f)-T(t)\}-(dT/dt)_{nat}(t_f-t)]/w, \qquad (6\text{-}1)$$

where C_{tot} represents the total heat capacity excluding the configurational part of the sample, T the observed temperature of the cell, t_f the final time of the observation at which the relaxation has completed to within the precision of the measurement, $(dT/dt)_{nat}$ the temperature-drift rate due to the slight incompleteness of the adiabatic control, and w the mass of the sample.

The volume relaxation of the sample was measured in the high precision mode of the volume measurement system described in Chapter 4. The departure from the equilibrium configurational volume at time t was calculated by

$$\Delta V_C(t) = \{V(t)-V(t_f)\}/w + \int_t^{t_f} [dV_{sr}^*/dT]\{dT(t)/dt\}dt/w, \qquad (6\text{-}2)$$

where V is the observed volume of the sample room and V_{sr}^* the volume of the sample room excluding the configurational part of the sample. The second term in the right-hand side of eq. 6-2 corresponds to the correction for the thermal expansion caused by

the temperature change due to the enthalpy relaxation. The magnitude of this term was ca. 10 % of the first term through the measurement.

It took ca. 3.5 days to obtain constant temperature and volume drifts within the resolution of each measurement (temperature: 100 μK, volume: 2×10^{-6} cm^3). As a reference experiment, the sample was rapidly cooled down to 365 K ($\approx T_g$ + 12 K), where the sample was free from any relaxation processes in the relevant time scale. It took ca. 30 min to obtain thermal equilibrium in the cell. In the measurement of the structural relaxation, therefore, the temperature and volume measurements were started at 30 min after the rapid cooling.

6-3 Results

Fig. 6-1 shows the relaxation functions corresponding to $\Delta H_C(t)$ (open circles) and $\Delta V_C(t)$ (closed circles) measured simultaneously. The abscissa of the graph is the time t and its origin is the time at which the rapid cooling was finished. The relaxation functions (ϕ) were derived by scaling $\Delta H_C(t)$ and $\Delta V_C(t)$ by the amplitudes of the relaxation; i.e.,

$$\phi(t) = \Delta H_C(t)/\Delta H_C(t_i) \text{ or } \Delta V_C(t)/\Delta V_C(t_i). \qquad (6\text{-}3)$$

Here, t_i = 30 min (1.8 ks), which is the initial time of the measurements. $(dT/dt)_{nat}$ used in the calculation of $\Delta H_C(t)$ was

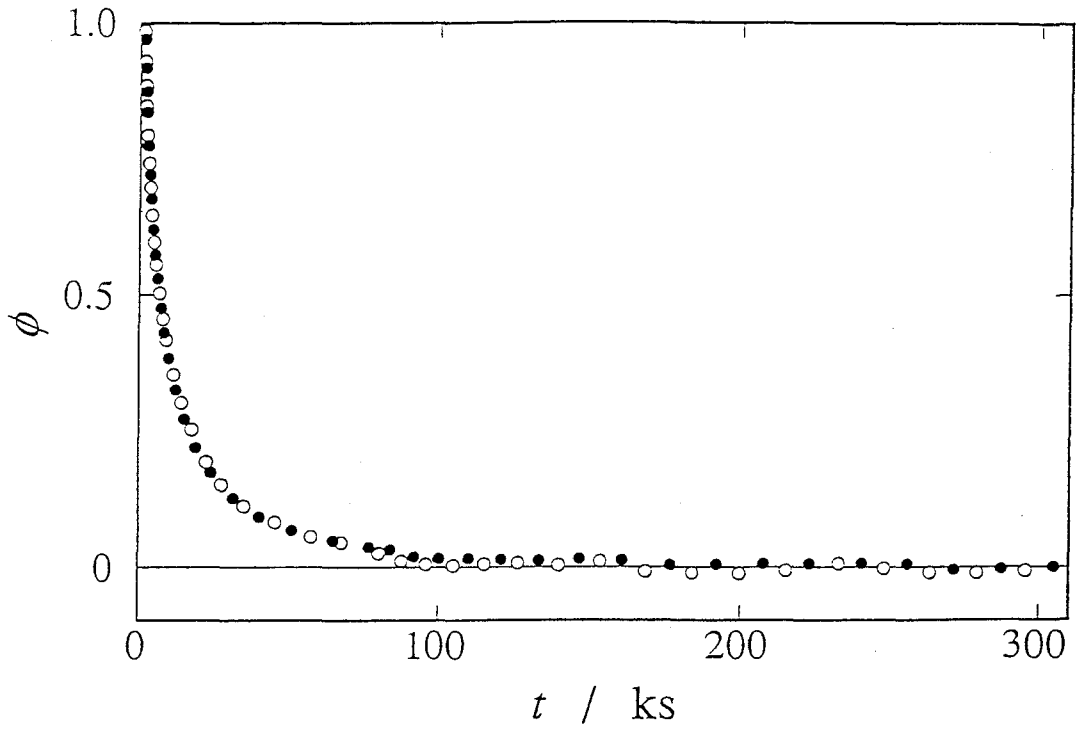

Fig. 6-1. Relaxation functions of glassy atactic polystyrene for the configurational enthalpy (open circles) and volume (closed circles) relaxations measured simultaneously.

estimated to be -4.07×10^{-8} K s^{-1} from the least-squares fit using $T(t)$ data in the period t = 160 - 305 ks. $\Delta H_C(t_i)$ and $\Delta V_C(t_i)$ were 0.817 $J\ g^{-1}$ and 0.637 $mm^3\ g^{-1}$, respectively. These amplitudes correspond to ca. 20 mK of temperature and 0.27 V of output signal of the Magnesensor, respectively.

It was found that the relaxation functions for enthalpy and volume after t_i were similar to each other within the experimental errors. The present data themselves are quite significant as the first successful data of the simultaneous measurement of the enthalpy and volume relaxation near T_g. It is noteworthy that the precision of the volume measurement was better than that of the enthalpy measurement.

6-4 Discussion

6-4-1 Examination of the Fictive Temperature Concept

The experimental data of ΔH_C and ΔV_C measured simultaneously are plotted in Fig. 6-2 by the open circles. This graph gives the relaxation path of the glassy polystyrene in the ΔH_C-ΔV_C plane. The relaxation proceeds from the upper-right to the lower-left in the graph and terminates at the origin corresponding to the equilibrium state. The solid line in Fig. 6-2 represents the equilibrium line; i.e., the ΔH_C - ΔV_C relation in the equilibrium states at various temperatures under atmospheric pressure. This line was calculated from the experimental data of the excess heat capacity and thermal expansivity above T_g.

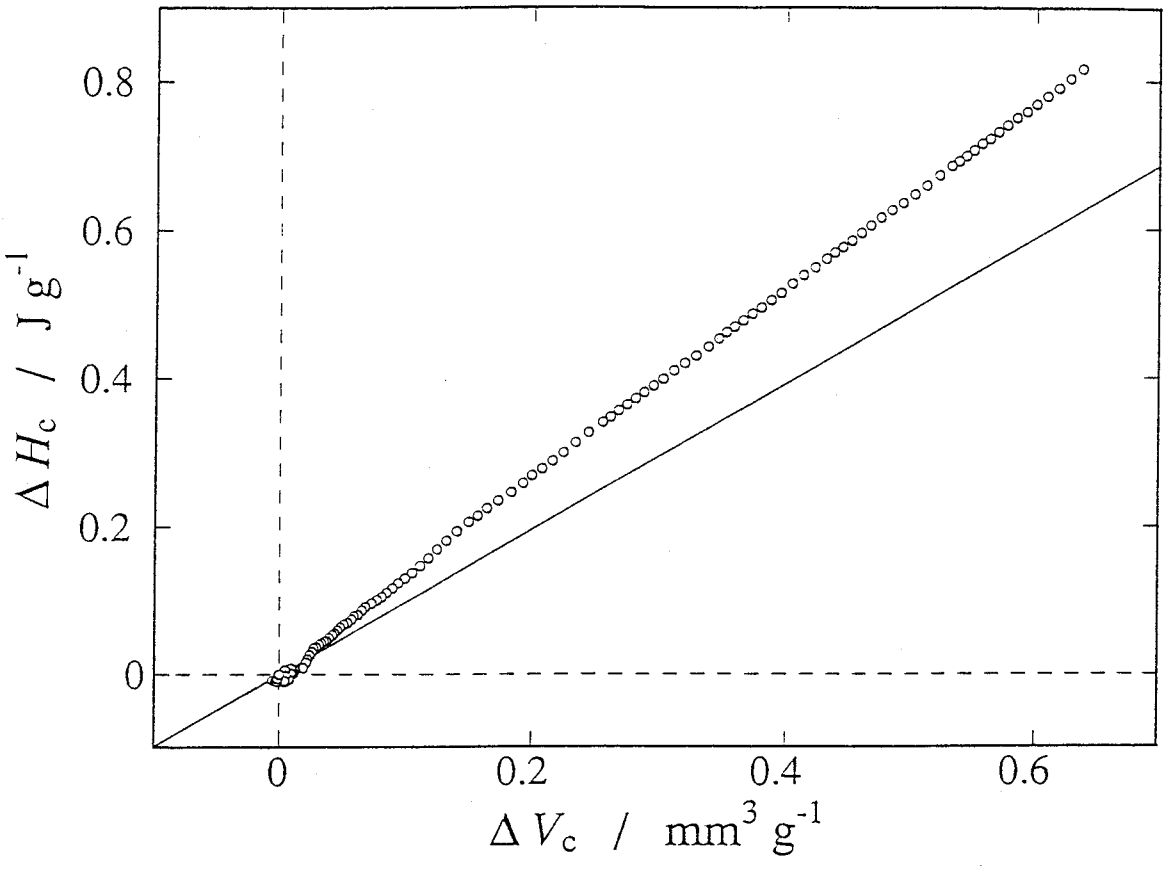

Fig. 6-2. Relaxation path of glassy atactic polystyrene in the ΔH_C-ΔV_C plane. The solid line represents the equilibrium line.

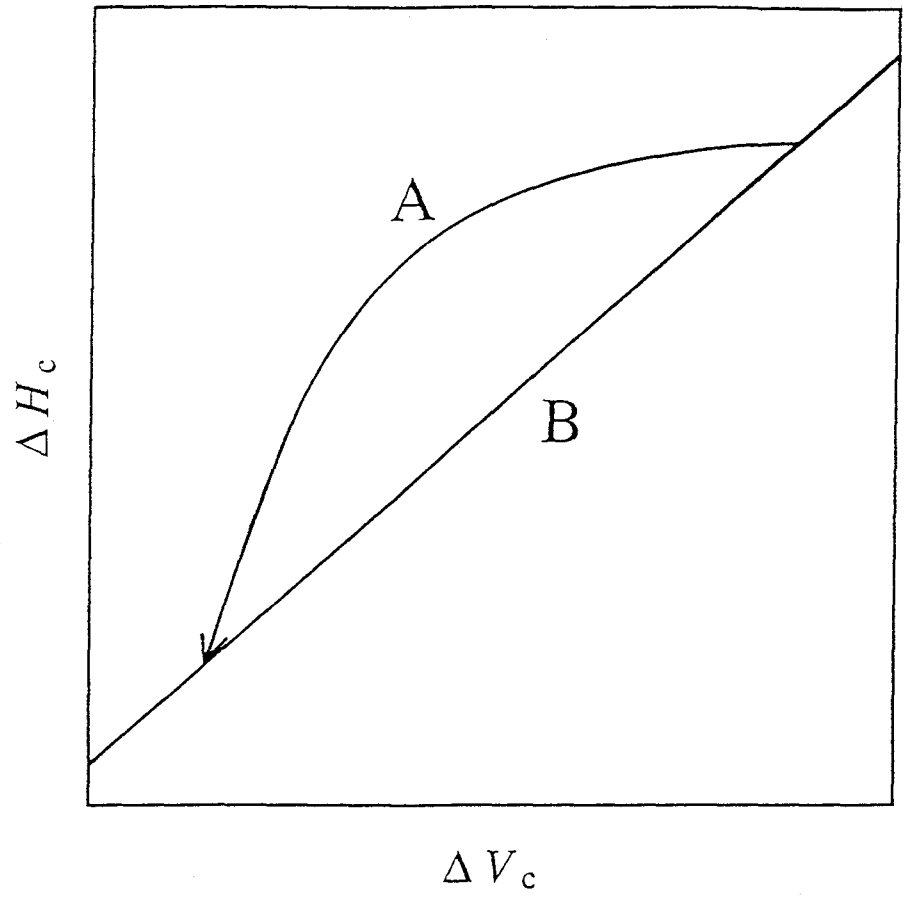

Fig. 6-3. Schematic diagram of the relaxation path in the ΔH_C-ΔV_C plane. See text for the details.

The relaxation path in the ΔH_C-ΔV_C plane was found to be almost straight. This is expected from the result described in the last section; i.e., the relaxation functions of the enthalpy and volume are similar to each other. The most important result in this chapter is that the observed relaxation path did not coincide with the equilibrium line. This indicates that the fictive temperature concept is invalid in the structural relaxation of polystyrene even in a close vicinity of equilibrium state.

Since the sample was in the equilibrium state before the rapid cooling, the initial point of the relaxation path should lie on the equilibrium line. This means that the whole relaxation path in the ΔH_C-ΔV_C plane is not straight but convex and initially the volume relaxed faster than the enthalpy. This is schematically shown by Fig. 6-3. The line A corresponds to the observed relaxation path and the line B the equilibrium line.

It is very important to determine whole relaxation path in the ΔH_C-ΔV_C plane experimentally. The improvement of the apparatus and some advanced data analysis (e.g. deconvolution of the structural relaxation and thermal equilibration allowing for temperature distribution in the cell) are necessary to obtain the relaxation data within 30 min of the rapid cooling.

6-4-2 Gibbs Free Energy Surface and Relaxation Path

In this section, the Gibbs energy surface is considered as the functions of the departure from the equilibrium configurational energy (ΔE_C) and the departure from the equilibrium configurational volume (ΔV_C). ΔE_C is derived from ΔH_C by

$$\Delta E_C = \Delta H_C - P_0 \Delta V_C, \tag{6-3}$$

where P_0 is the external pressure (0.1 MPa). In practice, however, ΔH_C was used as ΔE_C without any correction because the second term in the right-hand side of eq. 6-3 was negligibly small (0.01 % of ΔH_C).

The departure from the equilibrium configurational Gibbs free energy (ΔG_C) is expressed as

$$\Delta G_C = \Delta E_C + P_0 \Delta V_C - T_0 \Delta S_C, \tag{6-4}$$

where T_0 is the external temperature (353 K) and ΔS_C the departure from the equilibrium configurational entropy. Expanding ΔG_C about its minimum (i.e. equilibrium state) in powers of ΔE_C and ΔV_C as far as the second order term, one obtains

$$\Delta G_C = (\partial^2 G_C/\partial E_C{}^2)\Delta E_C{}^2/2 + (\partial^2 G_C/\partial E_C \partial V_C)\Delta E_C \Delta V_C + (\partial^2 G_C/\partial V_C{}^2)\Delta V_C{}^2/2. \tag{6-5}$$

The second differential coefficients of G_C in eq. 6-5 can be calculated from ΔC_p, $\Delta\alpha$ and $\Delta\varkappa$ by

$$\begin{pmatrix} (\partial^2 G_C/\partial E_C{}^2) & (\partial^2 G_C/\partial E_C \partial V_C) \\ (\partial^2 G_C/\partial E_C \partial V_C) & (\partial^2 G_C/\partial V_C{}^2) \end{pmatrix} = \frac{1}{kT_0} \begin{pmatrix} (T_0 \Delta C_p - 2T_0 P_0 V_0 \Delta\alpha + P_0{}^2 V_0 \Delta\varkappa) & (T_0 V_0 \Delta\alpha - P_0 V_0 \Delta\varkappa) \\ (T_0 V_0 \Delta\alpha - P_0 V_0 \Delta\varkappa) & (T_0 V_0 \Delta\varkappa) \end{pmatrix}^{-1}. \tag{6-6}$$

where V_0 is the equilibrium volume of the sample, k the Boltzmann constant. Using the experimental values of ΔC_p, $\Delta\alpha$ and V_0 obtained in Chapter 5 and the literature value of $\Delta\varkappa$ [8], ΔG_C was numerically expressed by

$$\begin{aligned}(\Delta G_C/\mathrm{Jg^{-1}}) = {} & 3.29\times10^{-5}\,(\Delta E_C/\mathrm{Jg^{-1}})^2 \\ & -4.15\times10^{-5}\,(\Delta E_C/\mathrm{Jg^{-1}})(\Delta V_C/\mathrm{mm^3g^{-1}}) \\ & +2.08\times10^{-5}\,(\Delta V_C/\mathrm{mm^3g^{-1}})^2. \end{aligned} \qquad (6\text{-}7)$$

Fig. 6-4 shows the ΔG_C contour map in the ΔE_C-ΔV_C plane. In Fig. 6-4, the lines A and B represent the experimental relaxation path and the equilibrium line, respectively. These lines correspond to the lines in the ΔE_C-ΔV_C plane in Fig. 6-3.

According to the linear non-equilibrium thermodynamics [9], the relaxation rates of configurational energy and volume are given by

$$\begin{aligned} -(dE_C/dt) &= L_{EE}(\partial G_C/\partial E_C) + L_{EV}(\partial G_C/\partial V_C) \\ -(dV_C/dt) &= L_{EV}(\partial G_C/\partial E_C) + L_{VV}(\partial G_C/\partial V_C), \end{aligned} \qquad (6\text{-}8)$$

respectively. Here, L_{EE}, L_{EV} and L_{VV} are constants. $L_{EE} > 0$ and $L_{VV} > 0$ from the thermodynamic consideration. If $L_{EV} = 0$, eqs. 6.8 asserts that the relaxation path lies in the lower-right area of the equilibrium line (line B) as shown by the line C in Fig. 6-4. The simplest case is that if $L_{EE} = L_{VV}$, the relaxation progresses through the steepest-gradient path in the ΔG_C surface.

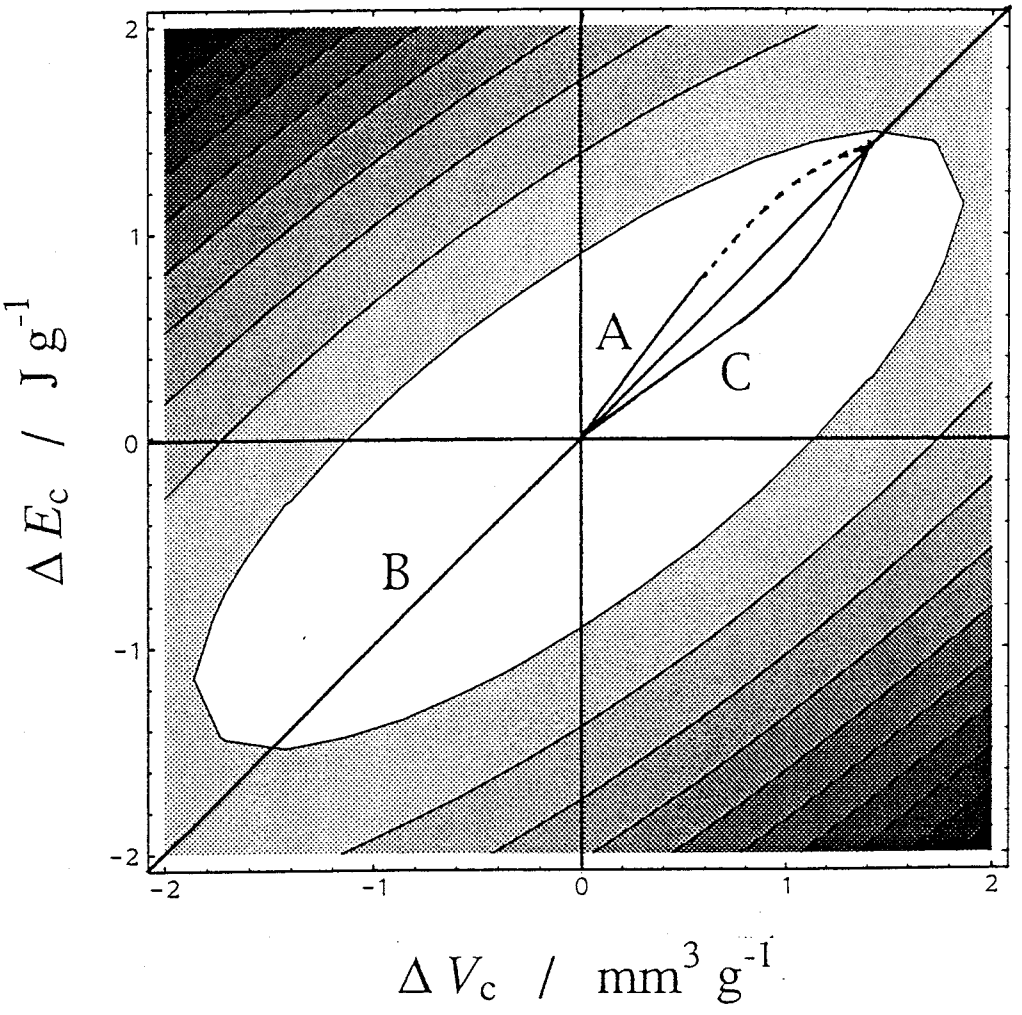

Fig. 6-4. Contour map of the departure from the equilibrium configurational Gibbs free energy of atactic polystyrene in the ΔE_C-ΔV_C plane. See text for the details.

As discussed in Section 6-4-1, the whole relaxation path is a convex locating in the upper-left area of the equilibrium line (line B). This indicates that the enthalpy and volume relaxations are coupled with each other, i.e., $L_{EV} \neq 0$.

To make further discussion on the relaxation path, a number of different relaxation paths should be determined experimentally on the ΔG_C surface. The relaxation measurements after much more rapid cooling are desirable for determination of the paths much different from the present one. Another significant experiment is to make the pressure jumps (rapid increase of pressure) [8,10] to the glass transition region and follow the relaxation under pressure. This method will provide the relaxation paths quite different from those obtained by the temperature jump (rapid cooling). After the accumulation of the relaxation paths, it will be possible to identify the internal thermodynamic parameters which dominate the progress of the structural relaxation in the glassy states. Gupta's multiparameter theory [11], in which the fictive temperature and the fictive pressure are taken as the internal parameters, is the first one to be examined.

References to Chapter 6

[1] K. Takeda, O. Yamamuro and H. Suga, J. Phys. Chem. Solids, 52 (1991) 607.

[2] H. Fujimori, Y. Adachi and M. Oguni, Phys. Rev., B46 (1992) 14501.

[3] R.W. Randell, K.L. Ngai, G.R. Fong and J.J. Aklonis, Macromolecules, 20 (1987) 1070.

[4] A.J. Kovacs, Fortschr. Hochpolym. -Forsch., 3 (1963) 394.

[5] G.W. Scherer, J. Am. Ceram. Soc., 67 (1984) 504.

[6] K Adachi and T. Kotaka, Polymer J. 14 (1982) 959.

[7] A.Q. Tool and C.G. Eichlin, J. Am. Chem. Soc., 54 (1931) 491.

[8] J.J. Tribone and J.M. O'Reilly, J. Polym. Sci. Polym. Phys. Ed., 27 (1989) 837.

[9] S. R. DeGroot and P. Mazur, Non-Equilibrium Thermodynamics (North-Holland, Amsterdam, 1963).

[10] O. Yamamuro, S. Takahara and H. Suga, J. Non-Cryst. Solids, in press.

[11] P.K. Gupta, J. Non-Cryst. Solids, 102 (1988) 231.